U.PORTO

BIOTECNOLOGIA MOLECULAR E CELULAR APLICADA ÀS CIÊNCIAS DA SAÚDE

Target-to-treat nanotherapy for rheumatoid arthritis

Virgínia Adorinda Moura Gouveia

D

2020

U.PORTO

Virgínia Adorinda Moura Gouveia. Target-to-treat nanotherapy for rheumatoid arthritis

D.ICBAS 2020

Target-to-treat nanotherapy for rheumaoid arthritis

Virgínia Adorina Moura Gouveia

SEDE ADMINISTRATIVA

INSTITUTO DE CIÊNCIAS BIOMÉDICAS ABEL SALAZAR

FACULDADE DE FARMÁCIA

U.PORTO

BIOTECNOLOGIA MOLECULAR E CELULAR APLICADA ÀS CIÊNCIAS DA SAÚDE

Target-to-treat nanotherapy for rheumatoid arthritis

Virgínia Adorinda Moura Gouveia

D

2020

Virgínia Adorinda Moura Gouveia

TARGET-TO-TREAT NANOTHERAPY FOR RHEUMATOID ARTHRITIS

Tese de Candidatura ao grau de Doutor em Biotecnologia Molecular e Celular Aplicada às Ciências da Saúde;
Programa Doutoral da Universidade do Porto (Instituto de Ciências Biomédicas de Abel Salazar e Faculdade de Farmácia)

Orientador – Professora Doutora Maria de La Salette de Freitas Fernandes Hipólito Reis Dias Rodrigues

Categoria – Professor Associado

Afiliação – Faculdade de Farmácia da Universidade do Porto

Co-orientador – Professor Doutor António da Fonseca Oliveira

Categoria – Professor Catedrático Convidado

Afiliação – Instituto de Ciências Biomédicas Abel Salazar da Universidade do Porto

Co-orientador – Professor Doutor Giuseppe Battaglia

Categoria – Professor

Afiliação – Department of Chemistry, Faculty of Mathematics and Physical Sciences of University College London

Não vos inquieteis, pois,
com o dia de amanhã: o amanhã se ocupará de si.
A cada dia basta o seu trabalho!

Sermão da Montanha
Segundo São Mateus 5,1-7,29

Agradecimentos

Antes de mais gostaria de prestar alguns agradecimentos àquelas pessoas que, de alguma forma, me ajudaram na realização desta dissertação e que a tornaram num desafio muito gratificante e sem dúvida enriquecedor.

Em primeiro lugar sou muita grata à Professora Doutora Salette pela sua orientação no decurso do meu doutoramento, por todo apoio prestado nesta aventura de 4 anos. Por me ter dado o privilégio de trabalhar consigo e demonstrado ser uma referência no pequeno grande mundo da nanotecnologia, pela sua experiência, profissionalismo e dedicação no seu trabalho. Pelo seu positivismo, apoio incondicional e carinho nas minhas crises existenciais. Todas as conversas, de perto ou de longe, e conselhos que me deu foram essenciais para o meu crescimento primeiro como pessoa e jovem cientista. Muito Obrigada Professora Salette!

Ao Professor António Oliveira, o meu Muito Obrigado pela orientação, preocupação, incentivo e apoio prestados durante o meu doutoramento, pela sua experiência e disponibilidade em partilhar conhecimentos comigo.

Also, I would like to express my deepest gratitude to Beppe for the valuable opportunity of being part of his research group at University College London. For all the knowledge, constructive criticism and guidance that led me to grow as a young scientist. You have always motivated and supported me to want more and to be better. It has been a memorable experience and a pleasure to be part of Molecular Bionics Lab. Beppe, grazie mille per aver fiducia in me!

I am very grateful to my mentor Loris. Thank you for believing in me since the moment I start working with you. Your support, knowlege and constant unconditional help made this thesis possible and opened my eyes to what Science and team work can really be. Thank you for being by my side every step of the way in this adventure. Grazie mille maestro!

À Cláudia um especial agradecimento por ser incansável ao longo desta aventura. Porque sempre me motivaste e apoiaste a querer mais e a querer ser melhor. Porque sempre estiveste disponível de braços abertos para me ajudar em tudo que fosse necessário. E sem ti não seria a cientista que sou hoje! Cláudia Maria, Muito Obrigada pelo apoio incondicional e pela amizade.

Também não me posso esquecer do apoio e carinho de todos os membros do Molecular Biophysics and Biotechnology Lab, em especial do meu trio Biotech, Joaninha e o José, que comigo percorreram este trilho. Por todos os momentos vividos, de trabalho, mas também de muita alegria, generosidade e partilha, a todos Muito Obrigada!

I would also like to thank all members of the Molecular Bionics Lab for making me feel so welcome and for providing a good working environment. In particular, to Senio, Ciro, Cesare, Azzurra, Gabriele, Alessandro, Edo, Aroa, Laura, Safa, Chiara and Barbara, for being always available for helping me at all times. Thank you! Também gostaria de agradecer às minhas Dianas, sempre atenciosas para comigo em todos momentos. E alguns verdadeiramente inesquecíveis! Muito Obrigada meninas!

Sem sombra de dúvida quero agradecer também aos meus amigos da vida, em especial à Sofia Coura, Sara Asus, Pedro Xuxa, Rita Panela, Paula e João por todos os mimos e carinho. E aos meus companheiros londrinos, Laly, Márcio e Maya pelo apoio nesta etapa tão importante da minha vida.

O sincero Muito Obrigado aos meus pais e irmão, que mesmo longe sempre desejaram e proporcionaram um melhor futuro para mim, em constante apoio, incentivo e amor incondicional. E não posso deixar de agradecer à minha família também por todo o apoio e carinho, com especial apreço aos meus tios e primo.

Um especial Muito Obrigada ao meu melhor amigo, namorado e futuro marido, Joel, por me ter acompanhado e incentivado ao longo desta aventura com muita paciência, incentivo, amor e carinho. E assim a ti dedico esta dissertação.

Por fim, mas não a menos importante, agradeço ao Professor Doutor Mário Barbosa e à Comissão Científica do Programa Doutoral do BiotechHealth pela oportunidade de fazer parte deste programa doutoral, permitindo assim o meu enriquecimento científico e aquisição de competências transversais que foram essenciais para a minha formação como jovem cientista.

Um muito obrigado a todos!

Funding

I thank for the received financial support from FCT (Fundação para a Ciência e Tencnologia) through the FCT PhD Programmes and by POCH (Programa Operacional Potencial Humano), specifically by the Doctoral Programme on Cellular and Molecular Biotechnology Applied to Health Sciences (BiotechHealth) for the grant PD/BD/128388/2017. This work has also received financial support from FCT/MCTES throught national funds UID/QUI/50006/2019 and from the Exploratory project IF/00293/2015 – Upgrading rheumatoid arthritis treatment through a targeted nanotherapeutic approach.

Publicações

Ao abrigo do disposto do número 2, alínea a) do artigo 31º do Decreto-Lei no 115/2013 de 7 de Agosto, fazem parte integrante desta tese de doutoramento as seguintes publicações:

V. M. Gouveia, C. Nunes, S. Reis (2018) *Chapter 13: Innovative Target-to-Treat Nanostrategies for Rheumatoid Arthritis*. Nanoparticles in the Life Sciences and Biomedicine. Pan Stanford Publishing.
ISBN: ISBN 978-1-351-20735-5

V. M. Gouveia, J. Lopes-de-Araújo, S. A. Costa Lima, C. Nunes, S. Reis (2018) *Hyaluronic Acid-conjugated pH-sensitive Liposomes for Targeted Delivery of Prednisolone on Rheumatoid Arthritis Therapy*. Nanomedicine – Future Medicine.
DOI: 10.2217/nnm-2017-0377

V. M. Gouveia, L. Rizzello, C. Nunes, A. Poma, L. Ruiz-Perez, A. Oliveira, S. Reis, G. Battaglia (2019) *Macrophage targeting pH Responsive polymersomes for glucocorticoid therapy*. Pharmaceutics.
DOI: 10.3390/pharmaceutics11110614

Resumo

A artrite reumatoide é a doença crónica inflamatória autoimune, com a maior prevalência em todo o mundo, atingindo quase 1% da população. Se não for diagnosticada precocemente e tratada adequadamente, a progressão da doença pode levar à deformação severa das articulações e, eventualmente, à perda da sua funcionalidade, prejudicando assim o cotidiano das pessoas com esta doença.

As atuais normas de tratamento incluem o uso de glucocorticoides e medicamentos antirreumáticos modificadores da doença, cujo potencial terapêutico é, no entanto, limitado por graves efeitos secundários. Assim, a fim de melhorar as necessidades dos pacientes e da clínica no tratamento da artrite reumatoide, proponho uma nanoterapia inovadora, idealizada para direcionar e tratar a artrite inflamatória, com o objetivo final de alcançar a remissão da doença.

Esta tese apresenta inovadoras estratégias que exploram os potenciais benefícios da nanomedicina para superar as desvantagens a que os fármacos convencionais estão associados na terapia crónica. Numa abordagem passo a passo, os estudos *in vitro* e *in vivo* revelaram que os sistemas de entrega de fármacos desenvolvidos apresentam a capacidade de se acumularem nas articulações inflamadas e favorecerem a sua entrega seletiva no local alvo. Deste modo, melhoram a eficácia terapêutica dos fármacos na supressão completa da progressão da artrite, enquanto reduz o risco de efeitos colaterais.

Neste sentido, a nanoterapia desenvolvida apresenta todos os requisitos com alto potencial terapêutico para ser clinicamente transferível para o tratamento da artrite reumatoide.

Abstract

Rheumatoid arthritis is the chronic immune-mediated inflammatory disease with the highest prevalence worldwide, striking nearly 1% of the population. If not early diagnosed and properly treated, disease progression may lead to the severe deformity of joints and, eventually, to the loss of their functionality. Thus, causing impairment in the daily lives of people affected by this disorder.

Current treatment guidelines include glucocorticoids and disease-modifying anti-rheumatic drugs, which therapeutic potential is however hampered by deleterious side-effects. Thus, in order to improve the patients and clinics needs in the treatment, I propose here an innovative nanotherapy that is specifically designed to target and treat inflammatory arthritis, aiming to pursuit the final goal of disease remission.

This thesis presents a rationale target-to-treat strategy, which explores the potential benefits of lipid and polymer-based nanomedicines to overcome the drawbacks that conventional drugs entail in chronic therapy. In a step-by-step approach, the *in vitro* and *in vivo* studies revealed the ability of the developed nanomedicines to accumulate within inflamed joints and to enhance the selective delivery of loaded drug on-site. Hence, improving the drug therapeutic efficacy in the complete abrogation of arthritis progression, while reducing the risk of side-effects.

To this respect, the target-to-treat nanotherapy designed here has all the requirements of high therapeutic potential to be clinically transferable for the treatment of rheumatoid arthritis.

Table of contents

List of abbreviations and symbols viii

List of figures xiii

List of tables xx

Thesis layout xxii

Chapter 1 | 1

Motivation and goals 2

Chapter 2 | 5

Innovative target-to-treat nanostrategies for rheumatoid arthritis 6

Appendix 37

Chapter 3 | 38

I. Hyaluronic acid-conjugated pH-sensitive liposomes for targeted delivery of prednisolone on rheumatoid arthritis therapy 39

Supplementary information 52

Appendix 55

II. Macrophage targeting pH responsive polymersomes for glucocorticoid therapy 60

Supplementary information 76

III. pH-responsive polymersomes in the control of arthritic inflammation *in vitro* 82

Supplementary information 110

IV. pH-NITRA: pH-responsive nano immuno therapy for rheumatoid arthritis 113

Chapter 4 | 136

Conclusion and future perspectives 137

List of abbreviations and symbols

A

AbIA antibody-induced arthritis

ACR american college of rheumatology

AIA adjuvant-induced arthritis

ANOVA analysis of variance

ATRP atom-transfer radical polymerisation

AUC area under the curve

B

BE bone erosion

BMS betamethasone hemisuccinate

BSA bovine serum albumin

BSP betamethasone sodium phosphate

C

CD cartilage damage

CD cluster of differentiation

cDNA complementary deoxyribonucleic acid

CHEMS cholesteryl hemisuccinate

CIA collagen-induced arthritis

CLSM confocal laser scanning microscopy

CO_2 carbon dioxide

cps counts per second

CV cardiovascular

C_t cycle threshold

Cy cyanine

D

D_h hydrodynamic diameter

DLS dynamic light scattering

DMARD disease-modifying anti-rheumatic drug

DMEM Dulbecco's modified eagle medium

DMSO dimethyl sulfoxide

DOTAP 1,2-dioleoyl-3-trimethylammonium-propane

DNA deoxyribonucleic acid

DPBS Dulbecco's phosphate-buffered saline

DPPE 1,2-dipalmitoyl-*sn*-glycero-3-phosphoethanolamine

DTT dithiothreitol

DXP dexamethasone phosphate

E

EE encapsulation efficiency

EDTA ethylenediaminetetraacetic acid

ELISA enzyme linked immunosorbent assay

EPR enhanced permeation and retention

ELS electrophoretic light scattering

EULAR European league against rheumatism

F

FA folic acid

FBS fetal bovine serum

FR folate receptor

Fw forward

G

GADPH glyceraldehyde 3-phosphate dehydrogenase

GC glucocorticoid

GR glucocorticoid receptor

H

HA hyaluronic acid

HCL hydrochloric acid

HDAC2 histonedeacetylase-2

H&E haematoxylin and eosin

HFLS human fibroblast like synoviocytes

HPLC high-performance liquid chromatography

I

ID injected dose

IL interleukin

IL-RA interleukin receptor antagonist

IND indomethacin

IP intraperitoneal

IVIS *in vivo* imaging system

K

K_0 zero-order release constant

K_1 first-order release constant

K_e elimination rate

K_{HC} Hixson–Crowell rate constant

K_H Higuchi dissolution constant

K_{KP} Korsmeyer–Peppas drug release rate constant.

K_p partition coefficient

L

LC loading capacity

LDH lactate dehydrogenase

LE loading efficiency

Lipo liposome

LipoHA HA-conjugated pH-sensitive liposome

Log logarithm

LPS lipopolysaccharide

M

MMP matrix metalloprotease

MPS methylprednisolone hemisuccinate

MTT thiazolyl blue tetrazolium bromide

MTX methotrexate

MW molecular weight

N

NaOH sodium hydroxide

NBD N-(7-nitro-2,1,3-benzodiazole-4-yl)

NFκB nuclear factor-κB

NMR nuclear magnetic resonance

NP nanoparticle

P

PAGE polyacrylamide gel electrophoresis

PAMAM polyamidoamine

PBS phosphate-buffered saline

PCR polymerase chain reaction

PDI poydispersity index

PDP prednisolone disodium phosphate

PDPA poly(2-(diisopropylamino)ethyl methacrylate)

PEG polyethylene glycol

pKa acid dissociation constant

PLA poly(lactic acid)

PLGA poly(lactic-co-glycolic acid)

PLP prednisolone phosphate

PMA phorbol 12-myristate 13-acetate

PMPC poly(2-methacryloyloxyethyl phosphorylcholine)

Psome polymersome

PVDF polyvinylidene difluoride

Q

qPCR quantitative polymerase chain reaction

R

r^2 coefficient of determination

RA rheumatoid arthritis

RANKL receptor activator of nuclear factor-κB

RES reticuloendothelial system

RGD tripeptide Arginine-Glycine-Aspartate

RIPA radioimmunoprecipitation

RNA ribonucleic acid

RPL13A ribosomal protein L13A

Rpm rotations *per* minute

RT room temperature

RT-qPCR real-time quantitative polymerase chain reaction

Rv reverse

S

sCT salmon calcitonin

SDS sodium dodecyl sulfate

SD standard deviation

SEM standard error of the mean

SEAP secreted embryonic alkaline phosphatase

siRNA small interfering ribonucleic acid

SM synovial membrane

SR scavenger receptor

T

$t_{1/2}$ half-life

TBST tris-buffered saline tween-20

TCZ tocilizumab

TEM transmission electronic microscope

THP1 human leukemic monocytes

TFA trifluoroacetic acid

TNFα tumour necrosis factor-α

TRAIL TNF-related apoptosis-inducing ligand

U

UV ultraviolet

V

VECs vascular endothelial cells

VEGF vascular endothelial growth factor

Vis visible

α alpha

β beta

Δ delta

κ kappa

φ phi

λ wavelength

μ micro

3D three-dimensional

List of figures

Chapter 2 |

Figure 1. Target-to-treat strategies for RA. 11

Figure 2. Targeting strategies for RA. 16

Chapter 3 | **I**

Figure 1. H nuclear magnetic resonance (NMR) spectrum of hyaluronic acid (HA)–1,2-dipalmitoyl-sn-glycero-3-phosphoethanolamine (DPPE) conjugate. H NMR spectra of HA and DPPE are presented in Supplementary Figure S1. 43

Figure 2. Transmission electron microscopy representative images of prednisolone disodium phosphate-loaded pH-sensitive liposomes in buffered solutions at pH 7.4 (A & C) and pH 5.0 (B & D). 44

Figure 3. *In vitro* release profiles of prednisolone disodium phosphate from pH-sensitive liposomes in mimicked acidic and physiological conditions at 37ºC. Data represent the average ± standard deviation (n = 3). Statistical significant differences (*p < 0.05) between buffered solutions at pH 7.4 and 5.0 at each time point. ... 45

Figure 4. Cell viability and cytotoxicity of pH-sensitive liposomes. Cell viability assessed by MTT (A & B) and cytotoxicity effect measured by LDH release (C & D) on L929 fibroblast (A & C) and RAW 264.7 macrophage (B & D). Data represent the average ± standard deviation (n = 5 of two independent assays). Statistical significant differences when comparing liposomes-loading PDP either with empty ones (*p < 0.05) or PDP solution control (#p < 0.05) at each concentration, and between conjugated and unconjugated liposomal formulations (·p < 0.05). 47

Figure 5. Cellular uptake of N-(7-nitro-2,1,3-benzodiazole-4-yl)-fluorescent pH-sensitive liposomes. L929 fibroblast (A) and RAW 264.7 macrophage (B) cell lines.

Data represent the average ± standard deviation (n = 3 of two independent assays). Statistical significant differences when comparing unconjugated liposomes with conjugated ones (*p < 0.05). 48

Figure 6. Effect of low temperature and pathway mechanism inhibitors on the uptake of N-(7-nitro-2,1,3-benzodiazole-4-yl)-fluorescent pH-sensitive liposomes by L929 fibroblast and RAW 264.7 macrophage. Data represent the average ± standard deviation (n = 3). Statistical significant differences when comparing with control at 37ºC (*p < 0.05). 49

Figure S1. ^{1}H-NMR spectra of HA and DPPE molecules. 52

Figure S2. Stability studies conducted with weekly assessment on the physicochemical parameters of HA conjugated pH-sensitive liposomes indicated that storage at 4oC protected from light preserved the liposomes properties for one month. Data express the average ± standard deviation (n=3). Statistical significant differences (* P<0.05) when comparing with week 0. 54

Chapter 3 | II

Figure 1. (a) Representative TEM images of empty (top) and PDP loaded PMPC-PDPA polymersomes (bottom) produced via film rehydration method (200 nm scale bar). (b) PDP cumulative release profile in each tested pH condition over 50 h at 37ºC. Data express as mean ± SD (n = 3). (c) Cy5- release profile in each tested pH condition over 50 h at 37ºC. Data express as mean ± SD (n = 3). (c) Cy5-PMPC-PDPA polymersomes normalised fluorescent intensity relative to the nucleus signal measured as a function of time upon uptake by macrophages. Data express the mean ± SD (10 images for n = 2). Cell viability assay after 24 h incubation with increasing concentrations of (d) unloaded PMPC-PDPA polymersomes (Psome), (e) either free PDP or PDP loaded polymersomes (Psome:PDP). Data express PMPC-PDPA polymersomes (Psome), (e) either free PDP or PDP loaded polymersomes (Psome:PDP). Data express as mean ± SD (n = 3). 68

Figure 2. Representative CLSM images of Cy5-PMPC-PDPA polymersomes (green fluorescence intensity signal) cellular uptake overtime (scale bar: 25 μm). Staining of the cell nuclei (blue fluorescence intensity signal) with Hoechst 33342 and cell

membrane (red fluorescence intensity signal) with far-red CellMask™. The yellow fluorescence intensity signal corresponds to the co-localisation (merge) of the Cy5-PMPC-PDPA polymersomes and cell membrane fluorescence signals. 69

Figure 3. *In vitro* inflammation-related cellular studies on M1-macrophages after incubation with either PMPC-PDPA polymersomes (Psome), free PDP or PDP loaded polymersomes (Psome:PDP). (a, b) CLSM imaging of NFκB (red fluorescence intensity signal) translocation from cytoplasm to the nucleus (blue fluorescence intensity signal) and co-localisation analysis (pink fluorescence intensity signal). Data express as mean ± SD (5 images for n=2). (c) SEAP assay for the quantification of NfκB nuclear translocation. Data express as mean ± SD (n=3). (d) RT-qPCR of pro-inflammatory genes expression levels. Data express as mean ± SD (n=3). (e) ELISA for IL6 and TNFα protein secretion levels. Data express as mean ± SD (n=4). In all experiments, the differences were statistically significant when *p<0.05, **p<0.01, ***p<0.001 and ****p<0.0001. 71

Figure S1. Chemical structure of (a) $PMPC_{25}$-$PDPA_{68}$ and (b) Cy5-$PMPC_{25}$-$PDPA_{70}$. ... 78

Figure S2. DLS data on the hydrodynamic diameter (Dh) and polydispersity index (PDI) values of all formulations of unloaded and PDP loaded PMPC-PDPA polymersomes (n = 3). Analysis on the PDI values below 0.2 indicates a formulation of polymersomes with monodisperse and homogeneous size distribution [3]. (b) TEM representative image of Cy5-PMPC-PDPA polymersomes produced via film rehydration method (200 nm scale bar). (c) DLS data on the number of PMPC-PDPA polymersomes as a function of the Dh. Analysis on the drug loading capacity represented as the number of PDP molecules per polymersome as a function of their size. (d) Cryo-TEM representative image of PMPC-PDPA polymersomes produced via pH-switch method (200 nm scale bar). (e) Chemical structure and electrostatic surfaces of prednisolone disodium 21-phosphate (PDP) and respective representation of the electrostatic surfaces. 79

Figure S3. Cell viability assay after 48 h incubation with increasing concentrations of (a) unloaded PMPC-PDPA polymersomes, (b) either free PDP or PDP-loaded polymersomes (Psome:PDP). 80

Chapter 3 | III

Figure 1. (A) TEM micrograph of Mtx-loaded PMPC-PDPA polymersomes (100 nm scale bar). (B) Analysis on the drug loading capacity represented as the number of Mtx molecules per polymersome as a function of their hydrodynamic diameter (D_h) measured by DLS. (C) Drug release profiles of Mtx from PMPC-PDPA polymersomes in pH 5.0, 6.5 and 7.4 buffer solutions at 37ºC for 50 hours (n = 3). 95

Figure 2. (A) CLSM images of Cy5-PMPC-PDPA polymersome (green fluorescence intensity signal) uptake by LPS-activated macrophages overtime. 3D image corresponds to the 24-hour time point. Staining of the cell nuclei (blue fluorescence intensity signal) with Hoechst 33342 and cell membrane (red fluorescence intensity signal) with far-red CellMask™. (B) Cell uptake profile of Cy5-PMPC-PDPA polymersomes normalised fluorescent intensity relative to the nucleus signal measured as a function of time. Data express the mean ± SEM (10 images for n=2). (C) Cell viability assay in LPS-activated macrophages after 24 hours incubation with increasing concentrations of either free Mtx or Mtx loaded PMPC-PDPA polymersomes. Data express as mean ± SD (n=3). 96

Figure 3. (A) CLSM images of Cy5-labelled PMPC-PDPA polymersome (green fluorescence intensity signal) uptake by TNFα-activated synoviocytes over time. 3D image corresponds to the 10-hour time point. Staining of the cell nuclei (blue fluorescence intensity signal) with Hoechst 33342 and cell membrane (red fluorescence intensity signal) with far-red CellMask™. (B) Cell uptake profile of Cy5-PMPC-PDPA polymersomes normalised fluorescent intensity relative to the nucleus signal measured as a function of time. Data express the mean ± SEM (10 images for n=2). (C) Cell viability assay in TNFα-activated synoviocytes after 24 hours incubation with increasing concentrations of either free Mtx or Mtx loaded PMPC-PDPA polymersomes. Data express as mean ± SD (n=3). 97

Figure 4. (A) SRBI and CD36 cell surface proteins expression levels in non- and activated macrophages and synoviocytes detected by western blot assay (n=3). The SRBI and CD36 were revealed using specific antibodies and glyceraldehyde 3-phosphate dehydrogenase (GAPDH) was used as the loading control. (B) Fold change expression normalised to non-activated control. Data express as mean ± SD (n=3). The differences relative to the non-activated control were statistically significant for *p<0.05, **p<0.01, ***p<0.001 and ****p<0.0001. 98

Figure 5. CLSM images of NFκB (red fluorescence intensity signal) translocation from cytoplasm to the nucleus (blue fluorescence intensity signal) in (A) LPS-activated macrophages and (C) TNFα-activated synoviocytes. (B) Quantitative imaging co-localisation (pink fluorescence intensity signal) analysis after 24 hours treatment with either free Mtx or Mtx-loaded PMPC-PDPA polymersomes. Data express as mean ± SEM (5 images for n=2). The differences relative to activated cells control were statistically significant when *p<0.05, **p<0.01, ***p<0.001 and ****p<0.0001. 99

Figure 6. ELISA analysis on the TNFα and IL6 protein secretion levels in (A, B) LPS-activated macrophages and (C, D) TNFα-activated synoviocytes after 24 hours incubation with increasing concentrations of either free Mtx or Mtx-loaded PMPC-PDPA polymersomes. Data express as mean ± SD (n=3). 101

Figure 7. RT-qPCR on the gene expression levels in (A) LPS-activated macrophages and (B) TNFα-activated synoviocytes after 24 hours incubation with either free Mtx or Mtx-loaded PMPC-PDPA polymersomes. Data express as mean ± SD (n=3). The differences relative to non-treated control were statistically significant for *p<0.05, **p<0.01, ***p<0.001 and ****p<0.0001. 102

Figure S1. (A) Log $D_{o/w}$ calculations for Mtx at different pH conditions using the MarvinSketch calculator (Chemaxon). (B) Absorption spectra and second-derivative spectra of Mtx at pH 7.4 (25 μM) (blue lines) incubated in with increasing concentrations of PMPC-PDPA polymersomes at 37 ºC (gray lines) (0 – 120 μM). Graphic represents the fitting curve of the experimental second-derivative spectrophotometric data using a nonlinear least squares regression method at wavelength 255 nm where the scattering is eliminated [55]. The partition coefficients are then calculated by fitting the equation to experimental derivative spectrophotometric data through a nonlinear regression method, where the adjustable parameters are D_p and K_p [55]. D, D_w and D_p correspond to the second derivative of total, aqueous and polymer absorbance of Mtx, respectively; K_p is the partition coefficient (M^{-1}), [polymer] the PMPC-PDPA concentration ($mol.L^{-1}$) and Vϕ the polymer molar volume ($L.mol^{-1}$). 110

Figure S2. TEM micrograph of Cy5-PMPC-PDPA polymersomes produced by solvent-switch method (100 nm scale bar). 112

Figure S3. Cell viability of 24 hours treatment with unloaded PMPC-PDPA polymersomes in inflammation-activated macrophages and synoviocytes. …… 112

Chapter 3 | IV

Figure 1. (A) Representative TEM image of Mtx-loaded pH-NITRA polymersomes (100 nm scale bar). (B) Analysis on the drug loading capacity represented as the number of Mtx molecules per PMPC-PDPA polymersome as a function of their hydrodynamic diameter (Dh) measured by DLS. …… 120

Figure 2. (A) The blood plasma concentration-time profiles of Cy7-labelled pH-NITRA after intraperitoneal injection in healthy and AIA Wistar rats. The plasma concentrations of Cy7-labelled pH-NITRA are expressed in $\mu g.mL^{-1}$. Pharmacokinetic parameters – terminal half-life ($t_{1/2}$), elimination rate (Ke), area under the curve (AUC) – regarding the plasma concentration-time profiles of Cy7-labelled pH-NITRA after intraperitoneal injection of healthy and AIA Wistar rats. (C) The injected dose of Cy7-labelled pH-NITRA (% ID) in the spleen, kidney, liver, heart, after 24 hours intraperitoneal injection in healthy and AIA Wistar rats. (D) The % ID of Cy7-labelled pH-NITRA per gram of organ tissue weight. (E, F) IVIS images of the right hind and front paws of healthy and AIA Wistar rats. Data express the mean ± SEM (n=3). …… 122

Figure 3. (A) Paws arthritic inflammation score over the 15 days period of treatment. Data defined as the mean ± SEM of the sum of the partial scores of each affected joint. (B) Representative images of the left hind paw of a healthy and adjuvant-induced arthritis (AIA) Wistar rat. (C) Ankle perimeter of hind paws over the 15 days of treatment. (D) Variation of the ankle swelling percentage of the hind paws after the 15 days of treatment. (E) Body weight of all animals over the 15 days of treatment. (F) Variation of the body growth percentage of animals after the 15 days of treatment. Data express the mean ± SEM (n=5 per experimental group). Statistical analysis for * $p \leq 0.05$, ** $p \leq 0.01$, *** $p \leq 0.001$ and **** $p \leq 0.0001$. ……125

Figure 4. (A) H&E histological representative images of the left hind paw of each experimental animal group (scale bar: 500 μm; SM: synovial membrane; CD: cartilage damage; BE: bone erosion). Histological evaluation: (B) Sublining layer infiltration score (0 = none to diffuse infiltration, 1 = lymphoid cell aggregate, 2 =

lymphoid follicles, 3 = lymphoid follicles with germinal centre formation); (C) Lining layer cell number score (0 = fewer than three layers, 1 = three to four layers, 2 = five to six layers, 3 = more than six layers); (D) Bone erosion score (0 = no erosions, 1 = minimal, 2 = mild, 3 = moderate, 4 = severe); (E) Cartilage damage score (0 = normal, 1 = irregular, 2 = clefts, 3 = clefts to bone); (F) Global severity score (0 = no signs of inflammation, 1 = mild, 2 = moderate, 3 = severe). Data express the mean ± SEM. Statistical analysis versus the AIA experimental group (* $p \leq 0.05$, ** $p \leq 0.01$, *** $p \leq 0.001$ and **** $p \leq 0.0001$) and the pH-NITRA:Mtx experimental group (# $p \leq 0.1$ and * $p \leq 0.05$). 127

Figure 5. Inflammation-related cytokine analysis in the serum of animals after the 15 days of treatment. Data express the mean ± SEM (n=5 per experimental group). Statistical analysis versus the AIA experimental group (* $p \leq 0.05$, ** $p \leq 0.01$, *** $p \leq 0.001$ and **** $p \leq 0.0001$) and the pH-NITRA:Mtx experimental group (# $p \leq 0.1$). 128

Chapter 4 |

Figure 1. Target-to-treat nanotherapy for rheumatoid arthritis: from idea to clinics. 139

List of tables

Chapter 2 |

Table 1. PEGylated target-to-treat nanocarriers for RA. 14

Table 2. FA nanocarriers targeting synovial cells. 18

Table 3. HA nanocarriers targeting synovial cells. 21

Table 4. RGD nanocarriers targeting synovial cells. 22

Table 5. Target-to-treat nanocarriers toward cytokines. 24

Chapter 3 | I

Table 1. Characterization of developed pH-sensitive liposomes. 43

Table 2. Correlation coefficient (r^2) and k values from various drug release models for each developed liposomal formulation (n = 3). 46

Chapter 3 | II

Table S1. Mathematical models for drug-release kinetics. 80

Table S2. Correlation coefficient (r^2) from various drug release mathematical models for each pH profile. 80

Table S3. Forward (Fw) and reverse (Rv) gene sequences of designed primers (PRIMER-BLAS; Sigma-Aldrich) used for gene expression studies. 81

Chapter 3 | III

Table S1. Mathematical models for drug-release kinetics. 111

Table S2. Correlation coefficient (r^2) from various drug release mathematical models for each pH profile. 111

Table S3. Forward (Fw) and reverse (Rv) gene sequences of designed primers (PRIMER-BLAS; Sigma-Aldrich) used for gene expression studies. 111

Thesis layout

This thesis is organized in 4 chapters, based on the publications originated from this PhD.

Chapter 1

Motivation and goals

This chapter presents the motivation and the research goals need to be attained to develop an innovative target-to-treat nanotherapy for rheumatoid arthritis.

Chapter 2

Innovative target-to-treat nanostrategies for rheumatoid arthritis

In this chapter, the state of the art on rheumatoid arthritis, its diagnosis, current treatment options and, more importantly, the last decade of research on the most promising nanomedicines are presented. For this purpose, in here it is included a book chapter entitled: Innovative Target-to-Treat Nanostrategies for Rheumatoid Arthritis, published in *Nanoparticles in Life Sciences and Biomedicine* by Pan Stanford Publishing (2018) that includes a more detail narrative on the disease pathogenesis focusing in how to treat and target rheumatoid arthritis.

Chapter 3

This chapter comprises the progress beyond the state of the art presented in the format of four original research articles:

I. Hyaluronic acid-conjugated pH-sensitive liposomes for targeted delivery of prednisolone on rheumatoid arthritis therapy

(published in *Nanomedicine Future Medicine*, 2018)

II. Macrophage targeting pH responsive polymersomes for glucocorticoid therapy

(published in *Pharmaceutics*, 2019)

III. pH-responsive polymersomes in the control of arthritic inflammation *in vitro*

(to be submitted)

IV. pH-NITRA: pH-responsive nano immuno therapy for rheumatoid arthritis

(to be submitted)

Chapter 4

Conclusion and future perspectives

This chapter includes a conclusion regarding the major findings and future research work. Alongside the value, impact and future perspectives of the proposed target-to-treat nanotherapy for rheumatoid arthritis are presented.

Chapter 1

Motivation and goals

Rheumatoid arthritis (RA) is a chronic inflammatory autoimmune disease characterised by the progressive inflammation and severe damage of joints synovial tissues [1, 4]. Although not regarded as a lethal, RA causes severe implications in the daily lives of patients affected by it as a consequence of disease progression and comorbidities [5-9]. Currently there is not resultative cure for this disease and its treatment still remains a challenge [10-12]. The European League Against Rheumatism and American College of Rheumatology endorse the early intervention in RA treatment to pursuit the complete disease remission [10-12]. The primary focus of treatment guidelines is to relieve the pain and discomfort of the patients caused by arthritis [7, 11, 12]. And, then to abrogate the progressive synovial inflammation to prevent the irreversible destruction of joints that ultimately leads to disability [7, 11, 12].

The treatment guidelines recommend the use of conventional disease-modifying anti-rheumatic drugs (DMARDs) as a monotherapy, or in combination with glucocorticoids (GCs) as part of the initial treatment strategy [10-12]. The implementation of biologic DMARDs in RA treatment should be only consider for patients with adverse prognostic signs, and preferentially in combination with methotrexate [10-12]. Methotrexate is a conventional DMARD well-known for its effectiveness in reducing or annulling the arthritic inflammation symptoms and signs [7, 10-12]. As well as, in preventing joint damage with the aim to interfere with the disease progression [7, 10-12]. GCs, such as prednisolone, should only be at low dose for a short time, which then should be tapered as rapidly as clinically feasible [7, 10-12]. Particularly due to the chronic component of the disorder, the prolonged use of current therapeutics intensifies the deleterious side-effects and the increased risk of comorbidities, which, in turn, often leads to patient non-compliance [7, 10-13].

RA is associated with a broad health and social burden. This does not only involve the cost related to the quality of life of people suffering from RA. But also, social-economic costs related to the disease-related work invalidity and early retirement. As the debilitating impairment of joint function can significantly affect the work productivity [8, 14, 15]. In addition, RA treatment entails high medical costs in terms of medication, physiotherapy and joint replacement surgery [8, 14, 15]. Overall, the mean annual cost per patient has been estimated to be around € 13,500 in Europe, of which medical costs and medication represent about one-third [8, 15]. The costs in the United States are much higher (€ 21,000), mainly due to the greater implementation of biologic therapies [8, 15]. The total cost impact of

this disease tends to exacerbate as the population ages and morbidity increases [8, 14, 15].

In this sense, the aim of this thesis is to take RA treatment to a new level by designing an innovative nanotherapy able to overcome the therapeutic limitations related to the long-term use of DMARDs and GCs with an improved cost-benefit ratio. Thereby, the nanomedicine proposed in this thesis aims to bring both health and economic benefits for patients and healthcare system, respectively. At the end, the aim is to encourage the future clinic implementation of nanotherapies for RA treatment.

A rationale target-to-treat strategy is presented, which explores the potential of pH-responsive nanomedicines to attain the above-mentioned goals. In a step-by-step approach, the nanomedicine presents ideal characteristics to enhance the stability, the specificity and the bioavailability of loaded drug within the inflamed disease-tissue. Hence, this enhance the on-site drug therapeutic efficacy, while reducing the risk of well-known adverse off-site activity. In this framework, the following objectives were pursuit for the development of a target-to-treat nanotherapy:

- Production and physicochemical characterisation of nanomedicines loaded with either prednisolone or methotrexate.
- Assessment of cell viability, targeting and uptake of developed nanomedicines using *in vitro* cellular models.
- Assessment of the *in vitro* therapeutic efficacy of developed nanomedicines using cellular models of inflammation.
- Assessment of the pharmacokinetics and biodistribution of developed nanomedicines *in vivo.*
- Assessment of the safety and biocompatibility of developed nanomedicines *in vivo* using an establish animal model of arthritis.
- Assessment of the *in vivo* therapeutic efficacy of developed nanomedicines.

Therefore, unlike conventional RA therapies, the proposed nanotherapies promise to target and treat arthritic inflammation, which, in turn, might lead to disease remission with negligible side-effects.

References

1 McInnes IB, O'Dell JR. State-of-the-art: rheumatoid arthritis. Ann Rheum Dis 2010;69(11):1898-906.

2 Helmick CG, Felson DT, Lawrence RC, et al. Estimates of the prevalence of arthritis and other rheumatic conditions in the United States. Part I. Arthritis Rheum 2008;58(1):15-25.

3 Lawrence RC, Felson DT, Helmick CG, et al. Estimates of the prevalence of arthritis and other rheumatic conditions in the United States. Part II. Arthritis Rheum 2008;58(1):26-35.

4 Firestein GS. Evolving concepts of rheumatoid arthritis. Nature 2003;423(6937):356-61.

5 van der Linden MP, le Cessie S, Raza K, et al. Long-term impact of delay in assessment of patients with early arthritis. Arthritis Rheum 2010;62(12):3537-46.

6 Gouveia VM, Lima SA, Nunes C, Reis S. Non-Biologic Nanodelivery Therapies for Rheumatoid Arthritis. J Biomed Nanotechnol 2015;11(10):1701-21.

7 Smolen JS, Steiner G. Therapeutic strategies for rheumatoid arthritis. Nat Rev Drug Discov 2003;2(6):473-88.

8 Lundkvist J, Kastäng F, Kobelt G. The burden of rheumatoid arthritis and access to treatment: health burden and costs. Eur J Health Econ 2008;8 Suppl 2:S49-60.

9 Upchurch KS, Kay J. Evolution of treatment for rheumatoid arthritis. Rheumatology (Oxford) 2012;51 Suppl 6:vi28-36.

10 Singh JA, Saag KG, Bridges SL, et al. 2015 American College of Rheumatology Guideline for the Treatment of Rheumatoid Arthritis. Arthritis Rheumatol 2016;68(1):1-26.

11 Kay J, Upchurch KS. ACR/EULAR 2010 rheumatoid arthritis classification criteria. Rheumatology (Oxford) 2012;51 Suppl 6:vi5-9.

12 Smolen JS, Landewé R, Breedveld FC, et al. EULAR recommendations for the management of rheumatoid arthritis with synthetic and biological disease-modifying antirheumatic drugs: 2013 update. Ann Rheum Dis 2014;73(3):492-509.

13 Agca R, Heslinga SC, Rollefstad S, et al. EULAR recommendations for cardiovascular disease risk management in patients with rheumatoid arthritis and other forms of inflammatory joint disorders: 2015/2016 update. Ann Rheum Dis 2017;76(1):17-28.

14 Kobelt G, Jönsson B. The burden of rheumatoid arthritis and access to treatment: outcome and cost-utility of treatments. Eur J Health Econ 2008;8 Suppl 2:95-106.

15 Smolen J, Aletaha D. The burden of rheumatoid arthritis and access to treatment: a medical overview. Eur J Health Econ 2008;8 Suppl 2:S39-47.

Chapter 2

Innovative target-to-treat nanostrategies for rheumatoid arthritis

Virgínia M. Gouveia [1], Cláudia Nunes [1] and Salette Reis [1]

[1] UCIBIO, REQUIMTE, Department of Chemical Sciences, Faculty of Pharmacy, University of Porto, 4050-313 Porto, Portugal

Original book chapter published in Nanoparticles in Life Sciences and Biomedicine, Pan Stanford Publishing (2018)
ISBN 978-1-351-20735-5

Chapter 13

Innovative Target-to-Treat Nanostrategies for Rheumatoid Arthritis

Virgínia Moura Gouveia, Cláudia Nunes, and Salette Reis
UCIBIO, REQUIMTE, Department of Chemical Sciences, Faculty of Pharmacy, University of Porto, Portugal
virginia.mgouveia@gmail.com

RA is a chronic inflammatory and autoimmune disease that manifests in the synovium of joints, hence causing severe functional limitations. Currently, available treatment options include glucocorticoids (GCs) and disease-modifying antirheumatic drugs (DMARDs), used either in monotherapy or in combination therapy. Nevertheless, treatment options only suppress inflammatory symptoms and not the irreversible joint damage. Thus, the disease's chronic nature and off-target therapy often lead to serious adverse side effects. To overcome the drawbacks of conventional therapies, there is increasing interest in nanotherapy. The increasing interest in the development of therapeutic delivery systems at the nanoscale level promises to revolutionize RA treatment management. Nanocarriers' huge potential is based on targeting strategies to selectively aim for and treat inflamed synovial tissues, allowing in situ therapeutic

Nanoparticles in Life Sciences and Biomedicine
Edited by Ana Rute Neves and Salette Reis

ISBN 978-981-4745-98-7 (Hardcover), 978-1-351-20735-5 (eBook)
www.panstanford.com

efficacy and hence remission of disease activity. The therapeutic potential of target-to-treat nanostrategies, aiming to defeat disease progression over the last 10 years of research, is reviewed in this section.

13.1 Rheumatoid Arthritis

Rheumatoid arthritis (RA) is a chronic systemic inflammatory autoimmune disease that afflicts approximately 1% of the population worldwide [1]. Particularly, the average prevalence rates is higher in North America and in northern European countries, compared with southern Europe and developing countries [2].

RA is mainly characterized by progressive inflammation of the synovial tissue of multiple body joints and hence structural joint damage [1, 2]. At the early stage, disease manifestations are the swelling and pain of joints, especially small joints with frequent movement, such as wrists, neck, hands, and feet. Symptoms in weight-bearing joints, such as hips, knees, spine, and ankles, develop later. RA may also affect tissues and organs, which makes it a systemic disease. In later stages, the chronic inflammatory nature of this disease leads to cartilage degradation, bone erosion, and joint stiffness as the disease progresses [1, 3]. In fact, the joint's inflammation is the hallmark of RA to measure disease severity [1, 3].

In that way, although not regarded as a lethal disease, depending on the severity, RA causes severe functional joint limitations [1]. Plus, long-term joint disability and, ultimately, implications for patients´ quality of life shorten their mean life expectancy by approximately 10 years [4].

13.2 Treat with What?

There is no cure for RA. During the first half of the 20th century the disease's progression from symptom onset to major joint deformity was often inevitable [5]. The European League Against Rheumatism (EULAR) and American College of Rheumatology (ACR) guidelines for RA treatment crucially acclaim an early intervention, immediately after disease diagnosis, to delay the beginning of joint damage [6, 7].

So, joint replacement surgery doesn't have to be the final outcome, and patients with RA can maintain a comfortable and active lifestyle with the more suitable treatment [8]. Clinically, the requirements for the management of RA are relied on primarily to provide the patient symptomatic relief, then slow down the disease's inflammatory activity, and finally amend the course of disease remission, hence preventing irreversible joint destruction [9, 10]. Nowadays, EULAR and ACR recommendations for early RA treatment include the use of glucocorticoids (GCs) in combination therapy, preferably with synthetic [6, 7]. Then, further introduction of biological disease-modifying antirheumatic drugs (DMARDs) in the treatment regime should be restricted to patients with advanced prognostic RA signs that did not responded adequately to the previous treatments [6].

GCs, such as prednisolone, methylprednisolone, dexamethasone, and budesonide, represent highly effective drugs in the control of the inflammatory response in the synovium and additionally promote rapid pain relief and reduce the swelling and stiffness manifested in arthritic joints [3, 11, 12]. These steroidal drugs inhibit the inflammatory reaction by controlling synovial neovascularization, thus reducing the release of endothelial growth factors and consequently the migration of leukocytes [3, 11, 13]. Moreover, GCs further prevent inflammation through downregulation of specific pro-inflammatory cytokines expression [3, 11, 13]. Although GCs are the most potent anti-inflammatory drugs in suppressing earlier disease symptoms, the long-term use and high doses can cause severe side effects [10, 12], namely impaired wound healing, skin atrophy, hypertension, weight gain, increased risks of cardiovascular (CV) diseases, osteoporosis, muscle atrophy, glaucoma, gastric ulcer, and manifestation of latent diabetes, leading ultimately to premature mortality [10, 12]. Additionally, their low bioavailability and off-targeted biodistribution profile often limit their therapeutic efficiency in controlling RA symptoms. Thereby, GCs are usually used in low doses in combination therapies meant to control inflammatory symptoms during periods when the disease activity is at its peak [10]. Contrary to GCs, which are mainly used for the symptomatic relief rather than remission of disease activity, synthetic DMARDs such as methotrexate (MTX), sulfasalazine, and also gold salts have specific antirheumatic activity to prevent disease progression [10]. The exact mechanism of action of synthetic

DMARDs is still unclear. Nonetheless evidence indicates that these drugs modulate inflammatory and immune responses [10, 14]. Specifically, MTX is the most used synthetic DMARD in the treatment of both early and established RA, as it has a rapid onset of action, as well as high, prolonged anti-inflammatory efficacy [10]. However, despite proven therapeutic efficacy, the long-term use of MTX is hampered by serious systemic effects, including infection, hepatitis, cirrhosis, and renal dysfunction, often resulting in the cessation of therapy [13, 15]. Furthermore, synthetic DMARDs aren't known for having a direct activity on the relief of inflammatory symptoms, as the suppression of immunologic response is not apparent until months after treatment begins [5, 10]. Therefore, EULAR and ACR recommendations for the treatment of early RA stages support the use of synthetic DMARDs in combination therapy with GCs in low doses and only for short time periods [6, 15].

In the last decade, significant advances in the treatment of RA have been emerging with the introduction of biologic DMARDs, especially for patients who do not respond to treatment with synthetic DMARDs.

Biologic DMARDs are genetically engineered molecules, including antibodies and nucleic acids (deoxyribonucleic acid [DNA] or small interfering ribonucleic acid [siRNA]), able to control inflammatory and autoimmune responses and further modulate disease progression, leading to a more effective prevention of joint disability [16]. The biologic agents' mechanism of action enables the inhibition of the activity of specific inflammatory mediators, like cytokines and chemokines, or their receptors and block the interaction of immune cells with VECs, thereby reducing the migration of immune cells into the synovium [16]. Therapies using biologic agents for the treatment of RA are being developed continuously, including tumor necrosis factor-α (TNF-α) antagonists (such as etanercept, infliximab, and adalimumab), interleukin (IL)-1 receptor antagonist (IL-1RA) anakinra, and IL-6RA tocilizumab [3]. However, despite the promising progress in enhancing RA treatment, the widespread distribution of these biologic molecules in off-target tissues results in severe systemic side effects, requiring repeated and expensive long-term treatment to achieve therapeutic efficiency, which often leads to patient noncompliance [3, 16]. Additionally, treatment-related immune system depressions enhance the possibility of

occurrence and re-emergence of viral and bacterial infections (e.g., tuberculosis), as well as increased risk of multiple sclerosis and congestive heart failure [3, 16].

Owing to the above-mentioned limitations, the ideal therapy for RA remains a challenge. Despite current available therapies being highly effective in the inhibition of the inflammatory and immune responses of RA, there are important issues that should be regarded about their therapeutic efficacy and safety, especially upon long-term administration.

13.3 Target What?

Although the exact origin of RA onset remains unknown, it is believed that arthritic inflammation is triggered by an autoimmune system response attacking the joint's synovium [1]. The synovial membrane of an arthritic joint becomes thicker, and the synovium undergoes a sustained inflammatory reaction, ultimately resulting in cartilage tissue damage. The innate immune system response is tangled in synovial pathophysiology, which mainly involves the recruitment of inflammatory cells to the synovium and intracellular signaling pathways for cellular activation and hence enduring inflammation [17].

Inflammatory diseases are commonly characterized by the enhanced permeability of the vasculature tissue, allowing the migration of immune cells, especially T and B cells, to the inflamed tissue [17]. Conversely, B cells mediate the immunologic process by promoting synovial vascularization and angiogenesis [18–20]. T cells are responsible for initiating the disease progression, followed by inflammation [21]. In early synovitis, the inflammatory response is mediated by synovial cells with the production of inflammatory mediators like cytokines and chemokines, which leads to the early recruitment of inflammatory cells to the synovium [17–19]. The synovial inflammation endures through activation of inflammatory cells. In turn, the process of joint destruction is mediated by the activation of intracellular signaling pathways, involving transcription factors, cytokines, chemokines, growth factors, cellular ligands, and adhesion molecules [17]. In the synovium, activated macrophages play a crucial role in perpetuating chronic inflammatory reaction

through overproduction of pro-inflammatory cytokines and chemokines, such as TNF-α, IL-1β, and IL-6, which stimulate the proliferation of synovial fibroblasts, also known as synoviocytes [17–19].

Both TNF-α and IL-1β induce activated synoviocytes differentiation and proliferation of osteoclasts, leading to synovial pannus formation [17]. Additionally, IL-6 acts with IL-1β, stimulating synoviocytes to produce tissue degrading matrix metalloproteases (MMPs), which are responsible for cartilage tissue destruction and further bone erosion [18, 19, 22]. Remarkably, synovial fibroblasts are considered to be responsible for the progressing inflammation from one arthritic joint to other unaffected joints, the role bearing resemblance to that of metastatic tumor cells in cancer [23].

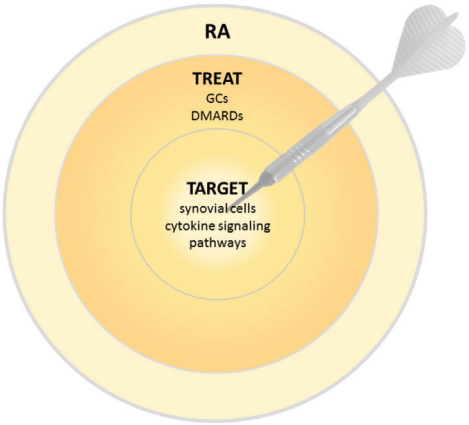

Figure 13.1 Target-to-treat strategies for RA.

Likewise, synoviocytes play a disease-promoting role by the activation of vascular endothelial growth factor (VEGF), inducing synovial vascularization and prominent angiogenesis, comparable to the one that occurs during tumor growth [20, 24]. Cells found within the synovium, mainly macrophages and synoviocytes, are major players in maintaining disease activity mediated by cytokine-dependent pathways. Through cellular interactions between these cells and the innate immune system, plus the production of inflammatory mediators, as well as their involvement in angiogenesis, synovial cells are responsible for the perpetuation of

joint inflammation and ultimately the joint's destruction [17]. In this regard, synovial cells and cytokines (Fig. 13.1) have moved into the spotlight as interesting targets for the specific and selective delivery of therapeutic agents for RA treatment.

13.4 Target-to-Treat Nanostrategies

The main drawback of current therapies is the drug off-target activity that increases the risk of off-target toxic effects. Progress in the field of nanotherapy promises interesting selective strategies, based on nanocarriers that deliver therapeutic agents to disease-affected tissues and cells, promoting in situ drug activity and overcoming potential adverse effects on normal tissues. Nanocarrier selectivity can be achieved through a process known as targeting, which basically depends on the properties of the system allowing the delivery of the drug into the site of action [12, 25]. One of the attractive properties of drug delivery systems is their nanometric size, which increases the surface area relatively to the volume, allowing a higher biological interaction and enhanced cell uptake [26]. Moreover, molecules' encapsulation within nanocarriers is useful either to provide protection from physiological degradation or for off-target activation in blood circulation [26]. Therefore, unlike conventional RA therapy, target-to-treat nanostrategies promise to increase stability, specificity, and bioavailability of therapeutic agents in the inflamed tissue and hence enhance their efficiency, while reducing the risk of well-known systemic side effects.

Nanocarriers are useful for increasing the stability of the drug during the long circulation time in blood and resistance to degradation until they reach the disease-affected tissues. In fact, intravenous NP administration often results in rapid plasma protein recognition and hence clearance by cells of the reticuloendothelial system (RES), mainly the cells of the liver and spleen [12, 25, 27]. To avoid NP clearance by RES cells and hence increase their half-life in blood circulation, the nanocarriers should be sterically stable in physiologic fluids [25]. Polymer conjugation is an efficient and well-known approach to modifying the pharmacokinetic properties of NPs. The most successful polymer conjugation is with PEG chains,

or PEGylation [28]. NP PEGylation increases the hydrophilicity, as it generates a protective layer over the surface [25, 28]. Thus, the presence of highly hydrated PEG chains results in repulsive interactions with plasma proteins and cellular biological components and, consequently, provides serum stability [29]. Additionally, conjugated PEG chains confer to the NPs the ability of passive tissue targeting, as a result of leaky vasculature and inadequate lymphatic drainage, an effect known as enhanced permeation and retention (EPR) [25, 30]. Whereas lymphatic drainage in inflamed synovial tissues appears to be still functioning, the emphasis is the prominent angiogenesis, similar to that in tumor tissues [21, 25, 30]. Indeed, synovial tissue is characterized by significantly increased vascular permeability, which allows PEGylated NPs to passively accumulate within the inflamed disease-tissue by the EPR effect, in an attempt to further enhance their cellular binding and uptake [21, 25].

The potential of PEGylated nanocarriers, including liposomes, micelles, and polymeric NPs, to passively target the site of inflammation and deliver drugs into it has been reported in several in vitro and in vivo studies (Table 13.1). For example, GC-loaded PEGylated liposomes were described by several authors to exhibit an enhanced passive accumulation within the synovium of arthritic joints compared to healthy joints upon intravenous administration [31–41]. Despite GCs playing a prominent role in the therapeutic management of RA, the occurrence of significant severe effects is a serious limitation with respect to the clinical application of GCs. In this way, Anderson and coworkers investigated the efficacy of intravenous injection of dexamethasone phosphate (DXP) PEGylated liposomes in comparison to the free drug in rats with established adjuvant-induced arthritis (AIA) [38]. Results show that inflammation in the AIA model was reduced, plus histological signs and expression of IL-1β and IL-6 by peritoneal macrophages were verified [38]. In fact, the suppression was long-lasting, as DXP-loaded PEG-conjugated liposomes considerably reduced the dose dependence by a factor of 3–10 compared to the injected free DXP [38]. Thereby, the therapeutic efficiency of DXP-loaded PEGylated liposomes was enhanced, limiting the unwanted toxicity of GC therapy in RA [38]. Similarly, Ishihara and colleagues obtained the same prolonged anti-inflammatory

Table 13.1 PEGylated target-to-treat nanocarriers for RA

Nanocarrier	Therapeutic agent	Preclinical tests	Ref.
Liposomes	PLP	In vitro	[31]
		fibroblast and macrophages	[32]
		cell lines	[33]
		In vivo	[34]
		AbIA murine model	[35]
Liposomes	DXP	In vivo	[36]
		CIA mouse model	[37]
		AIA rat model	[38]
Liposomes	BSP	In vivo	[39]
		AA mouse model	
Liposomes	MPS	In vivo	[40]
	BMS	AIA and AA rat models	[41]
Micelles	DXP	In vivo	[42]
		AbIA mouse model	
Polymeric	BSP	In vivo	[43]
nanoparticles		AA rat model	[44]
		AbIA mouse model	
Liposomes	MTX	In vivo	[45]
		AA rat model	
Metallic	Gold	In vivo	[46]
nanoparticles		CIA rat model	

AA, adjuvant arthritis; AbIA, antibody-induced arthritis; AIA, adjuvant-induced arthritis; BMS, betamethasone hemisuccinate; BSP, betamethasone sodium phosphate; CIA, collagen-induced arthritis; DXP, dexamethasone phosphate; MPS, methylprednisolone hemisuccinate; MTX, methotrexate; PLP, prednisolone phosphate.

effect with NPs of PLGA and poly(lactic acid) (PLA) conjugated with PEG for betamethasone sodium phosphate (BSP) delivery within the synovium [43, 44]. These polymeric NPs were then intravenously administered to rats with adjuvant arthritis (AA) and mice with anti-type II collagen antibody-induced arthritis (AbIA). In AA rats, a single injection of BSP-loaded PEGylated NPs resulted in 35% joint inflammation reduction within 1 day, which was maintained for 9 days [43]. On the other hand, in AbIA mice, a single injection resulted in complete remission of the inflammatory response after

1 week [43]. Moreover, the same authors have observed that due to PEG by the EPR effect BSP-loaded PEGylated NPs preferentially accumulated in the inflammatory lesion in AIA mice models [44]. Then, the loss of PEG and subsequent uptake by inflammatory macrophages allow intracellular drug release [44]. In another study, Hofkens and coworkers investigated the effect on the inhibition of protease expression after intravenous injection of prednisolone phosphate (PLP)-loaded liposomes in the AbIA murine model [33]. In vivo results revealed that a single injection promotes a noticeable suppression of synovial immune cell accumulation compared to the control [33]. Further in vitro experiments showed that there was efficient uptake of PLP-loaded PEGylated liposomes by macrophages and, consequently, an inhibition of the expression of IL-1β and MMPs in the synovium was observed after induced inflammation [33]. Thus, PEG-conjugated liposomes encapsulated with PLP could target the synovium, to internalize within macrophages and inhibit destruction of the cartilage matrix in AbIA model [33]. PEGylated nanocarriers increased drug therapeutic effect in arthritis models, possibly due to prolonged blood circulation, thus preventing interactions with RES cells. Moreover, the passive targeting of the inflamed synovial tissues increases the drug´s bioavailability in situ.

13.4.1 Synovial Cell Targeting

Over the years, targeting strategies (Fig. 13.2) have been explored to maximize a nanocarrier's selectivity to further allow specific NP-cell binding and uptake [12, 27]. In this context, the targeting potential is based on the unique pathophysiological features of RA, namely the accumulation of inflammatory cells within the synovium, the production of inflammatory mediators, and angiogenesis.

Targeting strategies take advantage of the roles of the cells found within the synovium. In contrast to other inflammatory diseases, arthritic inflammation involves the collaboration of numerous different cells, including mesenchymal cells (such as synovial fibroblast), macrophages, endothelial cells, dendritic cells, and other cells of the immune system [17, 19]. Thus, in addition to signaling pathophysiologic pathways, the cellular interactions in the synovium

are also the key to perpetuating cellular proliferation and chronic synovitis [17].

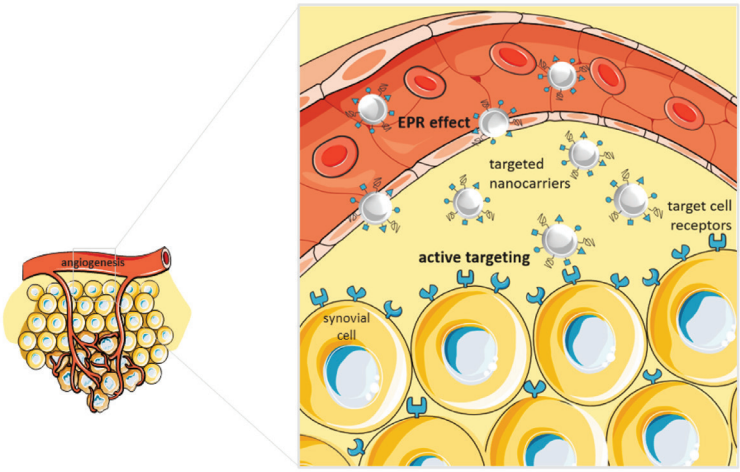

Figure 13.2 Targeting strategies for RA.

The activation of synovial mesenchymal cells, especially synoviocytes, is believed to be crucial in the pathogenesis involved in joint destruction through the synthesis of tissue-degrading molecules. Synoviocytes, which in healthy joints are involved in synovial homeostasis, also contribute directly to synovial chronic inflammation by excreting pro-inflammatory cytokines and chemokines for the signaling and proliferation of other mesenchymal and immune cells [17].

For example, T cell proliferation is enhanced by synovial fibroblasts through the release of IL-16. In addition, the activation of T cells in the synovium is believed to be strongly B cell dependent [17]. Remarkably, synoviocytes promote B cell survival and differentiation into plasma cells and produce B cell activation factors [17]. Conversely, macrophages that line the synovium play a key role in the inflammatory process, mainly by producing potent pro-inflammatory cytokines and chemokines that perpetuate inflammation [19]. Particularly, IL-1β and TNF-α stimulate synoviocyte activation and hence lead to irreversible joint destruction [19]. Furthermore, the inflamed synovium line is

characterized by an extensive accumulation of T cells, B cells, plasma cells, natural killer cells, and dendritic cells [17]. The interaction between these cells and macrophages results in the production of chemokines and the overexpression of chemokine receptors and other receptors [17, 19].

Therefore, cells found within the synovium are interesting target candidates for successful specific and selective intracellular NP delivery. To this end, active nanostrategies focus on the identification of effector ligands to target specific and selective cellular receptors by the nanocarrier. Depending on the cell of interest, several studies (Tables 13.2, 13.3, and 13.4) have reported the use of an FA, hyaluronic acid (HA), or cyclic Arg-Gly-Asp (RGD) peptide conjugated in nanocarriers for effector ligand-mediated targeting of the synovium.

13.4.1.1 FA targeting

Folic acid (FA) is a water-soluble vitamin that can induce receptor-mediated endocytosis, providing cytosolic drug delivery [47]. Folate receptors (FRs) are cysteine-rich cell surface glycoproteins that can exist in two isoforms: FRα and FRβ. Usually, FRα is addressed as a target for therapy and imaging in oncology, whereas FRβ has been reported in some studies as the cell effector receptor in inflammatory diseases. [48] This has unlocked the possibility to explore the potential of FA to target therapeutic agents to treat inflammatory RA. The feasibility of FRβ to mediate the active targeting delivery of nanocarriers is based on its specific overexpression on activated macrophages found in the synovial fluid, unlike the slight expression of this receptor on quiescent resident macrophages and other blood cells [49–52]. Activated macrophages are the key cells in RA pathogenesis that secrete multiple pro-inflammatory mediators with a central role in intracellular cytokine-mediated pathways involved in synovial inflammation and tissue-matrix degeneration [17].

Recent in vitro studies (Table 13.2) reported FRβ's potential to mediate specific delivery to activated macrophages in the synovial tissue of RA patients [47, 49, 51–54]. Likewise, in vivo studies on animal models of arthritis have shown that FA nanocarriers can selectively deliver therapeutic agents to joints' synovial tissues, showing reduced collateral toxicity comparing to normal tissues

[47, 51, 52, 55, 56]. Thomas and coworkers investigated the anti-inflammatory potential of FA-conjugated polyamidoamine (PAMAM) dendrimers to target macrophages and deliver loaded MTX in a collagen-induced arthritis (CIA) rat model [47]. The in vitro results showed that FA conjugation significantly increased PAMAM dendrimers' uptake rate via FR-mediated endocytosis expressed in activated synovial macrophages [47]. Moreover, in vivo studies revealed that FA-PAMAM dendrimers loaded with MTX increased the therapeutic anti-inflammatory index over free MTX. As arthritis-induced parameters of inflammation were reduced, an enhancement of the maximum tolerated dose in the used arthritic model was also observed [47]. Thus, the use of FA-targeted dendrimers to specifically delivery MTX into macrophages within the synovium can provide an efficient active targeting approach for RA treatment [47].

Table 13.2 FA nanocarriers targeting synovial cells

Nanocarrier	Therapeutic agent	Preclinical tests	Ref.
Dendrimers	MTX	In vitro macrophage cell line In vivo CIA rat model	[47]
Dendrimers	IND	In vivo AIA rat model	[57] [58]
Polymeric nanoparticles	IL-1 receptor antagonist gene	In vivo AIA rat model	[56] [55]
Lipid nanoparticles	NF-κB	In vitro macrophage cell line	[59]

AIA, adjuvant-induced arthritis; CIA, collagen-induced arthritis; FA, folic acid; IL, interleukin; IND, indomethacin; MTX, methotrexate; NF-κB, nuclear factor kappa B.

FA has been also used to achieve active targeting of macrophages in gene therapy. Fernandes and, later, Shi designed FA-conjugated chitosan NPs to deliver IL-1RA gene encoding plasmid DNA [55, 56]. The formulation administered intravenously in AIA rats showed to inhibit paw inflammation. Indeed, an improved transfection efficiency of FA-chitosan NPs loading IL-1RA resulted in a significant downregulation of TNF-α and IL-1β [55]. Further in vitro analysis of macrophages isolated from mouse arthritic joints suggested that IL-1RA plasmid DNA was efficiently and specifically delivered

through FR-mediated targeting of macrophages [56]. In another study, Hattori and colleagues investigated the intracellular delivery of a nuclear factor kappa B (NF-κB) decoy using FA-conjugated lipid-based NPs into macrophages [59]. NF-κB is a key regulator of gene transcription highly active in the synovial membrane. NF-κB-dependent signaling pathway in activated macrophages directly induce osteoclast for cartilage and bone destruction [17]. In vitro experiments suggested that FA-lipid NPs effectively delivered the NF-κB decoy into the macrophage's cytoplasm, resulting in an inhibitory effect on the translocation of NF-κB into the nucleus, providing protection against bone resorption by osteoclasts [59].

13.4.1.2 HA targeting

HA is a glycosaminoglycan responsible for cellular growth and tissue integrity maintenance, thus being an essential component of the extracellular matrix [60, 61]. HA has the potential to selectively bind to CD44 antigen spliced variant isoforms CD44v4 and v6, which are known to be involved in cell migration and in the regulation of inflammation through lymphocyte activation [60, 62, 63]. Several in vitro and in vivo studies have shown that inflamed synovial tissue contains high expression levels of the CD44 receptor on both synoviocytes and macrophages compared to healthy normal tissue [25, 61–65]. Therefore, CD44's importance in the chemotaxis phenomenon, as well as in mediating the specific binding of HA during inflammation, makes it a suitable candidate for the nanocarrier's specific delivery within the inflamed synovium.

Several studies (Table 13.3) have investigated the potential of HA for active targeting of synovial cells plus for the safe delivery of therapeutic agents in arthritis animal models. Shin and colleagues investigated the therapeutic effect of MTX-loaded HA-conjugated NPs in CIA mouse models [66]. In vivo studies showed that HA NPs preferentially accumulated in the inflamed joints and were substantially more potent than the free drug in controlling the clinical score of joint swelling [66]. These results suggest that the enhanced therapeutic efficiency of MTX might owe to the conjugate's ability to enable the release of MTX under acidic conditions found in both extracellular inflamed synovium and intracellular compartments of macrophages [66]. Further in vitro experiments revealed an efficient significant uptake of conjugated HA-MTX by the

activated macrophage cell line [66]. Similarly, Kamat and coworkers developed iron oxide–based magnetic NPs conjugated to HA to study their specific recognition by the CD44 receptor present on activated macrophages [67]. In vitro cell uptake studies also demonstrated significant uptake of HA NPs by an activated macrophage cell line [67]. Moreover, fluorescein contained on the NPs was found to be delivered to the cell nucleus [67]. This means that HA-conjugated nanocarriers are suitable for both molecular imaging and drug delivery and targeting of inflamed disease-tissue. In another study, not only is HA used as a targeting strategy, but Mero et al. and Ryan et al. have been using the polymeric properties of HA to develop NPs able to accumulate within the synovium and reduce the EPR-driven leakage from the synovial joint upon intra-articular injection. In vivo studies by Mero and colleagues revealed that salmon calcitonin (sCT)-conjugated HA NPs avoided EPR-driven leakage, and hence systemic off-target effects, known to occur upon intra-articular injection of sCT formulation in a CIA mouse model [68]. Conversely, Ryan and coworkers' investigation showed that sCT conjugation with HA NPs strongly inhibited the production of pro-inflammatory cytokine and matrix-degrading enzymes, such as MMPs [69]. Indeed, the NF-κB mouse model of arthritis and the rabbit model of early osteoarthritis used in the studies presented reduced signs of inflammation after treatment [69].

Synovial vascularization and prominent angiogenesis are crucial for enduring synovitis and progressive joint destruction [20]. Likewise, the VEGF and its receptor found in the synovium are essential elements for neovascularization [20]. In this regard, in addition to HA's synovial-targeting ability, Lee and coworkers developed a HA-conjugated tocilizumab (TCZ) gold NP, used simultaneously for a targeting and biologic therapeutic approach. TCZ is a monoclonal therapeutic IL-6 antibody against IL-6 signaling by binding to the interleukin-6 receptor (IL-6R) [73]. IL-6 present in the synovium actively contributes to the RA pathogenesis by stimulating synoviocyte cell proliferation and osteoclast activation, plus the production of MMPs, hence promoting cartilage destruction. Additionally, this pro-inflammatory cytokine influences the VEGF expression for the vascularization of inflamed synovial tissue. Therefore, IL-6 is an interesting cytokine target used for RA treatment [17]. Remarkably, the HA-gold NP TCZ complex

administered intravenously in a CIA mouse model, aside from being able to target synovial tissues and accumulate within the synovium, also reveals TCZ ability to target angiogenic blood vessels [72, 73]. The observed reduction of VEGF and IL-6 expression in the synovium suggests that treatment with the HA-gold NP TCZ complex had an anti-inflammatory and antiangiogenic effect in arthritic mouse models [72].

Table 13.3 HA nanocarriers targeting synovial cells

Nanocarrier	Therapeutic agent	Preclinical tests	Ref.
Polymeric nanoparticles	MTX	In vitro macrophage cell line In vivo CIA mouse model	[66]
Polymeric nanoparticles	γ-secretase	In vivo CIA mouse model	[70]
Polymeric nanoparticles	sCT	In vivo arthritis rabbit and NF-κB mouse models	[68] [69]
PEG-polymeric nanoparticles	TRAIL	In vivo CIA mouse model	[71]
Metallic nanoparticles	TCZ gold	In vivo CIA mouse model	[72]
Magnetic nanoparticles	Fluorescent imaging molecule	In vitro macrophage cell line	[67]
Polymeric nanoparticles	Photosensitizers	In vitro macrophage cell line	[62]

CIA, collagen-induced arthritis; HA, hyaluronic acid; MTX, methotrexate; NF-κB, nuclear factor kappa B; PEG, polyethylene glycol; sCT, salmon calcitonin; TCZ, tocilizumab; TRAIL, TNF-related apoptosis-inducing ligand.

An alternative therapeutic targeting and biologic approach was also investigated by Kim and colleagues [71]. Instead of IL-6, in this study proapoptotic members of the TNF family, such as tumor necrosis factor–related apoptosis-inducing ligand (TRAIL), were efficiently delivered in CIA mouse models using the HA targeting strategy. In fact, in vivo experiments suggested that HA conjugation to PEGylated NP loading TRAIL resulted in prolonged and sustained

delivery of TRAIL with increased therapeutic effect over the unconjugated PEG-TRAIL formulation [71].

13.4.1.3 RGD targeting

Synovial vascularization represents a potential therapeutic target area, possibly by being the first barrier that blood leukocytes face before their migration into the target synovial tissue [20]. In fact, the interaction between cell adhesion molecules expressed on the endothelial cells and migrating blood leukocytes may direct specific leukocyte subsets to the target tissue [20]. In this regard, some studies (Table 13.4) have been reporting cell adhesion receptors, such as integrins, expressed on endothelial cells as therapeutic targets for RA. Particularly, the RGD peptide displays high affinity to the αvβ3 integrin, which is overexpressed in VECs and macrophages in inflamed disease-tissues [74].

Table 13.4 RGD nanocarriers targeting synovial cells

Nanocarrier	Therapeutic agent	Preclinical tests	Ref.
PEG-liposomes	DXP	In vivo AIA rat model	[75]
PEG-liposomes	PLP core peptide	In vivo AIA rat model	[76]
Polymeric nanoparticles	MTX gold	In vivo CIA mouse model	[77]

AIA, adjuvant-induced arthritis; CIA, collagen-induced arthritis; DXP, dexamethasone phosphate; MTX, methotrexate; PEG, polyethylene glycol; PLP, prednisolone phosphate; RGD, Arg-Gly-Asp.

Koning and coworkers investigated the therapeutic efficacy of DXP-loaded RGD conjugated to PEGylated liposomes using an AIA rat model [75]. The in vivo results revealed that RGD-PEG liposomes' retention time at the inflammation site was greater compared with PEGylated ones. Besides, in vitro studies showed that RGD enhances the uptake in proliferating human VECs [75], thereby suggesting that the specific RGD targeting is more effective than the EPR effect in terms of targeting inflamed disease-tissue in early stages of arthritis [75]. Moreover, in vivo studies showed that a single intravenous injection of DXP-loaded RGD-PEG liposomes prolonged the anti-

inflammatory effect in arthritic joints, thus limiting off-target tissue toxicity [75]. Similarly, Vanniasinghe and colleagues developed RGD-PEG liposomes to deliver either PLP or an immunosuppressive core peptide within the synovium [76]. In this study, liposome formulations were tested in vitro regarding their ability to specifically internalize on both synovial fibroblast and endothelial cells [76]. Additionally, in vivo studies were performed using a rat model of AIA, revealing that the accumulation of RGD-PEG liposomes increased 7- to 10-fold in inflamed joints compared to unaffected joints [76]. Thereby, the specific delivery of loaded therapeutic agents to inflamed joints led to efficient and prolonged anti-inflammatory efficacy [76].

Lately, a strategy has been developed to improve the ability to mediate intracellular controlled delivery of nanocarriers, along with triggering the release of loaded therapeutic agents, by hyperthermia. To this end, Lee and coworkers developed MTX-loaded PLGA NPs coated with gold half-shell and conjugated to the RGD peptide [77]. In vivo results using CIA mice showed that RGD allowed tissue-specific accumulation of NPs and cell targeting through αVβ3 integrin [77]. Then, upon application of local near-infrared photothermic stimulation on arthritic joints, whereas heat was locally generated due to gold half-shells, a MTX intracellular release increase was observed [77]. Hence, prolonged therapeutic efficacy was observed when compared with that of the free drug, which simultaneously minimizes MTX-dose-related side effects in the treatment of RA [77]. Similarly, in another study, MTX-loaded PLGA NPs containing gold NPs were investigated for near-infrared photothermic application [78]. In vitro experiments suggested that the incorporation of gold NPs resulted in a temperature-dependent and sustained drug release profile [78]. Further results revealed that the successful uptake of MTX-loaded PLGA/gold NPs by macrophages led to a significant reduction of pro-inflammatory cytokine expression after induced inflammation [78], suggesting a hyperthermia therapy as a promising strategy to improve the drug´s anti-inflammatory efficiency [78]. Remarkably, gold has been also described to exhibit therapeutic potential in RA treatment. Indeed, Tsai and coworkers used gold NPs to target VEGF in human RA synovial fluid, showing that these NPs inhibit VEC proliferation and migration [46]. Additionally, in vivo studies in CIA mice revealed that intra-articular injection of gold NPs suppresses synovial cells'

inflammatory response, presenting reduced clinical, radiographic, and histologic arthritic features [46].

13.4.2 Cytokine Targeting

The imbalance of pro-inflammatory cytokines and anti-inflammatory cytokines plays a key role in the pathogenesis of RA. In the inflamed synovium, pro-inflammatory cytokines, such as TNF-α, IL-1, IL-6, IL-12, and chemokines, are elevated, whereas the levels of anti-inflammatory cytokines, such as IL-10 and IL-4, are reduced [17]. Aside from stimulate inflammatory cells' migration to the inflamed synovium, cytokines are also responsible for perpetuating both autoimmune and inflammatory responses [3]. Moreover, cytokine-dependent signaling pathways mediate cellular interactions within the synovium, leading to persistent disease activity and hence irreversible joint destruction [17].

Table 13.5 Target-to-treat nanocarriers toward cytokines

Nanocarriers	Therapeutic agent	Preclinical tests	Ref.
Polymeric nanoparticles	Etanercept	In vivo CIA rat model	[79]
Polymeric nanoparticles	TNF-α siRNA	In vivo AbIA mouse model	[80]
Polymeric nanoparticles	TNF-α siRNA	In vivo CIA mouse model	[81] [82]
Liposomes	TNF-α siRNA IL-1/IL-6/IL-18 siRNA	In vivo CIA mouse model	[83] [84]
Liposomes	TNF-α siRNA	In vivo CIA mouse model	[85] [86]
Liposomes	IL-10 plasmid DNA	In vivo CIA mouse model	[87] [88]
Polymeric nanoparticles	IL-2/IL-15Rβ siRNA	In vivo AIA rat model	[89] [90]
Polymeric nanoparticles	TNF-α siRNA	In vitro macrophage cell line	[91]

AbIA, antibody-induced arthritis; AIA, adjuvant-induced arthritis; CIA, collagen-induced arthritis; DNA, deoxyribonucleic acid; IL, interleukin; siRNA, small interfering ribonucleic acid; TNF-α, tumor necrosis factor-α.

The selective downregulation of inflammatory mediators either by preventing their expression or by antagonizing their receptors using antibodies is simultaneously a promising therapeutic approach as well as a targeting approach used in the treatment of RA. Thus, mainly due to their involvement within the pathogenesis of RA, cytokines have been used as targets for monoclonal antibody therapy in RA. Formulations of monoclonal antibodies effectively inhibit inflammation and synovial tissue damage. Still after systemic administration many patients continue to experience severe off-target side effects and less symptomatic relief [21]. Furthermore, cytokines can be targeted therapeutically by gene transfer and gene-silencing approaches. Gene therapy is based on the delivery of nucleic acids within the cell either for overexpression or for silencing of a target cytokine [92]. More recently, nanotechnology has been combined with gene therapy, offering an enhanced strategy for targeting and treating RA after it can potentially lead to a safer, more selective, and more efficient delivery of therapeutic gene at the inflamed disease-tissue, hence avoiding adverse off-target systemic toxicity.

In the last decade, several studies (Table 13.5) have been developed for treating synovial inflammation by silencing the expression of target pro-inflammatory cytokines with targeted gene delivery systems. Regarding gene delivery in vivo, cationic nanocarriers represent a safe and selective strategy once positively charged moieties enable electrostatic complexation with negatively charged nucleic acids, intracellularly promoting the nanocarriers' ability to mediate endosomal escape and improve cytosolic delivery. Cationic nanocarriers can be developed using cationic polymers, such as poly(ethylene imine) (PEI), poly-L-lysine, and chitosan, or cationic lipids, such as dioleoylphosphatidylethanolamine (DOPE) and dioleoyltrimethylammoniumpropane (DOTAP).

Pro-inflammatory cytokines, such as TNF-α, IL-1β, and IL-6, have a crucial role in inflammation. It is well known that TNF-α is mainly produced by macrophages that line the synovium [17]. TNF-α upregulates the production of IL-1β in loop response, hence enduring chronic inflammation. As both cytokines induce the expression of cell adhesion molecules on endothelial cells, they promote inflammatory and immune cells' migration into the synovium. In addition, these cytokines stimulate the production of chemokines important for

intracellular signaling events. At the same time, they increase synoviocytes' and chondrocytes' destructive potential by inducing the production of MMPs and other matrix-degrading enzymes responsible for cartilage erosion [17]. Among all pro-inflammatory cytokines, TNF-α siRNA–loaded nanotherapeutic approaches have been successful in the inhibition of TNF-α pro-inflammatory activity in animal models of arthritis. Komano and coworkers investigated the therapeutic potential of cationic liposomes loading TNF-α siRNA in a CIA mouse model [85]. Mice were intravenously injected with Cy5-labeled TNF-α siRNA–loaded liposomes, wherefore the Cy5 fluorescence was used to assess the tissue distribution. Results showed that the Cy5 intensity of fluorescence was higher in arthritic inflamed joints than in off-target tissues. In fact, the fluorescence remained higher up to 48 h after treatment. Further experiments suggested that Cy5 fluorescence intensity was higher in synovial macrophages cells than in splenocytes, bone marrow cells, and blood leukocytes. Thus, treatment with TNF-α siRNA–loaded liposomes resulted in significant decrease in arthritis severity, allowing an efficient and targeted gene delivery to the inflamed synovium [85]. Similarly, Khoury and colleagues developed DOPE cationic liposome for systemic delivery of TNF-α siRNA in a CIA mouse model [83]. Results revealed that blocking TNF-α receptors effectively decreases local and systemic inflammation, as well as prevents cartilage damage in arthritic mice [83]. The same authors, in another study, investigated gene silencing via siRNA of other well-known pro-inflammatory cytokines (IL-1β, IL-6, and IL-18) instead of TNF-α [84]. Treatment in established arthritic mice revealed that a combination of the three cytokine-specific siRNAs reduced all arthritic pathological features [83]. In fact, compared to TNF-α siRNA treatment, IL-1β/IL-6/IL-18 siRNA–loaded liposomes improved overall anti-inflammatory efficiency, preventing cartilage and bone destruction [83]. Thus, multi-IL-specific siRNA can be a promising biologic nanostrategy for improving RA treatment, possibly shifting the supremacy of anti-TNF agents for standard care in patients not responding to synthetic DMARDs.

Apart from liposomes for gene delivery, te Boekhorst and colleagues developed PLGA/DOTAP NPs for intra-articular injection of loaded TNF-α siRNA [80]. The intra-articular injection of TNF-α

siRNA–loaded NPs in the AbIA mouse model resulted in a significant reduction in the paw swelling and joint inflammation [80].

Synoviocytes have been reported to play a central role in the chronic nature of RA, being key cells to target as they participate in inflammatory events of joint damage through the production of many pro-inflammatory cytokines and MMPs [17]. Particularly, IL-15 has been shown to have a role in these events, as it induces the production of other cytokines, such as TNF-α and IL-17, by T cells through a cell contact–dependent mechanism [17]. In turn, T cells induce the expression of IL-15 and IL-6 by synoviocytes, creating a feedback loop that favors persistent synovial inflammation [17]. In this regard, PEI-nucleic acid complexes have been developed by Zhang et al. and Duan et al. to deliver siRNA targeting the IL-2 and IL-15 receptor β (IL-2/15Rβ) on synovial fibroblasts for RA therapy [89, 90]. In both studies, following intravenous administration in rats with AIA, IL-2/15Rβ siRNA–loaded PEI nanocomplexes effectively accumulated in arthritic paws and subsequently were internalized by inflamed synovial cells [89, 90]. Thereby, results revealed that PEI-mediated siRNA delivery has the potential to treat RA, as anti-IL-2/15Rβ siRNA treatment decreases disease progression in arthritic mice [89, 90].

In another study, Xiao and colleagues developed mannosylated PEI NPs loaded with anti-TNF-α siRNA to specifically target the mannose receptor overexpressed on macrophages found within the synovium line [91]. Both in vitro and ex vivo studies showed that mannosylated NPs were efficiently internalized by macrophages, hence mediating the local delivery of TNF-α siRNA [91]. More results showed an increased silencing of TNF-α expression, which improved the anti-inflammatory efficiency of RA treatment [91].

Chitosan-based nanocarriers have also been used for gene delivery and target synovial cells. Howard and coworkers formulated chitosan NPs encapsulating TNF-α siRNA, aiming to target resident peritoneal macrophages upon intraperitoneal administration in CIA mouse models [81]. In vivo results showed effective anti-inflammatory responses that involved the formulation silencing the TNF-α gene on macrophages [81]. With a similar intent, Lee and colleagues used thiolated glycol chitosan NPs, showing enhanced accumulation at the arthritic joint of CIA mouse model and also efficient in vitro TNF-α gene silencing [82].

The effectiveness of downregulation of pro-inflammatory cytokines in reducing inflammatory activity has been proven. Nonetheless, an alternative biologic strategy to pro-inflammatory-cytokine-targeting gene-silencing approach is the gene transfer of anti-inflammatory cytokines, such as IL-10. Despite IL-10's potent anti-inflammatory activity, its clinical use is hampered by serious cytokine-related side effects [87]. To overcome this problem, cationic liposomes were developed by Fellowes and colleagues for plasmid DNA coding of IL-10 gene delivery [87]. In vivo experiments revealed that a single intraperitoneal injection of cationic liposomes containing human IL-10 plasmid DNA in CIA mice resulted in significant anti-inflammatory efficacy [87]. In fact, the anti-inflammatory activity in arthritic joints was prolonged by up to 30 days after injection. Further experiments showed that high accumulation and overexpression of IL-10 plasmid DNA in synovial inflamed joints allowed efficient gene transfer by synovial macrophages [87].

Indeed, a growing number of nanocarriers have been developed either for selective downregulation of pro-inflammatory cytokines or for overexpression of anti-inflammatory cytokines, amending the course of RA biologic treatment and improving its cost-effectiveness.

13.5 Final Remarks

RA is a serious health problem, the actual treatment of which has high rates of patient noncompliance, as available treatment options either are associated with risk of infection and potentially deleterious side effects or entail high medical costs.

Owing to these limitations, the ideal therapy for RA remains a challenge. In the past decade, nanotherapy has emerged as an enhanced clinical approach for the treatment of RA. Innovative target-to-treat nanostrategies focused on the inflamed disease-tissue have proven to be safe and efficient in the long term. Unlike conventional pharmacologic therapy, target-to-treat nanotherapies embody the concept of a magic bullet, conceived by Paul Ehrlich, enabling antirheumatic therapeutic agents to be selectively delivered to their designated synovial targets, enhancing tissue specificity and hence their therapeutic efficacy, while diminishing off-target toxicities that compromise the effectiveness of RA treatment.

The uncovering of novel cellular and molecular synovial targets opens the gate for a new era of therapeutic intervention with tailored target-to-treat nanotherapies. The therapeutic potential of these targets lies in RA pathogenesis amending nanocarriers' synovial tissue-targeting ability. To this end, exploiting the leaky vasculature of inflamed tissues and synovial-targeting strategies might then lead to treatments with improved clinically relevant therapeutic potency and pharmacologic safety profiles.

Acknowledgments

The authors thank the European Union (FEDER funds POCI/01/0145/FEDER/007728) and National Funds (Fundação para a Ciência e a Tecnologia and Ministério da Educação e Ciência [FCT/MEC]) under the partnership agreement PT2020 UID/MULTI/04378/2013 for the financial support received. Virgínia Moura Gouveia and Cláudia Nunes also thank FCT for the PhD grant (PD/BD/128388/2017) and the investigator grant (IF/00293/2015), respectively.

References

1. Gouveia, V.M., et al. Non-biologic nanodelivery therapies for rheumatoid arthritis. *J Biomed Nanotechnol*, 2015, **11**(10):1701–1721.
2. Lundkvist, J., et al. The burden of rheumatoid arthritis and access to treatment: health burden and costs. *Eur J Health Econ*, 2008, **8**:S49–S60.
3. Quan, L.D., et al. The development of novel therapies for rheumatoid arthritis. *Expert Opin Ther Pat*, 2008, **18**(7):723–738.
4. Kvien, T.K. Epidemiology and burden of illness of rheumatoid arthritis. *Pharmacoeconomics*, 2004, **22**(2 Suppl 1):1–12.
5. Van Vollenhoven, R.F. Treatment of rheumatoid arthritis: state of the art 2009. *Nat Rev Rheumatol*, 2009, **5**:531–541.
6. Smolen, J.S., et al. EULAR recommendations for the management of rheumatoid arthritis with synthetic and biological disease-modifying antirheumatic drugs: 2013 update. *Ann Rheum Dis*, 2014, **73**(3):492–509.
7. Singh, J.A., et al. 2015 American College of Rheumatology guideline for the treatment of rheumatoid arthritis. *Arthritis Rheumatol*, 2016, **68**(1):1–26.

8. Firestein, G.S. Evolving concepts of rheumatoid arthritis. *Nature*, 2003, **423**:356–361.
9. Upchurch, K.S., et al. Evolution of treatment for rheumatoid arthritis. *Rheumatology (Oxford)*, 2012, **51**:vi28–36.
10. Lee, S.J., et al. Pharmacological treatment of established rheumatoid arthritis. *Best Pract Res Clin Rheumatol*, 2003, **17**(5):811–829.
11. Patel, J., et al. Novel drug delivery technologies for the treatment of rheumatoid arthritis. *Internet J Med Technol*, 2009, **5**.
12. Pham, C.T. Nanotherapeutic approaches for the treatment of rheumatoid arthritis. *Wiley Interdiscip Rev Nanomed Nanobiotechnol*, 2011, **3**(6):607–619.
13. Gaffo, A., et al. Treatment of rheumatoid arthritis. *Am J Health Syst Pharm*, 2006, **63**(24):2451–2465.
14. Montesinos, M.C., et al. The anti-inflammatory mechanism of methotrexate depends on extracellular conversion of adenine nucleotides to adenosine by ecto-5'-nucleotidase: findings in a study of ecto-5'-nucleotidase gene-deficient mice. *Arthritis Rheum*, 2007, **56**:1440–1445.
15. Susan Jung-Ah Lee, A.K. Pharmacological treatment of established rheumatoid arthritis. *Best Pract Res Clin Rheumatol*, 2003, **17**(5):811–829.
16. Keyser, F.D. Choice of biologic therapy for patients with rheumatoid arthritis: the infection perspective. *Curr Rheumatol Rev*, 2011, **7**(1):77–87.
17. Muller-Ladner, U., et al. Mechanisms of disease: the molecular and cellular basis of joint destruction in rheumatoid arthritis. *Nat Clin Pract Rheumatol*, 2005, **1**(2):102–110.
18. Karouzakis, E., et al. Molecular and cellular basis of rheumatoid joint destruction. *Immunol Lett*, 2006, **106**(1):8–13.
19. Kinne, R.W., et al. Cells of the synovium in rheumatoid arthritis. Macrophages. *Arthritis Res Ther*, 2007, **9**(6):224.
20. Szekanecz, Z., et al. Angiogenesis and vasculogenesis in rheumatoid arthritis. *Curr Opin Rheumatol*, 2010, **22**(3):299–306.
21. Tran, T.H., et al. Targeted delivery systems for biological therapies of inflammatory diseases. *Expert Opin Drug Deliv*, 2015, **12**(3):393–414.
22. Takayanagi, H., et al. Involvement of receptor activator of nuclear factor kappaB ligand/osteoclast differentiation factor in osteoclastogenesis from synoviocytes in rheumatoid arthritis. *Arthritis Rheum*, 2000, **43**(2):259–269.

23. Lefevre, S., et al. Synovial fibroblasts spread rheumatoid arthritis to unaffected joints. *Nat Med*, 2009, **15**(12):1414–1420.

24. Szekanecz, Z., et al. Angiogenesis and its targeting in rheumatoid arthritis. *Vascul Pharmacol*, 2009, **51**(1):1–7.

25. Bader, R.A. The development of targeted drug delivery systems for rheumatoid arthritis treatment, in *Rheumatoid Arthritis: Treatment*, Lemmey, A.B., ed. InTech, 2012.

26. Gill, S., et al. Nanoparticles: characteristics, mechanisms of action, and toxicity in pulmonary drug delivery: a review. *J Biomed Nanotechnol*, 2007, **3**:107–119.

27. Garg, A., et al. pH-Sensitive PEGylated liposomes functionalized with a fibronectin-mimetic peptide show enhanced intracellular delivery to colon cancer cell. *Curr Pharm Biotechnol*, 2011, **12**(8):1135–1143.

28. Ferrari, M., et al. Trojan horses and guided missiles: targeted therapies in the war on arthritis. *Nat Rev Rheumatol*, 2015, **11**(6):328–337.

29. Vanniasinghe, A.S., et al. The potential of liposomal drug delivery for the treatment of inflammatory arthritis. *Semin Arthritis Rheum*, 2009, **39**(3):182–196.

30. Elbayoumi, T.A., et al. Current trends in liposome research. *Methods Mol Biol*, 2010, **605**:1–27.

31. Hofkens, W., et al. Intravenously delivered glucocorticoid liposomes inhibit osteoclast activity and bone erosion in murine antigen-induced arthritis. *J Controlled Release*, 2011, **152**(3):363–369.

32. Hofkens, W., et al. Liposomal targeting of prednisolone phosphate to synovial lining macrophages during experimental arthritis inhibits M1 activation but does not favor M2 differentiation. *PLoS One*, 2013, **8**(2):e54016.

33. Hofkens, W., et al. Liposomal targeting of glucocorticoids to the inflamed synovium inhibits cartilage matrix destruction during murine antigen-induced arthritis. *Int J Pharm*, 2011, **416**(2):486–492.

34. Hofkens, W., et al. Safety of glucocorticoids can be improved by lower yet still effective dosages of liposomal steroid formulations in murine antigen-induced arthritis: comparison of prednisolone with budesonide. *Int J Pharm*, 2011, **416**(2):493–498.

35. Harigai, T., et al. Prednisolone phosphate-containing TRX-20 liposomes inhibit cytokine and chemokine production in human fibroblast-like synovial cells: a novel approach to rheumatoid arthritis therapy. *J Pharm Pharmacol*, 2007, **59**(1):137–143.

36. Rauchhaus, U., et al. Targeted delivery of liposomal dexamethasone phosphate to the spleen provides a persistent therapeutic effect in rat antigen-induced arthritis. *Ann Rheum Dis*, 2009, **68**(12):1933–1934.
37. Rauchhaus, U., et al. Separating therapeutic efficacy from glucocorticoid side-effects in rodent arthritis using novel, liposomal delivery of dexamethasone phosphate: long-term suppression of arthritis facilitates interval treatment. *Arthritis Res Ther*, 2009, **11**(6):R190.
38. Anderson, R., et al. Liposomal encapsulation enhances and prolongs the anti-inflammatory effects of water-soluble dexamethasone phosphate in experimental adjuvant arthritis. *Arthritis Res Ther*, 2010, **12**(4):R147.
39. van den Hoven, J.M., et al. Optimizing the therapeutic index of liposomal glucocorticoids in experimental arthritis. *Int J Pharm*, 2011, **416**(2):471–477.
40. Avnir, Y., et al. Amphipathic weak acid glucocorticoid prodrugs remote-loaded into sterically stabilized nanoliposomes evaluated in arthritic rats and in a Beagle dog: a novel approach to treating autoimmune arthritis. *Arthritis Rheum*, 2008, **58**(1):119–129.
41. Ulmansky, R., et al. Glucocorticoids in nano-liposomes administered intravenously and subcutaneously to adjuvant arthritis rats are superior to the free drugs in suppressing arthritis and inflammatory cytokines. *J Controlled Release*, 2012, **160**(2):299–305.
42. Crielaard, B.J., et al. Glucocorticoid-loaded core-cross-linked polymeric micelles with tailorable release kinetics for targeted therapy of rheumatoid arthritis. *Angew Chem Int Ed Engl*, 2012, **51**(29):7254–7258.
43. Ishihara, T., et al. Treatment of experimental arthritis with stealth-type polymeric nanoparticles encapsulating betamethasone phosphate. *J Pharmacol Exp Ther*, 2009, **329**(2):412–417.
44. Ishihara, T., et al. Preparation and characterization of a nanoparticulate formulation composed of PEG-PLA and PLA as anti-inflammatory agents. *Int J Pharm*, 2010, **385**(1–2):170–175.
45. Prabhu, P., et al. Investigation of nano lipid vesicles of methotrexate for anti-rheumatoid activity. *Int J Nanomed*, 2012, **7**:177–186.
46. Tsai, C.Y., et al. Amelioration of collagen-induced arthritis in rats by nanogold. *Arthritis Rheum*, 2007, **56**(2):544–554.
47. Thomas, T.P., et al. Folate-targeted nanoparticles show efficacy in the treatment of inflammatory arthritis. *Arthritis Rheum*, 2011, **63**(9):2671–2680.

48. Low, P.S., et al. Discovery and development of folic-acid-based receptor targeting for imaging and therapy of cancer and inflammatory diseases. *Acc Chem Res*, 2008, **41**(1):120–129.
49. van der Heijden, J.W., et al. Folate receptor beta as a potential delivery route for novel folate antagonists to macrophages in the synovial tissue of rheumatoid arthritis patients. *Arthritis Rheum*, 2009, **60**(1):12–21.
50. Xia, W., et al. A functional folate receptor is induced during macrophage activation and can be used to target drugs to activated macrophages. *Blood*, 2009, **113**(2):438–446.
51. Paulos, C.M., et al. Folate receptor-mediated targeting of therapeutic and imaging agents to activated macrophages in rheumatoid arthritis. *Adv Drug Deliv Rev*, 2004, **56**(8):1205–1217.
52. Paulos, C.M., et al. Folate-targeted immunotherapy effectively treats established adjuvant and collagen-induced arthritis. *Arthritis Res Ther*, 2006, **8**(3):R77.
53. Nagayoshi, R., et al. Effectiveness of anti-folate receptor beta antibody conjugated with truncated Pseudomonas exotoxin in the targeting of rheumatoid arthritis synovial macrophages. *Arthritis Rheum*, 2005, **52**(9):2666–2675.
54. Puig-Kroger, A., et al. Folate receptor beta is expressed by tumor-associated macrophages and constitutes a marker for M2 anti-inflammatory/regulatory macrophages. *Cancer Res*, 2009, **69**(24):9395–9403.
55. Shi, Q., et al. Hydrodynamic delivery of chitosan-folate-DNA nanoparticles in rats with adjuvant-induced arthritis. *J Biomed Biotechnol*, 2011, **2011**:148763.
56. Fernandes, J.C., et al. Bone-protective effects of nonviral gene therapy with folate-chitosan DNA nanoparticle containing interleukin-1 receptor antagonist gene in rats with adjuvant-induced arthritis. *Mol Ther*, 2008, **16**(7):1243–1251.
57. Chandrasekar, D., et al. The development of folate-PAMAM dendrimer conjugates for targeted delivery of anti-arthritic drugs and their pharmacokinetics and biodistribution in arthritic rats. *Biomaterials*, 2007, **28**(3):504–512.
58. Chandrasekar, D., et al. Folate coupled poly(ethyleneglycol) conjugates of anionic poly(amidoamine) dendrimer for inflammatory tissue specific drug delivery. *J Biomed Mater Res A*, 2007, **82**(1):92–103.
59. Hattori, Y., et al. Folate-linked lipid-based nanoparticles deliver a NFkappaB decoy into activated murine macrophage-like RAW264.7 cells. *Biol Pharm Bull*, 2006, **29**(7):1516–1520.

60. Sladek, Z., et al. Expression of macrophage CD44 receptor in the course of experimental inflammatory response of bovine mammary gland induced by lipopolysaccharide and muramyl dipeptide. *Res Vet Sci*, 2009, **86**(2):235–240.

61. Naor, D., et al. CD44 in rheumatoid arthritis. *Arthritis Res Ther*, 2003, **5**(3):105–115.

62. Schmitt, F., et al. Chitosan-based nanogels for selective delivery of photosensitizers to macrophages and improved retention in and therapy of articular joints. *J Controlled Release*, 2010, **144**(2):242–250.

63. Vachon, E., et al. CD44 is a phagocytic receptor. *Blood*, 2006, **107**(10):4149–4158.

64. Vachon, E., et al. CD44-mediated phagocytosis induces inside-out activation of complement receptor-3 in murine macrophages. *Blood*, 2007, **110**(13):4492–4502.

65. Golan, I., et al. Expression of extra trinucleotide in CD44 variant of rheumatoid arthritis patients allows generation of disease-specific monoclonal antibody. *J Autoimmun*, 2007, **28**(2–3):99–113.

66. Shin, J.M., et al. A hyaluronic acid-methotrexate conjugate for targeted therapy of rheumatoid arthritis. *Chem Commun (Camb)*, 2014, **50**(57):7632–7635.

67. Kamat, M., et al. Hyaluronic acid immobilized magnetic nanoparticles for active targeting and imaging of macrophages. *Bioconjug Chem*, 2010, **21**(11):2128–2135.

68. Mero, A., et al. A hyaluronic acid-salmon calcitonin conjugate for the local treatment of osteoarthritis: chondro-protective effect in a rabbit model of early OA. *J Controlled Release*, 2014, **187**:30–38.

69. Ryan, S.M., et al. An intra-articular salmon calcitonin-based nanocomplex reduces experimental inflammatory arthritis. *J Controlled Release*, 2013, **167**(2):120–129.

70. Heo, R., et al. Hyaluronan nanoparticles bearing gamma-secretase inhibitor: in vivo therapeutic effects on rheumatoid arthritis. *J Controlled Release*, 2014, **192**:295–300.

71. Kim, Y.J., et al. Ionic complex systems based on hyaluronic acid and PEGylated TNF-related apoptosis-inducing ligand for treatment of rheumatoid arthritis. *Biomaterials*, 2010, **31**(34):9057–9064.

72. Lee, H., et al. Hyaluronate-gold nanoparticle/tocilizumab complex for the treatment of rheumatoid arthritis. *ACS Nano*, 2014, **8**(5):4790–4798.

73. Nishimoto, N., et al. Study of active controlled tocilizumab monotherapy for rheumatoid arthritis patients with an inadequate response to methotrexate (SATORI): significant reduction in disease activity and serum vascular endothelial growth factor by IL-6 receptor inhibition therapy. *Mod Rheumatol*, 2009, **19**(1):12–19.
74. Cox, D., et al. Integrins as therapeutic targets: lessons and opportunities. *Nat Rev Drug Discov*, 2010, **9**(10):804–820.
75. Koning, G.A., et al. Targeting of angiogenic endothelial cells at sites of inflammation by dexamethasone phosphate-containing RGD peptide liposomes inhibits experimental arthritis. *Arthritis Rheum*, 2006, **54**(4):1198–1208.
76. Vanniasinghe, A.S., et al. Targeting fibroblast-like synovial cells at sites of inflammation with peptide targeted liposomes results in inhibition of experimental arthritis. *Clin Immunol*, 2014, **151**(1):43–54.
77. Lee, S.M., et al. Targeted chemo-photothermal treatments of rheumatoid arthritis using gold half-shell multifunctional nanoparticles. *ACS Nano*, 2013, **7**(1):50–57.
78. Costa Lima, S.A., et al. Temperature-responsive polymeric nanospheres containing methotrexate and gold nanoparticles: A multi-drug system for theranostic in rheumatoid arthritis. *Colloids Surf B*, 2015, **133**:378–387.
79. Jung, Y.S., et al. Temperature-modulated noncovalent interaction controllable complex for the long-term delivery of etanercept to treat rheumatoid arthritis. *J Controlled Release*, 2013, **171**(2):143–151.
80. te Boekhorst, B.C., et al. MRI-assessed therapeutic effects of locally administered PLGA nanoparticles loaded with anti-inflammatory siRNA in a murine arthritis model. *J Controlled Release*, 2012, **161**(3):772–780.
81. Howard, K.A., et al. Chitosan/siRNA nanoparticle-mediated TNF-alpha knockdown in peritoneal macrophages for anti-inflammatory treatment in a murine arthritis model. *Mol Ther*, 2009, **17**(1):162–168.
82. Lee, S.J., et al. TNF-alpha gene silencing using polymerized siRNA/thiolated glycol chitosan nanoparticles for rheumatoid arthritis. *Mol Ther*, 2014, **22**(2):397–408.
83. Khoury, M., et al. Efficient new cationic liposome formulation for systemic delivery of small interfering RNA silencing tumor necrosis factor alpha in experimental arthritis. *Arthritis Rheum*, 2006, **54**(6):1867–1877.

84. Khoury, M., et al. Efficient suppression of murine arthritis by combined anticytokine small interfering RNA lipoplexes. *Arthritis Rheum*, 2008, **58**(8):2356–2367.

85. Komano, Y., et al. Arthritic joint-targeting small interfering RNA-encapsulated liposome: implication for treatment strategy for rheumatoid arthritis. *J Pharmacol Exp Ther*, 2012, **340**(1):109–113.

86. Presumey, J., et al. Cationic liposome formulations for RNAi-based validation of therapeutic targets in rheumatoid arthritis. *Curr Opin Mol Ther*, 2010, **12**(3):325–330.

87. Fellowes, R., et al. Amelioration of established collagen induced arthritis by systemic IL-10 gene delivery. *Gene Ther*, 2000, **7**(11):967–977.

88. Kageyama, Y., et al. Plasmid encoding interleukin-4 in the amelioration of murine collagen-induced arthritis. *Arthritis Rheum*, 2004, **50**(3):968–975.

89. Zhang, T., et al. Systemic delivery of small interfering RNA targeting the interleukin-2/15 receptor beta chain prevents disease progression in experimental arthritis. *PLoS One*, 2013, **8**(11):e78619.

90. Duan, J., et al. Polyethyleneimine-functionalized iron oxide nanoparticles for systemic siRNA delivery in experimental arthritis. *Nanomedicine (Lond)*, 2014, **9**(6):789–801.

91. Xiao, B., et al. Mannosylated bioreducible nanoparticle-mediated macrophage-specific TNF-alpha RNA interference for IBD therapy. *Biomaterials*, 2013, **34**(30):7471–7482.

92. Robbins, P.D., et al. Gene therapy for arthritis. *Gene Ther*, 2003, **10**(10):902–911.

Appendix

Jenny Stanford Publishing Pte. Ltd.
Level 34, Centennial Tower
3 Temasek Avenue
Singapore 039190
Tel: +65 6549 7898
Fax: +65 6549 7001
Reg No: 200609521R

21st October 2019

To Whom It May Concern

Letter of Authorisation

We hereby approve the republication of Virgínia Moura Gouveia's chapter as follows for her PhD thesis.

Book: "Nanoparticles in Life Sciences and Biomedicine" (ISBN: 978-981-4745-98-7)
Chapter: Chapter 13: "Innovative target-to-treat nanostrategies for rheumatoid arthritis"

Thesis title: "Target-to-Treat Nanotherapy for Rheumatoid Arthritis"
Doctoral programme: Molecular and Cellular Biotechnology Applied to Health Sciences
Host institution: Abel Salazar Biomedical Sciences Institute and Faculty of Pharmacy, University of Porto
Doctoral candidate: Virginia Adorinda Moura Gouveia
Affiliation: LAQV, REQUIMTE, Department of Chemical Sciences, Faculty of Pharmacy, University of Porto, Portugal
Supervisor: Prof. Doutora Maria de La Salette de Freitas Fernandes Hipólito Reis Dias Rodrigues

Sincerely,

Jenny Rompas
Director and Publisher

Email: jenny@jennystanford.com

Chapter 3

I. Hyaluronic Acid-conjugated pH-sensitive Liposomes for Targeted Delivery of Prednisolone on Rheumatoid Arthritis Therapy

Virgínia M. Gouveia [1], José Lopes-de-Araújo [1], Sofia A. Costa Lima [1], Cláudia Nunes [1] and Salette Reis [1]

[1] LAQV,REQUIMTE, Department of Chemical Sciences, Faculty of Pharmacy, University of Porto, 4050-313 Porto, Portugal

Original research article published in Nanomedicine: Future Medicine (2018)
DOI: 10.2217/nnm-2017-0377

Research Article

For reprint orders, please contact: reprints@futuremedicine.com

Nanomedicine

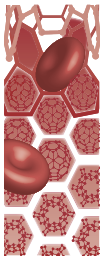

Hyaluronic acid-conjugated pH-sensitive liposomes for targeted delivery of prednisolone on rheumatoid arthritis therapy

Virgínia M Gouveia[1], José Lopes-de-Araújo[1], Sofia A Costa Lima[1], Cláudia Nunes[1] & Salette Reis*,[1]

[1]LAQV, REQUIMTE, Departamento de Ciências Químicas, Faculdade de Farmácia da Universidade do Porto, 4050-313 Porto, Portugal

*Author for correspondence: shreis@ff.up.pt

Aim: The treatment of rheumatoid arthritis remains a challenge as available therapies still entail the risk of deleterious off-target effects. The present study describes hyaluronic acid-conjugated pH-sensitive liposomes as an effective drug delivery-targeting strategy to synovial cells. **Materials & methods:** Therapeutic, cytotoxic and targeting potential of developed liposomes were studied *in vitro* using macrophages and fibroblasts cell lines.**Results & Conclusion:** Results suggest an enhanced cellular uptake of conjugated liposomes, mainly mediated by caveolae- and clathrin-dependent endocytosis. *In vitro* release studies demonstrated that prednisolone was preferentially released under acidic conditions mimicking intracellular endosomal compartments. Overall, results revealed that conjugated pH-sensitive liposomes are a promising nanoapproach for the targeted delivery of prednisolone within inflamed synovial cells for rheumatoid arthritis treatment.

First draft submitted: 15 December 2017; Accepted for publication: 7 March 2018; Published online: 23 May 2018

Keywords: corticosteroids • fibroblasts • hyaluronic acid • macrophages • pH-responsive liposomes

Rheumatoid arthritis (RA) is among the chronic autoimmune diseases with higher prevalence in the world, causing long-term disability and severe functional limitations on patient quality of life [1,2]. RA origin remains unknown, being then characterized by an autoimmunologic response attacking the joints synovium [1]. Neovascularization of the synovial tissue enables the migration of inflammatory cells to the synovium and of proinflammatory mediators for cellular activation that induce the destruction of cartilage and bone erosion, leading to synovial inflammatory activity that is related to hypoxia in the synovium [1]. The European League Against Rheumatism and the American College of Rheumatology preconize that is crucial an early intervention in RA treatment to slow down disease inflammatory progression and delay the beginning of irreversible joint damage [2–4]. In this context, immediately after diagnosis, the guidelines for treatment recommend the use of low-dose glucocorticoids, namely prednisolone, due to its rapid anti-inflammatory effect in suppressing the early arthritic symptoms [2–4]. Although prednisolone is highly effective in reducing inflammation, its long-term use is hampered by severe side effects, low drug bioavailability and off-targeted biodistribution profile, limiting its therapeutic efficiency [1]. In an effort to overcome these drawbacks, improve the therapeutic efficacy of prednisolone and eventually increase the duration of the therapy, hyaluronic acid (HA)-conjugated pH-sensitive liposomes were developed as a targeted drug delivery therapy strategy for RA. This approach relies on a nanobased drug delivery system that simultaneously takes advantage of the pathophysiological features of RA-like synovial neoangiogenesis [5] and acidic microenvironment of inflamed synovium [6], plus the HA ability to selectively target synovial cells [7,8] to promote a controlled prednisolone release. Among the cells found within the inflamed synovium, macrophages and fibroblasts are crucial in the progression of chronic inflammation by excreting proinflammatory mediators and trigger irreversible joint structural destruction [6,9,10]. Furthermore, HA is a naturally occurring glycosaminoglycan responsible for cellular growth and maintaining tissue integrity [11], which is already used as an approach for nanotherapy in RA [8,12,13]. Targeting strategies with

Future Medicine

HA-conjugated nanocarriers rely on its selective binding to CD44 cell receptor, overexpressed in activated cells found within the synovium and involved in the regulation of autoimmune response [7,8,11]. Hereby, this work presents a targeted RA therapy based on a nanotherapeutic approach relying on: enhanced vascular permeability of inflamed synovial tissues for liposome accumulation; HA-binding affinity to CD44 overexpressed in synovial cells to enable the targeted cellular uptake [7,8]; lipids pH sensitivity to acidic extracellular inflamed synovial tissue [5,6] and intracellular compartments, ensuring the controlled drug release in the cytosol and a reduced widespread of prednisolone off-target distribution. The combination of these strategies is innovative and promises to enable *in situ* drug bioavailability, while decreasing adverse off-target effects by selectively deliver prednisolone into the inflamed synovium. Thus, a synergic effect to improve the effectiveness of this potent conventional glucocorticoid on the inflammation site should be ensured.

Materials & methods

Materials

Sodium hyaluronate (MW: 320 kDa) was a kind gift from Genzyme Corporation (MA, USA). Prednisolone disodium phosphate (PDP) was purchase from Tokyo Chemical Industry Co. Ltd (Tokyo, Japan). 1,2-Dipalmitoyl-*sn*-glycero-3-phosphoethanolamine (DPPE) and *N*-(7-nitro-2,1,3-benzodiazole-4-yl)-DPPE (NBD-DPPE) were purchased from Avanti® Polar Lipids Inc. (AL, USA). Chloroform and methanol were acquired from ThermoFisher Scientific Inc. (Leicestershire, UK) and Atom Scientific (Cheshire, UK). Cholesteryl hemisuccinate (CHEMS), Triton™ X-100, thiazolyl blue tetrazolium bromide (MTT), trypan blue solution, dimethyl sulfoxide (DMSO, 99.9%), acetic acid (99.8%), triethylamine, ethyldimethyl-aminopropyl-carbodiimide, *N*-hydroxysuccinimide, chlorpromazine, filipin and cytochalasin-D were purchased from Sigma–Aldrich® (MO, USA). Fetal bovine serum, penicillin-streptomycin and DMEM were purchased from Gibco® by Life Technologies™ (ThermoFisher Scientific Inc.). Lactate dehydrogenase (LDH) cytotoxicity detection kit was acquired from Takara Bio, Inc. (Shiga, Japan). Murine L929 fibroblast and RAW 264.7 macrophages cell lines from the American Type Culture Collection (ATCC® TIB71™, Salisbury, UK). All chemicals and reagents used in the study were used without further purification.

Synthesis of HA-DPPE conjugate

The HA-DPPE conjugate synthesis was achieved using carbodiimide chemistry according with a modified method in the literature [11]. The three-step synthesis began with the activation of the hydroxysuccinimide ester of HA. Briefly, 1.0 mg of HA was dissolved in 50 ml of ultrapure water, followed by incubation with 0.5 g of ethyldimethyl-aminopropyl-carbodiimide and 0.52 g of *N*-hydroxysuccinimide at pH 4.0 for 2 h at 37°C. Followed by the addition of 100 mg of DPPE to the activated HA resulting solution and further pH adjustment to 8.6 (0.1 M borate buffer solution). This reaction was maintained for 24 h at 37°C, to allow the carboxyl groups of HA link to the amino groups of DPPE. Finally, the HA-DPPE conjugate was purified to remove unconjugated HA and other by-products, through dialysis against 1-l phosphate buffer for 48 h, using a cellulose dialysis bag (Cellu.Sep® T3 with a nominal molecular weight cutoff of 12–14 kDa). The solution was then lyophilized using a LyoQuest 85 plus v.407 Telstar freeze dryer (Telstar® Life Science Solutions, Terrassa, Spain), yielding a white dry powder. The characterization of the synthesized HA-DPPE conjugate was performed by ^{1}H nuclear magnetic resonance (NMR; Bruker Avance III) at 400 MHz in D_2O and DMSO at room temperature (RT) with tetramethylsilane as internal standard.

Preparation of pH-sensitive liposomes

pH-sensitive liposomes were prepared by the modified thin-film hydration method [14]. Briefly, DPPE:CHEMS and DPPE:CHEMS:DPPE-HA lipid solutions of 10 mM, respectively, in a molar ratio of 6.5:3.5 and 6.5:3.5:0.03, were prepared in a round-bottom flask by dissolving the amounts of lipids in a chloroform:methanol mixture (3:2). Whereas, for the formulations of drug-loaded liposomes, the amount of PDP was dissolved only in methanol and then slowly added to the remaining organic phase. The organic solvents were evaporated using a rotary-evaporator under a nitrogen flow, with the round-bottom flasks immersed in a bath at 42°C for approximately 40 min. The thin-lipid film was then hydrated with hepes-buffered solution at pH 7.4. Followed by 20 min of vigorous vortex stirring, the formulations were extruded three- and ten-times, respectively, through 600- and 100-nm polycarbonate filter membranes, under pressure of nitrogen gas and above the main phase transition temperature of the lipids mixture (>60°C).

pH-sensitive liposomes physicochemical characterization

Size, polydispersity index & zeta potential

Liposomal formulations were characterized in terms of size, size distribution (by the polydispersity index [PDI]) and zeta potential at 37°C using a ZetaPALS particle analyser (Brookhaven Instruments Corporation, NY, USA). The size and PDI were determined by dynamic light scattering with an average count rate between 300–500 kcps and zeta potential by electrophoretic light scattering using phase analysis light-scattering mode at an angle of 90°.

Drug loading capacity & entrapment efficiency

The drug loading capacity (LC) and entrapment efficiency (EE) percentages were determined, respectively, using Equations (1) and (2). The amount of free drug in the supernatant was quantified by absorbance at 247 nm using a UV–Vis spectrophotometer (V-660, Jasco Corporation, MD, USA). In order to separate the free unloaded drug, formulations were centrifuged in Amicom® ultra centrifugal filter devices of 50,000 nominal molecular weight limit (MERK Milipore Ltd, Cork, Ireland) at 2500 x*g* and RT for 10 min.

$$LC\ (\%) = \frac{Total\ amount\ of\ drug - Amount\ of\ free\ drug}{Total\ amount\ of\ lipid} \times 100 \qquad \text{(Equation 1)}$$

$$EE\ (\%) = \frac{Total\ amount\ of\ drug - Amount\ of\ free\ drug}{Total\ amount\ of\ drug} \times 100 \qquad \text{(Equation 2)}$$

All formulations were storage at 4°C and protected from light. Their stability regarding size, PDI, zeta potential, LC and EE was assessed for 1 month (Supplementary Material).

Morphology

Liposomes morphology was assessed by transmission electron microscopy (TEM; JEM-1400Plus, JEOL Inc., MA, USA) in different pH conditions. Briefly, samples of each liposomal formulation were diluted tenfold with either hepes buffer solution at pH 7.4 or acetate buffer solution at pH 5.0. Then, 10 µl of sample was placed over a 300-mesh copper grid followed by negative staining with 1% uranyl acetate for 5 s. The morphology of liposomes was then evaluated at RT with an accelerating voltage of 60 kV.

In vitro drug release study

The *in vitro* drug release study was performed using the dialysis method. Briefly, formulations of PDP-loaded liposomes were placed into a cellulose ester dialysis membranes (Float-a-Lyzer® G2, Spectrum Laboratories Inc., CA, USA), with 3.5–5 kDa nominal molecular weight cutoff, filled with 1 ml of the sample and 80 ml of outer buffer and maintained under sink conditions. The studies were performed with either hepes buffer solution at pH 7.4 or acetate buffer solution at pH 5.0, under continuous magnetic stirring at 37°C (RT 15 power, IKA Werke GmbH & Co. KG, Staufen im Breisgau, Germany). During 50 h at regular time intervals, 1 ml aliquots were withdrawn and the same volume of respective fresh buffer solution replaced to maintain the sink conditions. The PDP amount that passed through the dialysis membrane was quantified by measuring the absorbance at 247 nm using the UV-Vis spectrophotometer. Mathematical models for drug-release kinetics were applied to evaluate the mechanism of PDP release (Supplementary Material).

In vitro cellular studies

Murine L929 fibroblast and RAW 264.7 macrophages cell lines were cultured in DMEM supplemented with 10% fetal bovine serum and 1% penicillin-streptomycin, at 37°C with 5% CO_2. For all *in vitro* cellular assays, subculture of both cell lines was done at a proportion 1:4 at least once a week to achieve 80–90% cell confluence.

Cytotoxicity

In vitro cytotoxicity of both empty- and PDP-loaded liposomes was carried out in RAW macrophages and L929 fibroblasts using the MTT and LDH assays. Briefly, for MTT assay cells were seeded at a density of 5×10^4 cell per well in 96-well plates. After 3 h of incubation at 37°C with 5% CO_2, cells were treated with different

concentration of each liposomal formulation and free PDP. Control wells were treated with equivalent volumes of DMEM and a solution of 2% Triton X-100. After 24-h incubation at 37°C with 5% CO_2, the cell supernatant of each well was recovered and kept at 4°C for the LDH assay and a solution of 0.5 mg.ml^{-1} of MTT was added to the culture medium [15]. Followed by 2-h incubation at 37°C with 5% CO_2, the MTT solution was replaced by the same volume of DMSO to dissolve the formed formazan crystals. Then, the optical density was read by measuring absorbance at 590 and 630 nm using a microplate spectrophotometer (Synergy™ HT, Biotek, VT, USA).

For the LDH assay, plates containing the cell supernatant were centrifuged at 250 *g* and RT for 10 min to remove cellular debris or liposomes. Afterward, 100 µl was taken for LDH activity measurements according to the manufacturer's instructions. Briefly, 100 µl of the LDH cytotoxicity detection kit reaction mixture was added to each well and let to incubate in the dark for 12 min protected from light. The optical density was read by measuring absorbance at 490 and 630 nm using the microplate spectrophotometer. The results of cell viability and cytotoxicity were reported as the percentage of the metabolic and LDH activity of treated cells relatively to nontreated control cells.

Cellular uptake

Fluorescent liposomes were produced by the addition of NBD–DPPE at 1% mol of the amount of lipid in the organic phase upon thin-lipid film preparation. The cellular uptake of empty NBD-fluorescent liposomes was evaluated in both cell lines by flow cytometry. Briefly, cells were seeded at a density of 5 × 10^5 cell per well in 24-well plates and incubated at 37°C with 5% CO_2 for 20 h. To study the effect of incubation time, cells were incubated with NBD-fluorescent liposomal formulations for 1, 2, 4 and 6 h at 37°C with 5% CO_2. Then, after each incubation time, cells were washed twice with phosphate-buffered saline to remove any cellular debris or noninternalized liposomes. After trypsinization, cells were recovered in fresh DMEM and analyzed in a BD Accuri™ C6 flow cytometer (Biosciences, Erembodegem, Belgium) under the 488-nm excitation and 530-nm emission wavelengths. Prior to analysis, 0.11% trypan blue was added to each sample for 1 min to quench the NBD-fluorescent signal coming from liposomes adsorbed to the cell surface and dead cells were excluded by staining with propidium iodide. The results were reported as mean fluorescence intensity of cells with NBD-fluorescent liposomes and normalized relatively to the autofluorescence of cells in culture medium used as control.

Cellular uptake pathways

The internalization pathways involved in the cellular uptake of NBD-fluorescent liposomes were studied using flow cytometry. Briefly, cells were seeded at a density of 5 × 10^5 cell per well in 48-well plates and incubated at 37°C with 5% CO_2 for 20 h. Then, cells were preincubated for 30 min at 37°C with 5% CO_2 with three pharmacological pathway inhibitor solutions: chlorpromazine (10 µg.ml^{-1}), filipin (1 µg.ml^{-1}) or cytochalasin D (5 µg.ml^{-1}) [15,16]. Additionally, to study whether the cellular uptake was energy dependent, cells were incubated at 4°C for 30 min and then incubated with each one NBD-fluorescent liposomes for 1 h at 4°C. Prior flow cytometric analysis, cells were recovered in fresh DMEM as previously described. The results were reported as mean fluorescence intensity of cells with inhibitor and normalized relatively to the autofluorescence of cells incubated with no inhibitor at 37°C used as control.

Statistical analysis

Statistical analysis was performed using IBM® SPSS® Statistics software (v.22, NY, USA). Data were analyzed using one-way analysis of variance followed by Tukey *post hoc* test. The differences were statistically significant when the p-value was less than 0.05.

Results & discussion

HA-DPPE conjugate ^{1}H NMR characterization

The ^{1}H NMR spectrum of HA-DPPE conjugate presented on Figure 1 confirms the coupling of the HA to DPPE through the peaks at 1.46 ppm (CH_2CH_2NH) and at 5.91 ppm ($CH_2NH_2^+CO$) [17,18]. Also a peak at 2.12 ppm ($NHCOCH_3$) in the spectrum is also indicative of the presence of HA. Additionally, the DPPE characteristic peaks are represented at 0.87 ppm, corresponding to the terminal CH_3, and the methylene protons at 1.26 ppm [18].

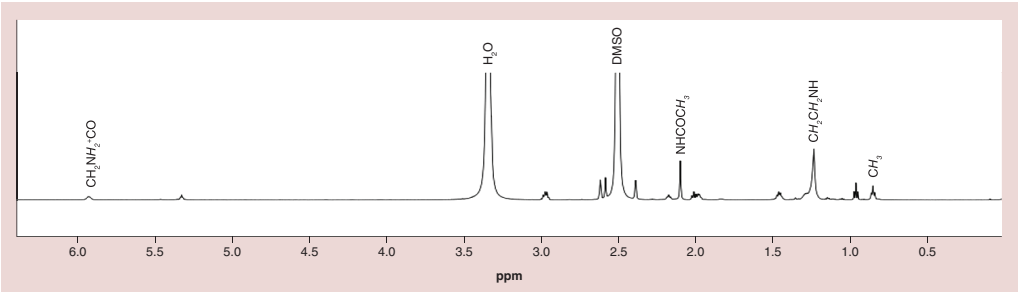

Figure 1. H nuclear magnetic resonance (NMR) spectrum of hyaluronic acid (HA)–1,2-dipalmitoyl-*sn*-glycero-3-phosphoethanolamine (DPPE) conjugate. H NMR spectra of HA and DPPE are presented in Supplementary Figure 1.

Table 1. Characterization of developed pH-sensitive liposomes.

		% EE	% LC	size (nm)	PDI	zeta potential (mV)
Lipo	empty	–	–	110 ± 1*	0.05 ± 0.01#	−36 ± 1#
	PDP	70 ± 2	45 ± 1	104 ± 3*	0.06 ± 0.03#	−33 ± 2#
	empty	–	–	114 ± 3#	0.10 ± 0.01#	−45 ± 2*
LipoHA	PDP	70 ± 1	45 ± 1	116 ± 3#	0.08 ± 0.02	−37 ± 3*

Data represent the average ± standard deviation (n = 3). Statistical significant differences between PDP loaded and empty pH-sensitive liposomes (*$p < 0.05$) or when comparing HA conjugated with unconjugated pH-sensitive liposomes (#$p < 0.05$).
EE: Entrapment efficiency; HA: Hyaluronic acid; LC: Loading capacity; PDI: Polydispersity index; PDP: Prednisolone disodium phosphate.

Characterization of pH-sensitive liposomes

Liposomes composed of DPPE:CHEMS (Lipo) or DPPE:CHEMS:DPPE-HA (LipoHA) loaded with PDP and empty were successfully produced and characterized in size, PDI and zeta potential. Additionally, drug-loaded liposomes were optimized for drug LC and EE. Results revealed for both formulations an average LC of 45% along with 70% of EE. In fact, a 45% of LC corresponds to 9 mg of entrapped prednisolone, which guarantees a therapeutic response. From the characterization of prepared pH-sensitive liposomes (Table 1), all formulations presented uniform vesicle sizes lower than 200 nm. Indeed, these sizes are described in the literature to be suitable for intravenous administration with long-circulating times in the bloodstream and enhanced ability to reach the synovium through the enhanced vascular permeability at the inflamed synovial region [5,19]. Moreover, at pH 7.4, HA is in the form of a sodium salt, which confers it a highly hydrophilicity. Thereby, the water molecules linked by hydrogen bonds to HA are oriented in a structured manner surrounding the polymer chain, thus creating a steric hydration shell [11]. This could enable stealth ability to liposomes, promoting long-lasting circulation. Further results on the characterization of liposomes revealed low PDI values (<0.2), indicating a homogeneous and monodisperse population of liposomes. Additionally, zeta potential revealed that the surface charge is beneath -30 mV, which is considered the reference value to prevent aggregation and hence liposomal monodispersity [20]. The negativity of liposomes surface was caused by the negatively charged terminal carboxylic group of CHEMS, as DPPE is a neutral zwitterionic molecule. Results revealed that HA provides a statistically significant increase of zeta potential value to -45 ± 2 mV when compared with Lipo (-36 ± 1 mV). Conversely, PDP association significantly decreased zeta potential values to -37 ± 3 mV, mainly due to the establishment of strong intermolecular interactions with HA. As negatively charged HA at pH 7.4 can establish electrostatic interactions with positively charged sodium groups of PDP [11]. Still, the zeta potential negativity of liposomes was not compromised, granting the shelf stability. Overall, HA conjugation did not influence PDP incorporation within pH-sensitive liposomes despite having an impact on vesicle size and zeta potential.

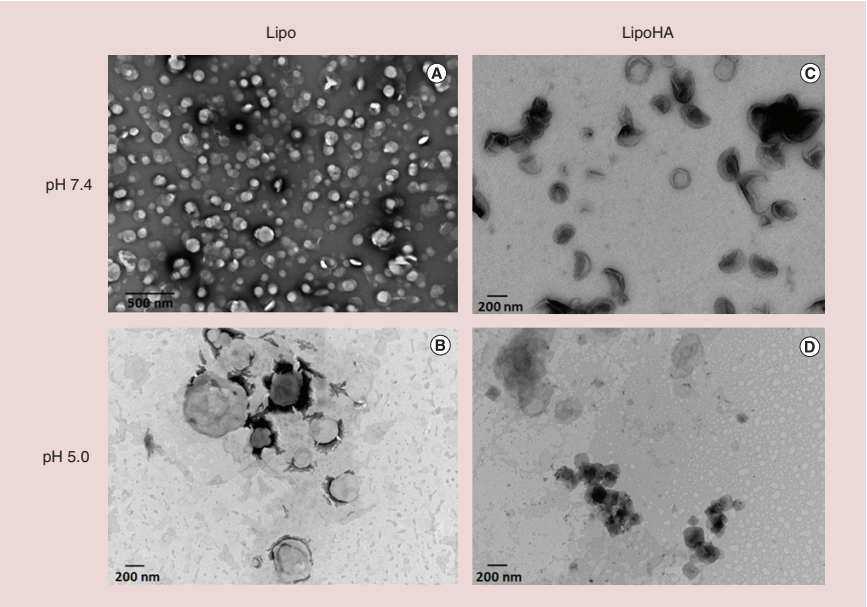

Figure 2. Transmission electron microscopy representative images of prednisolone disodium phosphate-loaded pH-sensitive liposomes in buffered solutions at pH 7.4 (A & C) and pH 5.0 (B & D).
HA: Hyaluronic acid.

Morphology

Morphology was assessed using TEM analysis and representative images of PDP-loaded liposomes are presented on Figure 2. Figure 2A and B illustrates pH-sensitive liposomes (Lipo) in buffered solutions, respectively, at pH 7.4 and 5.0. Under physiologic pH conditions (pH 7.4), the formulation exhibited liposomes with spherical shape morphology and homogenous sizes around 100 nm. Particularly on Figure 2A, the observed shadow blur can be related to sob-reposition of liposomes, possibly due to the high concentration of the sample. On Figure 2B, it can be observed that at pH 5.0, the liposomes did not lose the spherical shape, but there is a noticeable increase on the vesicle size (>200 nm) when compared with the ones in buffered solution at pH 7.4. Figure 2C and D presents HA-conjugated pH-sensitive liposomes (LipoHA) in buffered solutions, respectively, at pH 7.4 and 5.0. Vesicles on Figure 2C presented a ring morphology in both oval and spherical shapes. The appearance of the edge ring occurred likely due to electrostatic interactions established at pH 7.4 between negatively charged HA conjugated to the liposomes surface either with surrounding water or PDP molecules. Indeed, a decrease on the zeta potential values was found for LipoHA-loading PDP as compared with empty liposomes (Table 1). Remarkably, it was possible to observe that at pH 5.0 (Figure 2D), there is a complete loss of the liposomal structure. Instead of a spherical shape morphology, the observed square shape on Figure 2D may indicate the lamellar to hexagonal phase transition and the liposomes disassembly under acidic pH.

Drug release study

The *in vitro* drug release studies assess the ability of liposomes to mediate intracellular release of loaded drug and verify their pH-dependence. Therefore, the drug release profile was evaluated at 37°C under various pH conditions, namely acetate-buffered solution at pH 5.0, to mimic the acidic environment of inflamed synovial tissues and within intracellular compartments (as endosomes). Whereas, to mimic physiological pH conditions and evaluate inherent drug release in the bloodstream upon intravenous administration, hepes-buffered solution at pH 7.4 was used. The

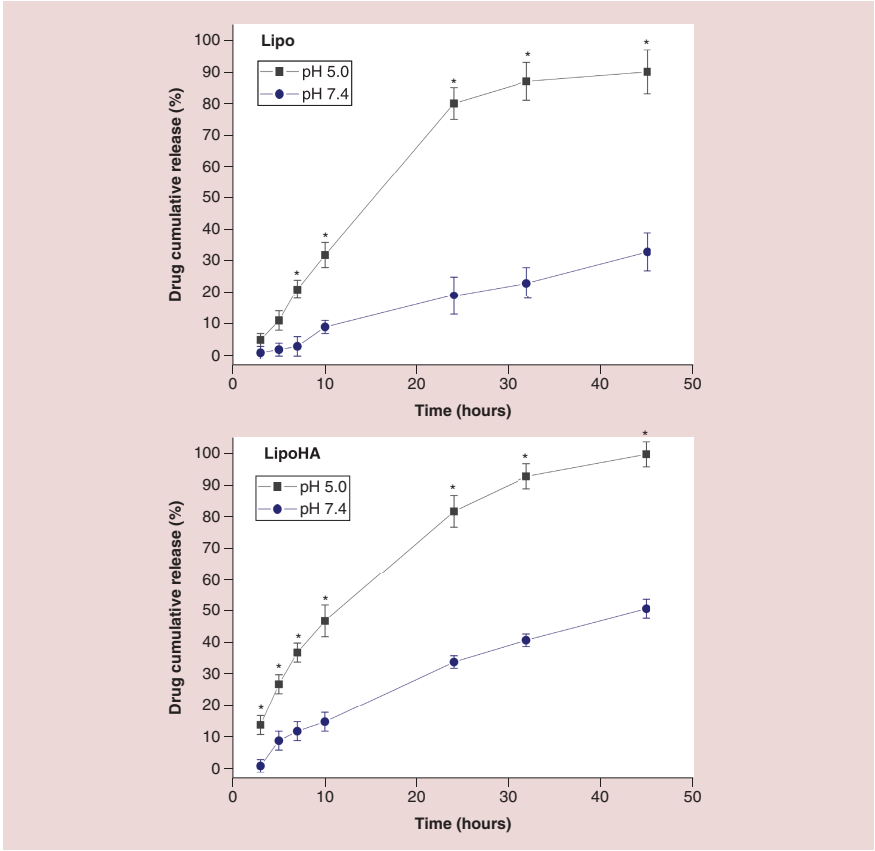

Figure 3. *In vitro* release profiles of prednisolone disodium phosphate from pH-sensitive liposomes in mimicked acidic and physiological conditions at 37°C. Data represent the average ± standard deviation (n = 3). Statistical significant differences (*$p < 0.05$) between buffered solutions at pH 7.4 and 5.0 at each time point.
HA: Hyaluronic acid.

results on the *in vitro* PDP release profile from liposomes presented in Figure 3 revealed that as expected on both liposomal formulations, the drug release rate in acidic pH conditions (pH 5.0) was higher than at pH 7.4. Thus, confirming the pH responsiveness of liposomes as an efficient trigger for liposomes disassembling and drug release. In fact, significant differences were observed when comparing cumulative amount of drug released from liposomes maintained at pH 7.4 with the ones at pH 5.0 in each time point. Moreover, under the acidic conditions, either Lipo or LipoHA released more than 90% of PDP in 45 h. While less than 50% of PDP was released during 50 h in physiological conditions, however, remaining enough loaded drug to exert its biologic effect once within cells.

The drug release data obtained were fitted to different models including zero-order and first-order equations, Higuchi, Hixson–Crowell and Korsmeyer–Peppas models to analyze the mechanism of drug release and the diffusion kinetics. The fitting of each model was evaluated based on the correlation coefficient (R^2) values obtained. The R^2 and the release rate constants (k) obtained for each model fit are presented in Table 2.

Results on Table 2 revealed that the best fit for the formulations with HA, as well as for Lip at pH 5, was obtained by the Higuchi model, which reveals that PDP release is caused primarily by a diffusion mechanism. Analyzing the

Table 2. Correlation coefficient (R^2) and k values from various drug release models for each developed liposomal formulation (n = 3).

Formulations	pH	Zero order		First order		Hixson–Crowell		Higuchi		Korsmeyer–Peppas	
		R^2	K_0	R^2	K_1	R^2	K_{HC}	R^2	K_H	R^2	K_{KP}
Lipo	7.4	†0.994	†8.6×10^{-5}	0.932	-2.4×10^{-4}	0.888	4.0×10^{-3}	0.965	6.5×10^{-4}	0.501	1.0×10^{-21}
	5.0	0.922	2.3×10^{-4}	0.981	-7.7×10^{-4}	0.840	3.0×10^{-3}	†0.997	†2.0×10^{-3}	0.269	3.0×10^{-21}
LipoHA	7.4	0.930	9.1×10^{-5}	0.989	-5.6×10^{-4}	0.607	1.9×10^{-3}	†0.993	†1.0×10^{-3}	0.418	9.0×10^{-23}
	5.0	0.829	1.4×10^{-4}	0.971	-9.3×10^{-4}	0.734	1.5×10^{-3}	†0.995	†2.0×10^{-3}	0.309	1.0×10^{-22}

†Represents models which best fits each release profile.
HA: Hyaluronic acid; K_0: Zero-order release constant; K_1: First-order release constant; K_{HC}: Hixson–Crowell rate constant; K_H: Higuchi dissolution constant; K_{KP}: Korsmeyer–Peppas drug release rate constant.

release rate constants (K_H), it is possible to observe that the HA conjugation does not interfere with the diffusion. Additionally, the drug release rate from LipoHA is faster at pH 5.0 than at pH 7.4. Conversely, results suggested that for Lipo at pH 7.4, the best fitting was obtained with the zero-order model, meaning that there was a constant release of PDP from the liposomes. Considering that only about 30% of PDP was released and that the EE is 70%, it is notorious that only the free PDP was released and that almost no PDP entrapped in the liposomes is released during the time of the experiments

In vitro cytotoxicity & cell viability study

In vitro cellular studies were carried out in RAW 264.7 macrophages and L929 fibroblasts cell lines to assess the cell viability and cytotoxicity of liposomal formulations. For both cell lines, results presented on Figure 4 revealed that empty Lipo and LipoHA exhibited over 85% cell viability within the concentration range between 0.19 and 3.0 mM, hence being biocompatible and noncytotoxic. In fibroblasts and macrophages, PDP-loaded pH-sensitive liposomes (Lipo:PDP) led to a significant statistical decrease in 30% of the mitochondrial metabolic activity assessed by the MTT assay, plus affected the membrane permeability only at the highest concentration (3.0 mM). A concentration-dependent effect was observed for the cell viability in the treatment with LipoHA-loading PDP (LipoHA:PDP) on both fibroblasts and macrophages lines (Figure 4A & B). Furthermore, LipoHA:PDP presented a statistically significant higher cytotoxic effect when compared with free PDP solution on fibroblasts (Figure 4C) and macrophages (Figure 4D), as result of a higher release of LDH enzyme and a reduced metabolic activity. These results suggested that observed cytotoxicity was due to HA conjugation, as it enables cellular uptake, hence increasing intracellular concentration of PDP and its cytotoxic effect.

In vitro cell uptake & pathway mechanism study

The cellular uptake efficiency of pH-sensitive liposomes was assessed using flow cytometry. The mean fluorescent intensity values obtained in fibroblasts and macrophages after incubation with NBD-fluorescent pH-sensitive liposomes, measure the liposome cellular uptake at each time point. Results on Figure 5 revealed cellular uptake time-dependence for both liposomal formulations. After 2 h of incubation, a significant increase on uptake by both cell types was observed for LipoHA when comparing to Lipo (Figure 5A & B). Further results suggested that most of liposomes were rapidly internalized within 2 h, as no statistical significant differences were observed between 2, 4 and 6 h of incubation (Figure 5A & B). Thus, uptake of Lipo carried out on both cell lines was almost completed within 2 h, oppositely to LipoHA uptake that increased after 2 h in both cell lines (Figure 5A), suggesting that HA conjugation enabled an efficient cellular uptake over time.

Liposomes can enter in cells via endocytosis or energy-independent nonendocytic pathways. To clarify the energy dependence and pathway mechanisms involved specific endocytic inhibitors were used. Namely, cells were preincubated at 4°C and with three pharmacological pathway inhibitors at 37°C: chlorpromazine and filipin, respectively, for clathrin- and caveolae-dependent endocytosis, and cytochalasin D for macropinocytosis [15,16,21]. Results on Figure 6 revealed that lower temperature (4°C) treatment led to a higher inhibitory effect (85%) on the uptake of LipoHA by fibroblasts, suggesting a full active energy-dependent endocytic process. Conversely, in macrophages low temperature inhibited the uptake by 50% as compared with uptake DMEM control at 37°C. Low temperature prevents passive uptake by increasing the rigidity of the plasma membrane [15], hence the results revealed that the LipoHA uptake can occur either by an active or passive energy-dependent endocytic process by macrophages. Further results on the endocytic pathway mechanism study revealed that, in fibroblasts

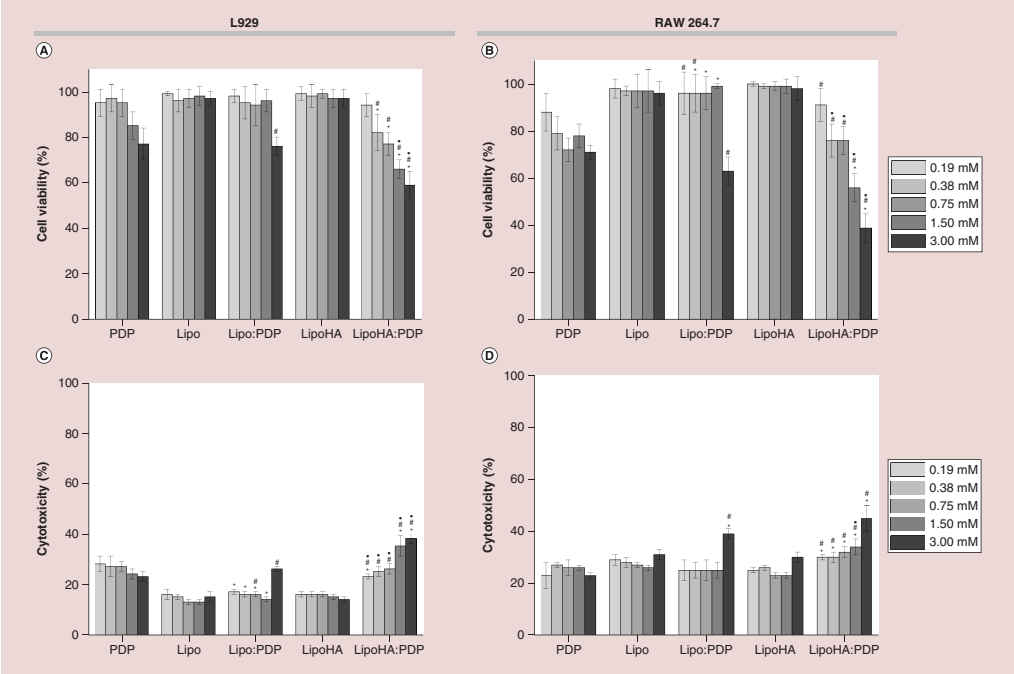

Figure 4. Cell viability and cytotoxicity of pH-sensitive liposomes. Cell viability assessed by MTT **(A & B)** and cytotoxicity effect measured by LDH release **(C & D)** on L929 fibroblast **(A & C)** and RAW 264.7 macrophage **(B & D)**. Data represent the average ± standard deviation (n = 5 of two independent assays). Statistical significant differences when comparing liposomes-loading PDP either with empty ones (*$p < 0.05$) or PDP solution control ($^{\#}p < 0.05$) at each concentration, and between conjugated and unconjugated liposomal formulations (•$p < 0.05$).
HA: Hyaluronic acid; MTT: Thiazolyl blue tetrazolium bromide; PDP: Prednisolone disodium phosphate.

the inhibition of clathrin-mediated endocytosis by chlorpromazine led to 40% reduction on the uptake, whereas inhibition of caveolae-mediated endocytosis by filipin resulted in less than 20% inhibition on the uptake of LipoHA (Figure 6). Additionally, inhibition of the macropinocytosis process resulted in about 30% reduction of the uptake by fibroblasts. Thereby, uptake process of LipoHA by fibroblasts in the presence of chlorpromazine exhibited a higher inhibitory effect when compared with the others pathway inhibitory treatments. Thus, suggesting a predominant clathrin-mediated endocytic uptake of LipoHA by fibroblasts. Further results on Figure 6 revealed that in macrophages LipoHA uptake was inhibited in 43 and 35%, respectively, in the presence of filipin and cytochalasin D. Equally, treatment with chlorpromazine led to about 30% inhibition on the uptake, suggesting that caveolae-mediated endocytosis and macropinocytosis processes are the main endocytic mechanisms involved in the uptake of LipoHA by macrophages. Overall, cell uptake and pathway mechanism studies suggested that HA conjugation specifically improved the liposomes cellular uptake overtime and that process is energy-dependent. Furthermore, LipoHA uptake actively occurs mainly by clathrin- and caveolae-mediated endocytosis. This outcome is consistent with previous studies, as clathrin-mediated endocytosis (or receptor-mediated endocytosis) is involved through the binding of HA to the CD44 cell receptor [7,8]. In its native form, HA is present as a high molecular mass polymer, but during inflammation smaller molecular fragments accumulate. Fragmented HA (<500 kDa, as the one used in this work) rather than the high molecular mass HA (>1 MDa) stimulates the cell-surface CD44 receptor. CD44 is critical to RA pathogenesis in leading to intracellular signaling of lymphocytes, expression of proinflammatory mediators and chemokines, hence cell proliferation [22]. Low-molecular fragments of HA also

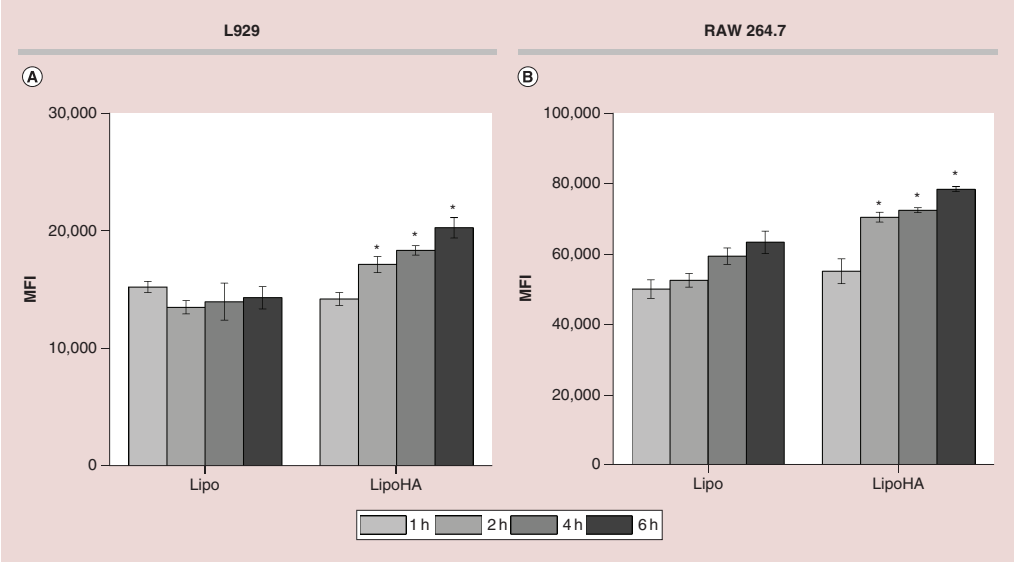

Figure 5. Cellular uptake of *N*-(7-nitro-2,1,3-benzodiazole-4-yl)-fluorescent pH-sensitive liposomes. L929 fibroblast **(A)** and RAW 264.7 macrophage **(B)** cell lines. Data represent the average ± standard deviation (n = 3 of two independent assays). Statistical significant differences when comparing unconjugated liposomes with conjugated ones (*$p < 0.05$).
HA: Hyaluronic acid.

stimulate angiogenesis, an important factor in inflammation, which enhance liposomal accumulation in the pannus through the enhanced permeability and retention effect [22]. HA has the potential to selectively bind to CD44, as it is overexpressed on the activated synovial macrophages and is involved in phagocytosis within the inflamed arthritic joint [23]. The enhanced expression of cell surface adhesion molecule CD44 was also found on fibroblast-like synoviocytes in the synovial pannus tissue relatively to healthy normal tissue [24]. Therefore, evidence of over and/or selective expression makes the CD44 cell surface receptor suitable for HA-targeted pH-sensitive liposomes in the treatment of RA.

The study of pathway mechanism involved in the liposomes uptake is important to understand their fate during the endocytic process, as clathrin and caveolae endocytosis mechanisms mediate the liposomes trafficking, respectively, to endosomes and caveosomes, followed by degradation processes in late endosomes and lysosomes [15]. Hence, under the acidic microenvironment the pH sensitivity trigger ensures that liposomes disassemble and the efficient release of drug molecules in the cytosol.

Conclusion

To selectively deliver prednisolone to the inflamed synovial tissue, HA-conjugated pH-sensitive liposomes were developed aiming a RA-targeted therapy. Liposomal formulations' evaluation in terms of liposomes' size, surface charge, size distribution, drug LC and EE shows that formulations presented optimized characteristics for either intravenous or intra-articular administration. Additionally, the morphological analysis allowed to assess vesicle's structural modification under acidic conditions and underlined differences between HA-conjugated and unconjugated pH-sensitive liposomes. The *in vitro* drug release profile revealed that pH responsiveness of developed pH-sensitive liposomes significantly enabled an increased drug release overtime under acidic pH at 37°C, mimicking either the extracellular inflamed synovium or intracellular endosomal compartments. *In vitro* cellular studies demonstrated the influence of HA conjugation in the intracellular accumulation of PDP, as HA-conjugated liposomes were effectively taken up by macrophages and fibroblasts through clathrin-mediated endocytosis. Taking

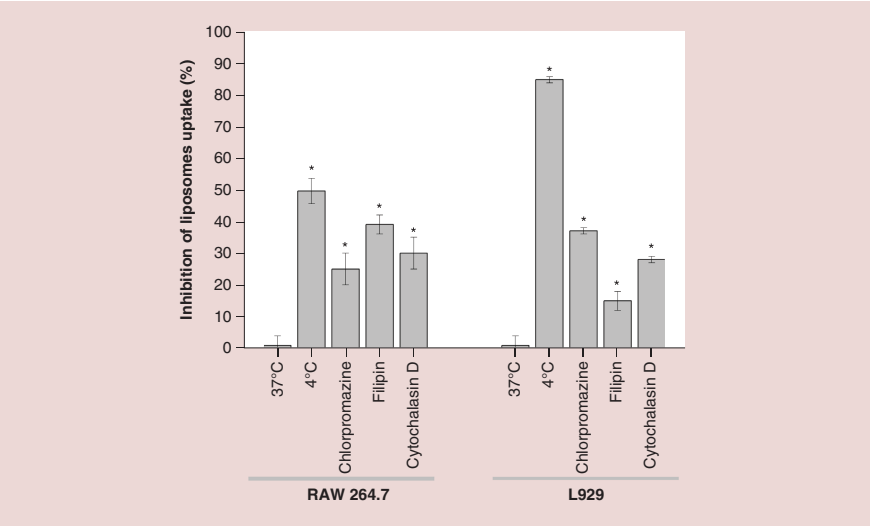

Figure 6. Effect of low temperature and pathway mechanism inhibitors on the uptake of *N*-(7-nitro-2,1,3-benzodiazole-4-yl)-fluorescent pH-sensitive liposomes by L929 fibroblast and RAW 264.7 macrophage. Data represent the average ± standard deviation (n = 3). Statistical significant differences when comparing with control at 37°C (*$p < 0.05$).

these *in vitro* study results, it is possible to realize the HA-conjugated pH-sensitive liposomes' huge potential as drug delivery systems to increase the bioavailability and improve the target therapeutic effectiveness of PDP *in situ*, while minimizing the well-known side effects. Therefore, being a promising therapeutic nanoapproach for an effective targeted RA treatment.

Summary points

Background

- Rheumatoid arthritis (RA) is a chronic inflammatory autoimmune disease affecting the synovial tissue of multiple body joints.
- Macrophages and fibroblasts are the key cells responsible for the RA progression.
- Prednisolone is administered during early stages of RA, but long-term dosages induce severe off-target effects.
- In this study, we propose the use of hyaluronic acid (HA)-conjugated pH-sensitive liposomes to deliver prednisolone within target synovial cells.

Results

- *In vitro* drug release studies revealed that prednisolone was preferentially released under acidic pH conditions like the ones presented either in the extracellular inflamed synovium or in the intracellular endosomal compartments.
- *In vitro* cellular studies on RAW 264.7 macrophages and L929 fibroblasts show that HA-conjugated pH-sensitive liposomes promote cellular uptake and enhance the cytotoxic effects of prednisolone disodium phosphate.

Discussion

- HA-conjugated pH-sensitive liposomes allow the targeted delivery of prednisolone within the inflamed synovial cells, enabling the *in situ* drug release and hence potentially reduce off-target toxicities.

Outlook

- HA-conjugated pH-sensitive liposomes revealed to be a promising nanotherapy to enhance the therapeutic efficacy and efficiency of prednisolone on RA long-term treatment.

Supplementary data

To view the supplementary data that accompany this paper please visit the journal website at: www.futuremedicine.com/doi/suppl/10.2217/nnm-2017-0377

Acknowledgements

The authors are also grateful to R Fernandes (Histology and Electron Microscopy Service – Instituto de Biologia Molecular e Celular [HEMS-I3S], University of Porto) for his expertise and technical assistance with TEM and Manuela Barros for administrative and technical support.

Financial & competing interests disclosure

The authors thank the received financial support from EU (FEDER funds POCI/01/0145/FEDER/007265) and National Funds (FCT/MEC, Fundação para a Ciência e a Tecnologia and Ministério da Educação e Ciência) under the Partnership Agreement PT2020 UID/QUI/50006/2013. This work was supported by FCT through the FCT PhD Programmes and by Programa Operacional Potencial Humano (POCH), specifically by the BiotechHealth Programe (Doctoral Programme on Cellular and Molecular Biotechnology Applied to Health Sciences). In this context, VM Gouveia and J Lopes-de-Araújo thank FCT and POCH for their PhD grants (PD/BD/128388/2017 and PD/BD/114012/2015, respectively). C Nunes also thanks FCT for the Investigator grant (IF/00293/2015) and respective exploratory project, which is in the framework of this work. SA Costa Lima thanks Operação NORTE-01-0145-FEDER-000011 for her Investigator contract. The authors have no other relevant affiliations or financial involvement with any organization or entity with a financial interest in or financial conflict with the subject matter or materials discussed in the manuscript apart from those disclosed.

No writing assistance was utilized in the production of this manuscript.

Ethical conduct of research

The authors state that they have obtained appropriate institutional review board approval or have followed the principles outlined in the Declaration of Helsinki for all human or animal experimental investigations. In addition, for investigations involving human subjects, informed consent has been obtained from the participants involved.

References

Papers of special note have been highlighted as: • of interest; •• of considerable interest

1 Gouveia VM, Lima SA, Nunes C, Reis S. Non-biologic nanodelivery therapies for rheumatoid arthritis. *J. Biomed. Nanotechnol.* 11(10), 1701–1721 (2015).

•• **Overview focus on the last decade research on drug delivery systems designed as nanostrategies for rheumatoid arthritis (RA) treatment.**

2 Davis JM, 3rd, Matteson EL, American College of Rheumatology, European League Against Rheumatism. My treatment approach to rheumatoid arthritis. *Mayo Clin. Proc.* 87(7), 659–673 (2012).

3 Smolen JS, Landewe R, Breedveld FC *et al.* EULAR recommendations for the management of rheumatoid arthritis with synthetic and biological disease-modifying antirheumatic drugs: 2013 update. *Ann. Rheum. Dis.* 73(3), 492–509 (2014).

• **Overview on the current recommendations for the management of RA and on the use of low-dose glucocorticoids should be considered as part of the initial treatment strategy.**

4 Singh JA, Saag KG, Bridges SL Jr *et al.* 2015 American College of Rheumatology guideline for the treatment of rheumatoid arthritis. *Arthritis Rheumatol.* 68(1), 1–26 (2016).

5 Leblond A, Allanore Y, Avouac J. Targeting synovial neoangiogenesis in rheumatoid arthritis. *Autoimmun. Rev.* 16(6), 594–601 (2017).

6 Fukamachi T, Wang X, Mochizuki Y, Maruyama C, Saito H, Kobayashi H. Acidic environments enhance the inhibitory effect of statins on proliferation of synovial cells. *Int. Immunopharmacol.* 17(1), 148–153 (2013).

•• **Provides evidence of acidic microenvironment of synovial tissues.**

7 Racine R, Mummert ME. Hyaluronan endocytosis: mechanisms of uptake and biological functions. In: *Molecular Regulation of Endocytosis.* Ceresa B (Ed). Intech, London, UK, 377–390 (2012).

8 Shin JM, Kim SH, Thambi T *et al.* A hyaluronic acid-methotrexate conjugate for targeted therapy of rheumatoid arthritis. *Chem. Commun.* 50(57), 7632–7635 (2014).

9 Neumann E, Lefevre S, Zimmermann B, Gay S, Muller-Ladner U. Rheumatoid arthritis progression mediated by activated synovial fibroblasts. *Trends Mol. Med.* 16(10), 458–468 (2010).

10 Weyand CM, Zeisbrich M, Goronzy JJ. Metabolic signatures of T-cells and macrophages in rheumatoid arthritis. *Curr. Opin. Immunol.* 46, 112–120 (2017).

11 Carole E, Schantéa GZ, Corinne H, Vandamme TF. Chemical modifications of hyaluronic acid for the synthesis of derivatives for a broad range of biomedical applications. *Carbohyd. Polym.* 85, 469–489 (2011).

12 Heo R, Park JS, Jang HJ *et al.* Hyaluronan nanoparticles bearing gamma-secretase inhibitor: *in vivo* therapeutic effects on rheumatoid arthritis. *J. Control. Rel.* 192, 295–300 (2014).

13 Lee H, Lee MY, Bhang SH *et al.* Hyaluronate-gold nanoparticle/tocilizumab complex for the treatment of rheumatoid arthritis. *ACS Nano* 8(5), 4790–4798 (2014).

14 Nunes C, Brezesinski G, Lopes D, Lima JL, Reis S, Lucio M. Lipid–drug interaction: biophysical effects of tolmetin on membrane mimetic systems of different dimensionality. *J. Phys. Chem. B* 115(43), 12615–12623 (2011).

15 Costa Lima SA, Reis S. Temperature-responsive polymeric nanospheres containing methotrexate and gold nanoparticles: a multi-drug system for theranostic in rheumatoid arthritis. *Colloids Surf. B Biointerfaces* 133, 378–387 (2015).

16 Lopes-De-Araujo J, Neves AR, Gouveia VM, Moura CC, Nunes C, Reis S. Oxaprozin-loaded lipid nanoparticles towards overcoming NSAIDs side-effects. *Pharm. Res.* 33(2), 301–314 (2016).

17 Abraham RJ, Griffiths L, Perez M. 1H NMR spectra. Part 30(+): 1H chemical shifts in amides and the magnetic anisotropy, electric field and steric effects of the amide group. *Magn. Reson. Chem.* 51(3), 143–155 (2013).

18 Arpicco S, Lerda C, Dalla Pozza E *et al.* Hyaluronic acid-coated liposomes for active targeting of gemcitabine. *Eur. J. Pharm. Biopharm. V* 85(3 Pt A), 373–380 (2013).

19 Blanco E, Shen H, Ferrari M. Principles of nanoparticle design for overcoming biological barriers to drug delivery. *Nat. Biotechnol.* 33(9), 941–951 (2015).

20 Honary S, Zahir F. Effect of zeta potential on the properties of nano-drug delivery systems – a review (part 2). *Trop. J. Pharm. Res.* 12(2), 265–273 (2013).

21 Kanlaya R, Sintiprungrat K, Chaiyarit S, Thongboonkerd V. Macropinocytosis is the major mechanism for endocytosis of calcium oxalate crystals into renal tubular cells. *Cell Biochem. Biophys.* 67(3), 1171–1179 (2013).

22 Naor D, Nedvetzki S. CD44 in rheumatoid arthritis. *Arthritis Res. Ther.* 5(3), 105–115 (2003).

•• **Provides evidence of CD44-hyaluronan interaction as a therapeutic target in RA.**

23 Schmitt F, Lagopoulos L, Kauper P *et al.* Chitosan-based nanogels for selective delivery of photosensitizers to macrophages and improved retention in and therapy of articular joints. *J. Control. Rel.* 144(2), 242–250 (2010).

24 Henderson KJ, Edwards JC, Worrall JG. Expression of CD44 in normal and rheumatoid synovium and cultured synovial fibroblasts. *Ann. Rheum. Dis.* 53(11), 729–734 (1994).

Supplementary Information

Hyaluronic acid conjugated pH-sensitive liposomes for targeted delivery of prednisolone: a new approach for rheumatoid arthritis therapy

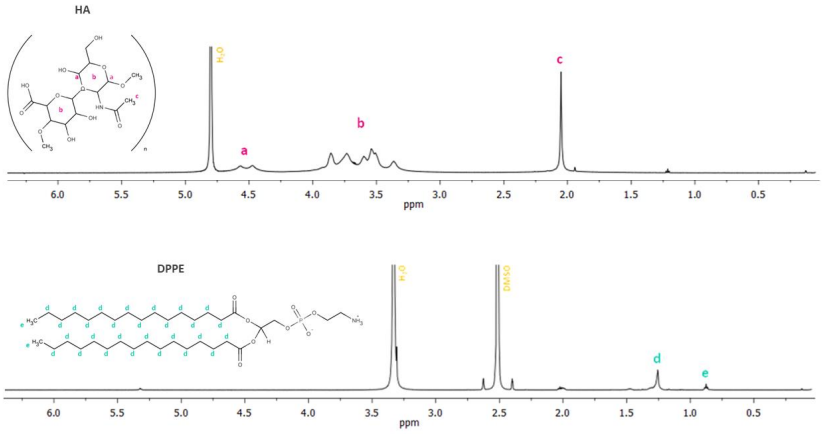

Figure S1 - ^{1}H-NMR spectra of HA and DPPE molecules.

Prednisolone release kinetics study

To examine the kinetics and mechanism of prednisolone (PDP) release from the liposomes, the data obtained from the *in vitro* release studies were analyzed by various mathematical models such as the zero and first order, Higuchi, Hixson–Crowell and Korsmeyer–Peppas models. The equations used were as follows:

Zero order release model: $Q = Q_0 + K_0t$

First order release model: $\text{Log } C = \text{Log } C_0 – k_1t / 2.303$

Higuchi release model: $Qt = k_H (t)^{0.5}$

Hixson-Crowell release model: $Q_0 1/3 – Q_t 1/3 = K_{HC}\, t$

Korsmeyer-Peppas release model: $F=M_t/M\ N = Kt^n$

where Q is the amount of drug released or dissolved; Q_0 is initial amount of drug in solution; C_0 is the initial concentration of drug; t is the time in hours; F is the fraction of drug release at time t; M_t/M is the fraction of drug released at time t; K are the rate constants for each model.

Zero order release model, refers to the process of constant drug release from a drug delivery device. The first-order equation represents a system where the release rate of the drug depends on the concentration of the drug in the system. Hixson-Crowell release model, describes the release from systems where there is a change in surface area and diameter of particles. The Higuchi model assumes that the drug´s release is caused primarily by a diffusion mechanism. The Korsmeyer–Peppas model provides insight into the type of drug release mechanism taking place from swellable devices.

Stability study

Stability studies conducted with weekly assessment on the physicochemical parameters of HA conjugated pH-sensitive liposomes indicated that storage at 4ºC protected from light preserved the liposomes properties for one month. Data express the average ± standard deviation (n=3). Statistical significant differences (* *P<0.05*) when comparing with week 0.

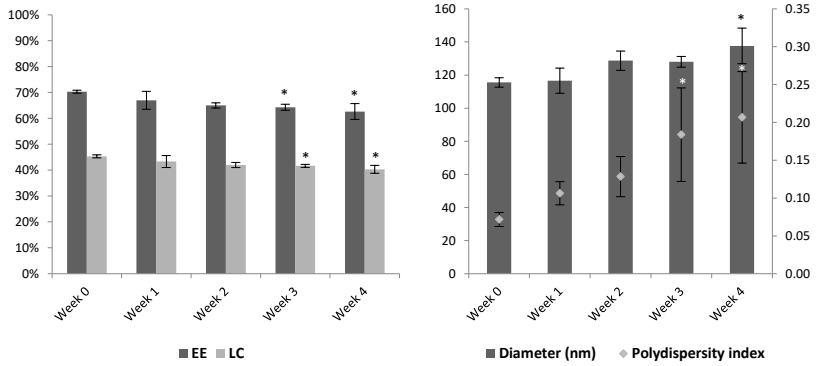

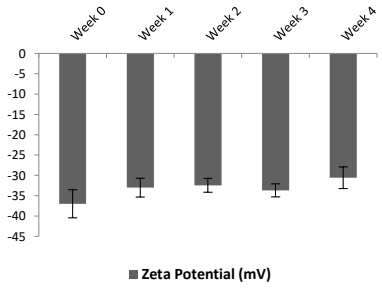

Appendix

Future Medicine Ltd LICENSE
TERMS AND CONDITIONS

May 23, 2019

This is a License Agreement between Virginia M. Gouveia ("You") and Future Medicine Ltd ("Future Medicine Ltd") provided by Copyright Clearance Center ("CCC"). The license consists of your order details, the terms and conditions provided by Future Medicine Ltd, and the payment terms and conditions.

All payments must be made in full to CCC. For payment instructions, please see information listed at the bottom of this form.

License Number	4594790270563
License date	May 14, 2019
Licensed content publisher	Future Medicine Ltd
Licensed content title	Nanomedicine
Licensed content date	Jan 1, 2006
Type of Use	Thesis/Dissertation
Requestor type	Author of requested content
Format	Print, Electronic
Portion	chapter/article
The requesting person/organization is:	Virginia Gouveia
Title or numeric reference of the portion(s)	Full Article
Title of the article or chapter the portion is from	Hyaluronic acid-conjugated pH-sensitive liposomes for targeted delivery of prednisolone on rheumatoid arthritis therapy
Editor of portion(s)	N/A
Author of portion(s)	N/A
Volume of serial or monograph.	N/A
Page range of the portion	
Publication date of portion	January 2020
Rights for	Main Product, any product related to main product, and other compilations/derivative products
Duration of use	Life of current and all future editions
Creation of copies for the disabled	no
With minor editing privileges	no
For distribution to	Worldwide
In the following language(s)	Original language of publication
With incidental promotional	no

use	
The lifetime unit quantity of new product	More than 2,000,000
Title	TARGET-TO-TREAT NANOTHERAPY FOR RHEUMATOID ARTHRITIS
Institution name	Abel Salazar Biomedical Sciences Institute and Faculty of Pharmacy, University of Porto
Expected presentation date	Jan 2020
Billing Type	Invoice
Billing Address	Virginia M. Gouveia R. Jorge de Viterbo Ferreira 228 Porto, Portugal 4050-313 Attn: Virginia M. Gouveia
Total (may include CCC user fee)	0.00 USD
Terms and Conditions	

TERMS AND CONDITIONS
The following terms are individual to this publisher:

None

Other Terms and Conditions:
STANDARD TERMS AND CONDITIONS

1. Description of Service; Defined Terms. This Republication License enables the User to obtain licenses for republication of one or more copyrighted works as described in detail on the relevant Order Confirmation (the "Work(s)"). Copyright Clearance Center, Inc. ("CCC") grants licenses through the Service on behalf of the rightsholder identified on the Order Confirmation (the "Rightsholder"). "Republication", as used herein, generally means the inclusion of a Work, in whole or in part, in a new work or works, also as described on the Order Confirmation. "User", as used herein, means the person or entity making such republication.

2. The terms set forth in the relevant Order Confirmation, and any terms set by the Rightsholder with respect to a particular Work, govern the terms of use of Works in connection with the Service. By using the Service, the person transacting for a republication license on behalf of the User represents and warrants that he/she/it (a) has been duly authorized by the User to accept, and hereby does accept, all such terms and conditions on behalf of User, and (b) shall inform User of all such terms and conditions. In the event such person is a "freelancer" or other third party independent of User and CCC, such party shall be deemed jointly a "User" for purposes of these terms and conditions. In any event, User shall be deemed to have accepted and agreed to all such terms and conditions if User republishes the Work in any fashion.

3. Scope of License; Limitations and Obligations.

3.1 All Works and all rights therein, including copyright rights, remain the sole and exclusive property of the Rightsholder. The license created by the exchange of an Order Confirmation (and/or any invoice) and payment by User of the full amount set forth on that document includes only those rights expressly set forth in the Order Confirmation and in these terms and conditions, and conveys no other rights in the Work(s) to User. All rights not expressly granted are hereby reserved.

3.2 General Payment Terms: You may pay by credit card or through an account with us payable at the end of the month. If you and we agree that you may establish a standing

account with CCC, then the following terms apply: Remit Payment to: Copyright Clearance Center, 29118 Network Place, Chicago, IL 60673-1291. Payments Due: Invoices are payable upon their delivery to you (or upon our notice to you that they are available to you for downloading). After 30 days, outstanding amounts will be subject to a service charge of 1-1/2% per month or, if less, the maximum rate allowed by applicable law. Unless otherwise specifically set forth in the Order Confirmation or in a separate written agreement signed by CCC, invoices are due and payable on "net 30" terms. While User may exercise the rights licensed immediately upon issuance of the Order Confirmation, the license is automatically revoked and is null and void, as if it had never been issued, if complete payment for the license is not received on a timely basis either from User directly or through a payment agent, such as a credit card company.

3.3 Unless otherwise provided in the Order Confirmation, any grant of rights to User (i) is "one-time" (including the editions and product family specified in the license), (ii) is non-exclusive and non-transferable and (iii) is subject to any and all limitations and restrictions (such as, but not limited to, limitations on duration of use or circulation) included in the Order Confirmation or invoice and/or in these terms and conditions. Upon completion of the licensed use, User shall either secure a new permission for further use of the Work(s) or immediately cease any new use of the Work(s) and shall render inaccessible (such as by deleting or by removing or severing links or other locators) any further copies of the Work (except for copies printed on paper in accordance with this license and still in User's stock at the end of such period).

3.4 In the event that the material for which a republication license is sought includes third party materials (such as photographs, illustrations, graphs, inserts and similar materials) which are identified in such material as having been used by permission, User is responsible for identifying, and seeking separate licenses (under this Service or otherwise) for, any of such third party materials; without a separate license, such third party materials may not be used.

3.5 Use of proper copyright notice for a Work is required as a condition of any license granted under the Service. Unless otherwise provided in the Order Confirmation, a proper copyright notice will read substantially as follows: "Republished with permission of [Rightsholder's name], from [Work's title, author, volume, edition number and year of copyright]; permission conveyed through Copyright Clearance Center, Inc. " Such notice must be provided in a reasonably legible font size and must be placed either immediately adjacent to the Work as used (for example, as part of a by-line or footnote but not as a separate electronic link) or in the place where substantially all other credits or notices for the new work containing the republished Work are located. Failure to include the required notice results in loss to the Rightsholder and CCC, and the User shall be liable to pay liquidated damages for each such failure equal to twice the use fee specified in the Order Confirmation, in addition to the use fee itself and any other fees and charges specified.

3.6 User may only make alterations to the Work if and as expressly set forth in the Order Confirmation. No Work may be used in any way that is defamatory, violates the rights of third parties (including such third parties' rights of copyright, privacy, publicity, or other tangible or intangible property), or is otherwise illegal, sexually explicit or obscene. In addition, User may not conjoin a Work with any other material that may result in damage to the reputation of the Rightsholder. User agrees to inform CCC if it becomes aware of any infringement of any rights in a Work and to cooperate with any reasonable request of CCC or the Rightsholder in connection therewith.

4. Indemnity. User hereby indemnifies and agrees to defend the Rightsholder and CCC, and their respective employees and directors, against all claims, liability, damages, costs and expenses, including legal fees and expenses, arising out of any use of a Work beyond the

scope of the rights granted herein, or any use of a Work which has been altered in any unauthorized way by User, including claims of defamation or infringement of rights of copyright, publicity, privacy or other tangible or intangible property.
5. Limitation of Liability. UNDER NO CIRCUMSTANCES WILL CCC OR THE RIGHTSHOLDER BE LIABLE FOR ANY DIRECT, INDIRECT, CONSEQUENTIAL OR INCIDENTAL DAMAGES (INCLUDING WITHOUT LIMITATION DAMAGES FOR LOSS OF BUSINESS PROFITS OR INFORMATION, OR FOR BUSINESS INTERRUPTION) ARISING OUT OF THE USE OR INABILITY TO USE A WORK, EVEN IF ONE OF THEM HAS BEEN ADVISED OF THE POSSIBILITY OF SUCH DAMAGES. In any event, the total liability of the Rightsholder and CCC (including their respective employees and directors) shall not exceed the total amount actually paid by User for this license. User assumes full liability for the actions and omissions of its principals, employees, agents, affiliates, successors and assigns.
6. Limited Warranties. THE WORK(S) AND RIGHT(S) ARE PROVIDED “AS IS”. CCC HAS THE RIGHT TO GRANT TO USER THE RIGHTS GRANTED IN THE ORDER CONFIRMATION DOCUMENT. CCC AND THE RIGHTSHOLDER DISCLAIM ALL OTHER WARRANTIES RELATING TO THE WORK(S) AND RIGHT(S), EITHER EXPRESS OR IMPLIED, INCLUDING WITHOUT LIMITATION IMPLIED WARRANTIES OF MERCHANTABILITY OR FITNESS FOR A PARTICULAR PURPOSE. ADDITIONAL RIGHTS MAY BE REQUIRED TO USE ILLUSTRATIONS, GRAPHS, PHOTOGRAPHS, ABSTRACTS, INSERTS OR OTHER PORTIONS OF THE WORK (AS OPPOSED TO THE ENTIRE WORK) IN A MANNER CONTEMPLATED BY USER; USER UNDERSTANDS AND AGREES THAT NEITHER CCC NOR THE RIGHTSHOLDER MAY HAVE SUCH ADDITIONAL RIGHTS TO GRANT.
7. Effect of Breach. Any failure by User to pay any amount when due, or any use by User of a Work beyond the scope of the license set forth in the Order Confirmation and/or these terms and conditions, shall be a material breach of the license created by the Order Confirmation and these terms and conditions. Any breach not cured within 30 days of written notice thereof shall result in immediate termination of such license without further notice. Any unauthorized (but licensable) use of a Work that is terminated immediately upon notice thereof may be liquidated by payment of the Rightsholder's ordinary license price therefor; any unauthorized (and unlicensable) use that is not terminated immediately for any reason (including, for example, because materials containing the Work cannot reasonably be recalled) will be subject to all remedies available at law or in equity, but in no event to a payment of less than three times the Rightsholder's ordinary license price for the most closely analogous licensable use plus Rightsholder's and/or CCC's costs and expenses incurred in collecting such payment.
8. **Miscellaneous.**
8.1 User acknowledges that CCC may, from time to time, make changes or additions to the Service or to these terms and conditions, and CCC reserves the right to send notice to the User by electronic mail or otherwise for the purposes of notifying User of such changes or additions; provided that any such changes or additions shall not apply to permissions already secured and paid for.
8.2 Use of User-related information collected through the Service is governed by CCC’s privacy policy, available online here:
http://www.copyright.com/content/cc3/en/tools/footer/privacypolicy.html.
8.3 The licensing transaction described in the Order Confirmation is personal to User. Therefore, User may not assign or transfer to any other person (whether a natural person or an organization of any kind) the license created by the Order Confirmation and these terms and conditions or any rights granted hereunder; provided, however, that User may assign

such license in its entirety on written notice to CCC in the event of a transfer of all or substantially all of User's rights in the new material which includes the Work(s) licensed under this Service.
8.4 No amendment or waiver of any terms is binding unless set forth in writing and signed by the parties. The Rightsholder and CCC hereby object to any terms contained in any writing prepared by the User or its principals, employees, agents or affiliates and purporting to govern or otherwise relate to the licensing transaction described in the Order Confirmation, which terms are in any way inconsistent with any terms set forth in the Order Confirmation and/or in these terms and conditions or CCC's standard operating procedures, whether such writing is prepared prior to, simultaneously with or subsequent to the Order Confirmation, and whether such writing appears on a copy of the Order Confirmation or in a separate instrument.
8.5 The licensing transaction described in the Order Confirmation document shall be governed by and construed under the law of the State of New York, USA, without regard to the principles thereof of conflicts of law. Any case, controversy, suit, action, or proceeding arising out of, in connection with, or related to such licensing transaction shall be brought, at CCC's sole discretion, in any federal or state court located in the County of New York, State of New York, USA, or in any federal or state court whose geographical jurisdiction covers the location of the Rightsholder set forth in the Order Confirmation. The parties expressly submit to the personal jurisdiction and venue of each such federal or state court.If you have any comments or questions about the Service or Copyright Clearance Center, please contact us at 978-750-8400 or send an e-mail to info@copyright.com.
v 1.1

Questions? customercare@copyright.com or +1-855-239-3415 (toll free in the US) or +1-978-646-2777.

Chapter 3

II. Macrophage targeting pH responsive polymersomes for glucocorticoid therapy

Virgínia M. Gouveia [1,2,3,4], Loris Rizzello [3,4,5], Cláudia Nunes [1], Alessandro Poma [3,4,6], Lorena Ruiz-Perez [3,4,7], António Oliveira [2], Salette Reis [1] and Giuseppe Battaglia [3,4,5,7,8]

[1] LAQV,REQUIMTE, Department of Chemical Sciences, Faculty of Pharmacy, University of Porto, 4050-313 Porto, Portugal

[2] Abel Salazar Biomedical Sciences Institute, University of Porto, 4050-313 Porto, Portugal

[3] Department of Chemistry, University College London, London WC1H 0AJ, UK

[4] Institute of Physics of Living Systems, University College London, London WC1H 0AJ, UK

[5] Institute for Bioengineering of Catalonia (IBEC), The Barcelona Institute of Science and Technology, 08028 Barcelona, Spain

[6] Division of Biomaterials and Tissue Engineering, UCL Eastman Dental Institute, University College London, London WC1X 8LD, UK

[7] EPSRC/JEOL Centre for Liquid Phase Electron Microscopy, University College London, London WC1H 0AJ, UK

[8] Catalan Institution for Research and Advanced Studies (ICREA), 08010 Barcelona, Spain

---

Original research article published in Pharmaceutics (2019)

DOI: 10.3390/pharmaceutics11110614

pharmaceutics

MDPI

Article

Macrophage Targeting pH Responsive Polymersomes for Glucocorticoid Therapy

Virgínia M. Gouveia [1,2,3,4], Loris Rizzello [3,4,5], Claudia Nunes [1], Alessandro Poma [3,4,6], Lorena Ruiz-Perez [3,4,7], António Oliveira [2], Salette Reis [1,*] and Giuseppe Battaglia [3,4,5,7,8,*]

1 LAQV/REQUIMTE, Department of Chemical Sciences, Faculty of Pharmacy, University of Porto, 4050-313 Porto, Portugal; virginia.mgouveia@gmail.com (V.M.G.); cdnunes@ff.up.pt (C.N.)
2 Abel Salazar Biomedical Sciences Institute, University of Porto, Portugal, 4050-313 Porto, Portugal; afonsecaoliveira1@gmail.com
3 Department of Chemistry, University College London, 20 Gordon Street, London WC1H 0AJ, UK; lrizzello@ibecbarcelona.eu (L.R.); a.poma@ucl.ac.uk (A.P.); l.ruiz-perez@ucl.ac.uk (L.R.-P.)
4 Institute of Physics of Living Systems, University College London, 20 Gordon Street, London WC1H 0AJ, UK
5 Institute for Bioengineering of Catalonia (IBEC), The Barcelona Institute of Science and Technology, Baldiri Reixac 10-12, 08028 Barcelona, Spain
6 Division of Biomaterials and Tissue Engineering, UCL Eastman Dental Institute, University College London, 256 Gray's Inn Road, London WC1X 8LD, UK
7 EPSRC/JEOL Centre for Liquid Phase Electron Microscopy, University College London, 20 Gordon Street, London WC1H 0AJ, UK
8 Catalan Institution for Research and Advanced Studies (ICREA), Passeig Lluís Companys 23, 08010 Barcelona, Spain
* Correspondence: shreis@ff.up.pt (S.R.); g.battaglia@ucl.ac.uk (G.B.); Tel.: +351-220-428-672 (S.R.); +44-20-7679-4688 (G.B.)

Received: 9 October 2019; Accepted: 12 November 2019; Published: 15 November 2019

check for updates

Abstract: Glucocorticoid (GC) drugs are the cornerstone therapy used in the treatment of inflammatory diseases. Here, we report pH responsive poly(2-methacryloyloxyethyl phosphorylcholine)–poly(2-(diisopropylamino)ethyl methacrylate) (PMPC–PDPA) polymersomes as a suitable nanoscopic carrier to precisely and controllably deliver GCs within inflamed target cells. The in vitro cellular studies revealed that polymersomes ensure the stability, selectivity and bioavailability of the loaded drug within macrophages. At molecular level, we tested key inflammation-related markers, such as the nuclear factor-κB, tumour necrosis factor-α, interleukin-1β, and interleukin-6. With this, we demonstrated that pH responsive polymersomes are able to enhance the anti-inflammatory effect of loaded GC drug. Overall, we prove the potential of PMPC–PDPA polymersomes to efficiently promote the inflammation shutdown, while reducing the well-known therapeutic limitations in GC-based therapy.

Keywords: inflammation; macrophages; glucocorticoid; polymersomes

1. Introduction

Inflammatory diseases comprise a vast range of disorders and conditions characterised by an uncontrolled over-activation of the immune system [1,2]. Inflammation is also indeed intimately related with the pathogenesis of many chronic autoimmune diseases, such as rheumatoid arthritis, lupus, psoriasis, and inflammatory bowel disorders [1,2]. Macrophages are a critical component of the innate immune system, and key cells in the initiation, maintenance, and resolution of inflammation [3–5]. These cells are professional phagocytes that are responsible for patrolling for pathogens, and modulating the inflammatory process [3–5]. Under inflammatory stimuli, macrophages become activated through

the interaction of the Toll-like receptors (class of proteins that play a key role in the innate immune system) with specific cytokines, such as interleukin-1β (IL1β), interleukin-6 (IL6) and tumour necrosis factor-α (TNFα), and/or bacterial lipopolysaccharides [3,4,6]. Once activated, macrophages initiate the nuclear factor-κB (NF-κB) translocation signalling pathway, which is a common pathological mechanism in several inflammatory diseases [2,7]. Thereby, activated macrophages are tangled in inflammatory response through the production of a wide range of molecules, such as cytokines, chemokines, inflammatory enzymes, and growth factors [2,7]. These molecules, as an immune-defensive mechanism, can act as both pro- or anti-inflammatory mediators, and thus induce either deleterious effects or promote the resolution of inflammation [2,7]. Macrophages play then a critical role in the balance between pro- and anti-inflammatory mediators to ultimately shutdown the outcomes of the inflammatory response [1,2,7]. This role identifies macrophages as both local and systemic key players in inflammatory diseases, and henceforth their efficient targeting is a crucial aspect. Glucocorticoids (GCs) are the cornerstone therapy used in the management of several inflammatory diseases, because of their strong anti-inflammatory and immunosuppressive properties [7–9]. One of these drugs, prednisolone, is highly effective in the suppression of inflammation-activated signalling, such as the NF-κB pathway [7–9]. Consequently, the drug-induced NF-κB regulation leads to the suppression of multiple pro-inflammatory cytokines, such as IL1β, IL6, and TNFα, which foster the inflammatory response [7,8,10,11]. Despite the effective anti-inflammatory mechanism of action of GCs, the lack of selectivity towards the inflamed tissues bestows the use of high doses, which further induce deleterious side effects [8,9,12]. Additionally, some cases of drug-resistance have been reported in patients with severe asthma, as well as, in other chronic obstructive pulmonary diseases [8,12]. This inevitably compromises the anti-inflammatory efficacy of GC-based therapy. Despite the advances in nanomedicine proved to improve the delivery of GCs, the translation into the clinic remains a challenge [9]. There is still the need to overcome some drawbacks particularly related to: (*i*) the safety and physiologic stability of the carrier itself, (*ii*) the ability to effectively and controllably release loaded cargo and, henceforth, (*iii*) the intracellular drug dose effectiveness. In this study, we propose polymersomes to enhance the anti-inflammatory properties of prednisolone disodium phosphate (PDP), while reducing the widespread off-target effects and the drug-resistance for the treatment of inflammatory disorders. Particularly, we used pH responsive polymersomes made of amphiphilic poly(2-methacryloyloxyethyl phosphorylcholine)–poly(2-(diisopropylamino)ethyl methacrylate) (PMPC–PDPA) diblock copolymers. The biocompatible nature of the PMPC block endows polymersomes with similar stealth properties to poly(ethylene glycol), thus being resistant to unspecific protein adhesion [13–15]. Additionally, PMPC binds to the scavenger receptor B type I (SR-BI) highly expressed in macrophages, which in turn enables the selective binding and internalisation of PMPC–PDPA polymersomes as we recently observed [13–16]. Whereas, the PDPA block bestows the pH responsive nature of polymersomes, as at pH lower than 6.2 (the PDPA pK_a) enables the polymersomes disassemble and hence release of loaded drug [17]. We have amply demonstrated [14,17–22] that such feature enables the intracellular cargo delivery, where the polymersome disassembly is confined within endosomes. Hence, the associated increase in osmotic pressure allows its endosomal escape and the release of loaded PDP molecules within the cell cytosol. In addition to this, during inflammation, particularly the most severe, the local environment pH can drop as low as to six due the cellular acidosis [23]. Herein, we studied the in vitro cellular uptake of PMPC–PDPA polymersomes, loaded PDP targeted release and hence its therapeutic effect in human macrophages.

2. Materials and Methods

2.1. Preparation of PMPC–PDPA Polymersomes

The $PMPC_{25}$–$PDPA_{68}$ and Cyanine5–$PMPC_{25}$–$PDPA_{70}$ copolymers were synthesised by atom-transfer radical polymerisation (ATRP) according to a previously published protocol [24,25] (details on supplementary materials about the experimental procedures and characterization).

Polymersomes made by self-assembly of the $PMPC_{25}$–$PDPA_{68}$ copolymers (Figure S1a) in aqueous solution were prepared under sterile conditions using the film rehydration method as previously reported [13,21,26–28] with some modifications. Briefly, 25 mg of $PMPC_{25}$–$PDPA_{68}$ copolymer was dissolved in an organic solution of 2:1 (*v/v*) chloroform:methanol (Sigma-Aldrich, Dorset, UK). The organic solvents were evaporated under vacuum oven at 38 °C for 24 h, resulting in a uniform polymeric thin film. Then, the film was rehydrated with Dulbecco's phosphate-buffered saline (DPBS, Sigma-Aldrich, Dorset, UK) at stable neutral pH for a final concentration of 5 mg/mL, and left under continuous magnetic stirring (200 rpm, RT15 power, IKA-Werke GmbH & Co. KG, Staufen, Germany) at room temperature for eight weeks.

Formulations of PMPC–PDPA polymersomes loading prednisolone disodium 21-phosphate (PDP, $C_{21}H_{27}Na_2O_8P$, MW 484.39, λ (250 nm), Tokyo Chemical Industry Co., Ltd., Oxford, UK) were prepared also using the film rehydration method by dissolving the drug in methanol during the organic phase prior to copolymer film formation. Additionally, for imaging fluorescence techniques, Cy5–PMPC–PDPA polymersomes were prepared using above-mentioned film rehydration method. Mainly, during the organic phase 10% (*w/w*) Cy5–$PMPC_{25}$–$PDPA_{70}$ (Figure S1b) was dissolved together with the $PMPC_{25}$–$PDPA_{68}$ copolymer. Afterwards, all formulations of PMPC–PDPA polymersomes were purified as previously described [29] firstly by centrifugation (2000 rcf, 20 min, 20 °C), following the size exclusion chromatography.

2.2. Characterisation Studies

2.2.1. Size and Size Distribution Study

The hydrodynamic diameter (D_h) and polydispersity index of PMPC–PDPA polymersomes were determined by dynamic light scattering (DLS) using the Zetasizer Nano ZS (Zen1600, Malvern Instruments Ltd., Worcestershire, UK) with a 633 nm HeNe laser in a scattering angle of 173°. Measurements were recorded at 20 °C in triplicate and samples were diluted for an average count rate between 100–300 kcps.

2.2.2. Morphology Study

The morphology and size of PMPC–PDPA polymersomes were analysed using the JEOL 100CX II transmission electronic microscope (TEM) (JEOL, Welwyn Garden City, UK) with a tungsten-filament 100 kV, and equipped with a Gatan Erlangshen ES500W camera. Prior to TEM imaging, samples were stained with 0.75% (*w/v*) phosphotungesteic acid (Sigma-Aldrich, Dorset, UK) in earlier prepared glow-discharged copper grids (Agar Scientific, Essex, UK), following a previously reported protocol [30].

2.2.3. Polymer and Drug Quantification Study

The amount of $PMPC_{25}$–$PDPA_{68}$ copolymer and loaded drug after purification process was determined by high-performance liquid chromatography (HPLC) using a Dionex Ultimate®3000 (Thermo Scientific, Dartford, UK) This instrument is equipped with a variable wavelength detector and a C18 analytical column (Jupiter Phenomenex 300A, 150 × 4.6 mm, 5 μm). The samples, previously diluted in DPBS at pH 2.0, were run according to a ramp gradient of eluent A [0.05% (*v/v*) trifluoroacetic acid (TFA, Thermo Fisher, Dartford, UK) in Milli-Q filtered H_2O] and eluent B [0.05% (*v/v*) TFA in methanol]: For 10 min from 5% to 100%; kept constant for 15 min and returned within 1 min to initial condition. By using the Chomeleon software (version 6.80, Thermo Scientific, Dartford, UK), the peak area was integrated at respective elution time and λ on the HPLC system to analyse the UV absorption of $PMPC_{25}$–$PDPA_{68}$ at λ (220 nm) and PDP at λ (250 nm). The amount of $PMPC_{25}$–$PDPA_{68}$ copolymer and PDP was quantified using their respective calibration curves. Further analysis on the drug encapsulation and loading efficiencies were determined using a previously reported method [18] (details on Supplementary Materials).

2.2.4. Drug Release Study

The PDP release study was performed using the dialysis method under sink conditions as previously described with some modifications [31]. Briefly, 1 mL of PDP loaded PMPC–PDPA polymersomes or free drug (at the same concentration of the loaded one) was filled in a cellulose ester dialysis membrane tube (3.5–5 kDa MWCO, Float-a-Lyzer G2, Spectrum Laboratories Inc., Sigma-Aldrich, Dorset, UK). Then, it was dialysed against 10 mL of outer buffer solution under continuous magnetic stirring (200 rpm, RT15 power, IKA-Werke GmbH & Co. KG, Staufen, Germany) at 37 °C for 50 h. These dialyses were carried out against three different outer buffer pH conditions: PBS solution at pH 7.4; acetate-buffered solution at pH 6.5 and 5.0. At regular time points, aliquots (200 µL) were withdrawn and the same volume of respective fresh buffered solution were replaced in order to maintain the sink conditions. The quantification of permeated drug aliquots throughout the 50 h was determined by measuring the UV absorbance of PDP at λ (250 nm) using the UV-Vis microplate spectrophotometer (Synergy HT, Biotek, Swindon, UK) and normalised to the free drug release profile. Mathematical models for drug-release kinetics (Table S1), including zero-order and first-order equations, Higuchi, Hixson–Crowell and Korsmeyer–Peppas models, were applied to each obtained profile to evaluate the mechanism of drug release (details on Supplementary Materials). The fitting of each model was evaluated based on the correlation coefficient (r^2) values for each model fit.

2.3. In Vitro Cellular Studies

2.3.1. Cell Culture and Differentiation

Human leukemic monocytes (THP-1) were cultured and maintained in RPMI-1640, containing 2 mM L-glutamine, 25 mM Hepes (Sigma-Aldrich, Dorset, UK) and supplemented with 10% (*v/v*) heat-inactivated fetal bovine serum (FBS, Sigma-Aldrich, Dorset, UK), 1% (*v/v*) penicillin-streptomycin (Sigma-Aldrich, Dorset, UK), and 0.1% (*v/v*) amphotericin B (Sigma-Aldrich, Dorset, UK). THP-1 cells were used for all in vitro experiments between passage numbers nine and twenty.

THP-1 Blue™ NF-κB reporter cells purchased from InvivoGen were maintained in the same cell culture medium plus supplemented with 100 µg/mL Normocin™ (InvivoGen, Toulouse, France). In addition, 10 µg/mL blastacidin (InvivoGen, Toulouse, France) was added to the growth medium every two passages to maintain selective pressure. The in vitro experiments with these cells were carried out between passage numbers three and nine.

Prior to all in vitro cellular studies, THP-1 cells differentiation into mature macrophages-like state (M0-macrophages) was induced through incubation with 10 ng/mL of phorbol 12-myristate 13-acetate (PMA, Sigma-Aldrich, Dorset, UK) for 48 h in a humidified atmosphere, 95% air, 5% CO_2 at 37 °C [6].

2.3.2. Cell Viability Assay

For the cell viability assay, THP-1 cells were seeded at a concentration of 5×10^3 cells per well in 96-well plates (CytoOne) and differentiated as mentioned above. Increasing concentrations of PMPC–PDPA polymersomes from 1.3 to 2.0 mg/mL were then incubated for 24 and 48 h in a humidified atmosphere, 95% air, 5% CO_2 at 37 °C. In another experiment, M0-macrophages were incubated with PMPC–PDPA polymersomes (<600 µg/mL) loaded with PDP in raging concentrations 2.5 to 40 µg/mL for 24 and 48 h in a humidified atmosphere, 95% air, 5% CO_2 at 37 °C. Additionally, free PDP in PBS solution raging the same concentrations of the loaded one was also incubated with M0-macrophages for 24 and 48 h. Control wells were incubated with equivalent volumes of cell culture medium and/or a solution of 10% (*v/v*) dimethyl sulfoxide (DMSO, Sigma-Aldrich, Dorset, UK) in DPBS. Later on, to evaluate the cytotoxicity of all treatments, the Real-Time-Glo™ MT Cell Viability Assay (Promega Corporation, Hampshire, UK) was used following the manufacturer protocol.

2.3.3. Cell Uptake Imaging

Cell imaging was performed using confocal laser scanning microscopy (CLSM, Leica SP8, Milton Keynes, UK). Firstly, THP-1 cells were seeded at a concentration of 5×10^4 cells per glass-bottom Petri dish (Ibidi) and differentiated as above mentioned. Cy5–PMPC–PDPA polymersomes (0.6 mg/mL) were then incubated for 0.5, 1, 2, 4, 6, 12, 24, and 48 h, in a humidified atmosphere, 95% air, 5% CO_2 at 37 °C. After each incubation time point, followed by three steps of DPBS washing, M0-macrophages were stained for CLSM live imaging. Hoechst 33342 (Sigma-Aldrich, Dorset, UK) and far-red Cell Mask™ (Life Technologies Ltd., Thermo Fisher Scientific, Renfrew, UK) were used for nuclear and cell membrane staining, respectively. At least 10 different regions of the Petri dishes were captured and analysed using the Fiji ImageJ software (version 2.0). For the quantification of Cy5–PMPC–PDPA polymersomes within macrophages, their fluorescent intensity signal was normalised relative to the nuclear intensity signal.

2.3.4. NF-κB Signalling Imaging and Quantification Assay

NF-κB signalling imaging was preformed using CLSM. Firstly, THP-1 cells were seeded at a concentration of 5×10^4 cells per glass-bottom Petri dish (Ibidi) and differentiated as above mentioned. Followed by M0-macrophage activation to M1 state, which was induced with incubation of 600 ng/mL of lipopolysaccharide (LPS, Sigma-Aldrich, Dorset, UK) for at least 6 h in a humidified atmosphere, 95% air, 5% CO_2 at 37 °C [6]. Then, M1-macrophages were incubated with PMPC–PDPA polymersomes (0.6 mg/mL), either free PDP or PDP loaded polymersomes (10 μg/mL) for 24 h in a humidified atmosphere, 95% air, 5% CO_2 at 37 °C. Following treatment, cells were washed with DPBS and fixed using 3.7% formaldehyde (Sigma-Aldrich, Dorset, UK) for 10 min at room temperature (RT). After fixation step, followed by DPBS washing for the membrane permeabilization step, cells were incubated with 0.2% Triton-X (Sigma-Aldrich, Dorset, UK) for a further 10 min at RT. Then, the immunostaining blocking was performed using 5% bovine serum albumin (BSA) (Sigma-Aldrich, Dorset, UK), to prevent unspecific antibody binding. After 1 h at RT, cells were incubated with NFκB p65 Antibody (F-6) Alexa Fluor® 647 (Santa Cruz Biotechnology Inc., Heidelberg, Germany) diluted in 1% BSA overnight in a humidified chamber at 4 °C. The following day, cells were washed with DPBS and the nucleus was stained with Hoescht 33342 (Sigma-Aldrich, Dorset, UK) for 10 min at RT, before visualisation under CLSM. At least 10 different regions of the petri dishes were acquired and the NF-κB nuclear translocation imaging analysis was evaluated by co-localisation (Pierce's coefficient values) of the NF-κB and nucleus fluorescence intensity signals using Fiji ImageJ software (version 2.0). Additionally, the quantification of macrophages inflammation levels related to the NF-κB signalling activity was carried out in the THP-1 Blue™ NF-κB reporter cells, as previously reported [32]. These cells are stably transfected and express a secreted embryonic alkaline phosphatase (SEAP) reporter gene driven by an interferon-β minimal promoter fused to five copies of the NF-κB transcription factor, which promotes cytokines production. Then, once the NF-κB translocation from the cytosol to the nucleus induces the secretion of the SEAP, this can be quantified by the absorbance read at λ (570 nm) using the UV-Vis microplate spectrophotometer (ELx800, BioTek, Swindon, UK). For the SEAP assay, THP-1 NF-κB reported cells were seeded at a concentration of 5×10^3 cells per well in 96-well plates (CytoOne) and differentiated as above-mentioned. Followed by M1-macrophage activation with 600 ng/mL of LPS for 6 h [6], cells were then incubated with each one of the treatments for more than 6 and 24 h in a humidified atmosphere, 95% air, 5% CO_2 at 37 °C. The detection and quantification of SEAP activity from the collected supernatant was then preformed according to the manufacturer.

2.3.5. RNA Extraction, Reverse Transcription, and Real-Time Quantitative Polymerase Chain Reaction

Analyses on the gene expression of inflammation-related markers, including TNFα, IL1β, IL6 and IL8, was assessed using real-time quantitative polymerase chain reaction (RT-qPCR). Firstly, THP-1 cells were seeded at a concentration of 10^6 cells per well in 96-well plates (CytoOne) and differentiated

as above-mentioned. Following the M1-macrophage activation with 600 ng/mL of LPS (non-treated control), cells were incubated either with PMPC–PDPA polymersomes (0.6 mg/mL), free PDP or PDP loaded polymersomes (10 μg/mL) for 6 h in a humidified atmosphere, 95% air, 5% CO_2 at 37 °C. Cells were then lysed and the RNA was extracted following the RNeasy mini kit (Qiagen, Manchester, UK) protocol pre-installed in the QIAcube (Qiagen, Manchester, UK). The total RNA concentration was measured with NanoDrop 8000 spectrophotometer (Fisher Scientific, Dartford, UK). Complementary DNA (cDNA) was synthesised from every 1 μg of total mRNA in 20 μL volume with QuantiTect Reverse Transcription Kit (Qiagen, Manchester, UK) according to the manufacture's protocol. This procedure provided a fast and efficient cDNA synthesis with integrated removal of genomic DNA contamination. Briefly, the sample of RNA is incubated at 42 °C for 2 min to effectively remove containing genomic DNA, then the reaction occurred for another 15 min at 42 °C and then inactivated at 95 °C. RT q-PCR reaction was performed on yield cDNA synthesised from each sample using QuantiTec® Rotor-Gene™ SYBR Green RT-PCR kit (Qiagen, Manchester, UK) using the Qiagility instrument software (Qiagen, Manchester, UK). This software enables rapid and high-precision system of sample preparation for RT-qPCR analysis, providing a step-by-step guidance for automatic calculation of all primers, cDNA template and Rotor-Gene SYBR Green master mixes needed for the reaction. The list of designed primers of each target gene and reference gene used for the gene expression experiments is in the Supplementary Information (Table S3). Following sample preparation, the PCR mixtures are placed in the Rotor-Gene Q cycler (Qiagen, Manchester, UK) and amplification process starts using the following protocol steps: Initial cycling step at 95 °C during 5 min for the DNA polymerase activation; followed by 40 cycles of 95 °C during 5 s for denaturation; and 60 °C during 10 s for combined annealing and extension for all primers. RT-qPCR data analysis of folds-changes in gene expression levels was determined by the—ΔΔCt method (details in supplementary materials), using cycle threshold (Ct) values acquired from the amplification curve using the Rotor-Gene Q instrumentation software (Qiagen, Manchester, UK).

2.3.6. Enzyme Linked Immunosorbent Assay

IL6 and TNFα protein levels secreted by macrophages were quantified by the enzyme linked immunosorbent assay (ELISA). Firstly, THP-1 cells were seeded at a concentration of 10^6 cells per well in 96-well plates (CytoOne) and differentiated as above mentioned. Following the M1-macrophage activation with 600 ng/mL of LPS (non-treated control), cells were incubated either with PMPC–PDPA polymersomes (0.6 mg/mL), free PDP or PDP loaded polymersomes (10 μg/mL) for 24 h in a humidified atmosphere, 95% air, 5% CO_2 at 37 °C. Cell supernatants were collected and then the ELISA technique was used following the manufacturer protocol (Invitrogen, Thermo Scientific, Dartford, UK).

2.4. Statistical Analysis

Statistical analyses were performed using GraphPad Prism (version 8.2.1). The difference between three and more groups was, respectively, analysed through one-way or two-way ANOVA multiple comparisons. Differences between two groups was evaluated by two-tailed Student's *t*-test. The differences were statistically significant when * $p < 0.05$, ** $p < 0.01$, *** $p < 0.001$ and **** $p < 0.0001$.

3. Results and Discussion

3.1. PMPC–PDPA Polymersomes Are Suitable Nanocarriers for PDP

The size of PMPC–PDPA polymersomes is one of the key factors to predict both their stability and behaviour in vivo, including circulation time, biodistribution, cell binding affinity, and uptake [20,22,33–35]. All the formulations of polymersomes were characterised in terms of size, distribution, and morphology by DLS and TEM. Light scattering analyses revealed that the loading of PDP drug into PMPC–PDPA polymersomes corresponds to an increase in size from an average hydrodynamic diameter (D_h) of 117 ± 5 to 178 ± 4 nm (Figure S2a). Such a change can be

attributed in part to the large number of drug molecules loaded within the polymersomes (defined as the drug loading efficiency; Figure S2c) and consequent swelling of the vesicles membrane. In addition, the amount of encapsulated PDP within PMPC–PDPA polymersomes, quantified using HPLC, resulted in 12% ± 4% of drug encapsulation efficiency (details in Supplementary Materials). TEM analyses of PMPC–PDPA polymersomes confirmed the formation of spherical vesicles with D_h size in agreement with the DLS measurements (Figure 1a, top image). While, TEM imaging of the PDP loaded polymersomes revealed the formation of vesicles with an oblate shape (Figure 1a, bottom image). The non-spherical nature of the polymersomes hinders the interpretation of the DLS size distribution and while the size increase can be still attributed to the drug loading, the tubular shapes might not be fitted by the traditional models based on spherical geometry. The PDP structure (Figure S2d) is partly polar and partly apolar (cholesterol-like) and such amphiphilic nature drives its insertion within the PDPA hydrophobic membrane of polymersomes. Additionally, the PDP anionic phosphate group could potentially interact with some residual positive charges still present in the PDPA block. Both interactions favour the encapsulation process and thus justify the very high loading numbers of drug molecules per polymersome (Figure S2c). In a previous work [26], we demonstrated that the inclusion of cholesterol, a molecule similar to PDP, within PMPC–PDPA polymersomes during the film hydration method stabilises the formation of tubular vesicles. Thus, we infer that the PDP insertion results in the formation of oblate polymersomes.

3.2. PMPC–PDPA Polymersomes Enable a pH-Controlled Drug Release

To prove the ability of PMPC–PDPA polymersome to release the PDP as a function of the environment pH, we measured the drug release under different pH conditions at 37 °C, mimicking the physiologic pH 7.4, the inflamed extracellular tissue (pH 6.5), and the intracellular compartments (pH 5.0). For PDP loaded polymersomes dialysed under conditions at pH 5.0, resulted in a biphasic drug release profile (Figure 1b) with an initial burst (immediate pulse of 55% within 1 h) followed by a sustained drug release overtime. As expected, under pH 5.0 conditions the PDPA amino groups (pKa 6.2; Figure S1a) get protonated and positively charged. The change of polarity makes the PDPA hydrophilic and hence the PMPC–PDPA copolymers are no longer capable of forming polymersomes driving a fast disassembly process [14,17–22] hence, resulting in a burst release of the majority of the PDP. The following sustained release suggests a mild interaction between the now cationic PDPA and the anionic PDP phosphate group. Results at pH 6.5 (Figure 1b) also suggest a timed sustained drug release profile (up to 22%) starting after 8 h under dialysis. The two effects are highly desirable within both the macrophage intracellular or inflamed milieu where the drug needs to be freed. The drug release profiles were analysed using several mathematical models (Table S1): Zero-order, first-order, Hixson–Crowell, Higuch, and Korsmeyer–Peppas. The regression coefficient (r^2) analyses (Table S1) confirm the Higuchi and zero-order as the best fitting model for pH 5.0 and pH 6.5, suggesting that the PDP release from the PMPC–PDPA polymersomes is indeed caused by a controlled diffusion mechanism [36,37]. This study proves not only the acidic pH responsiveness of the PDPA block to bestow the rapid disassemble of polymersomes, but also the drug release profile (Figure 1b) demonstrated the high stability of PMPC–PDPA polymersomes at physiologic pH 7.4.

3.3. PMPC–PDPA Polymersomes Enable a Rapid Intracellular Drug Delivery

PDP, similar to most glucocorticoids, downregulate inflammatory genes reversing histone acetylation binding to glucocorticoid receptors (GR) and thus triggering the recruitment of histonedeacetylase-2 (HDAC2) to the transcription complex [8]. Thus, the site of action of PDP is indeed the cytosol. Hence, the dynamics of cellular uptake of polymersomes by macrophages is a key parameter to achieve efficient intracellular delivery [35]. Cellular uptake studies of Cy5–PMPC–PDPA polymersomes (Cy5–Psome; Figure S2b) was assessed using live imaging CLSM. The amount of polymersomes increases in a time-dependent manner up to 48 h, resulting in a bimodal profile (Figure 1c), with a rapid internalisation within 3 h followed by a plateau. The PMPC–PDPA

polymersomes bind very quickly to the cell surface, saturating their receptors and dwell at the cell membrane for the first 30 min, as confirmed by the co-localisation of the merged fluorescence signals (Figure 2). A rapid and enhanced cellular uptake of PMPC–PDPA polymersomes was previously reported [15,20,21]. The internalisation mechanism is possibly due the combination of the intrinsic professional phagocytic activity of macrophages [3–5] and with the high affinity interaction of the PMPC block towards the scavenger receptor class B type I (SR-BI) [13–16]. This enables polymersomes to selectively bind to the SR-BI cell receptors, a process that triggers rapid internalisation within macrophages via endocytosis [13–15,19–22].

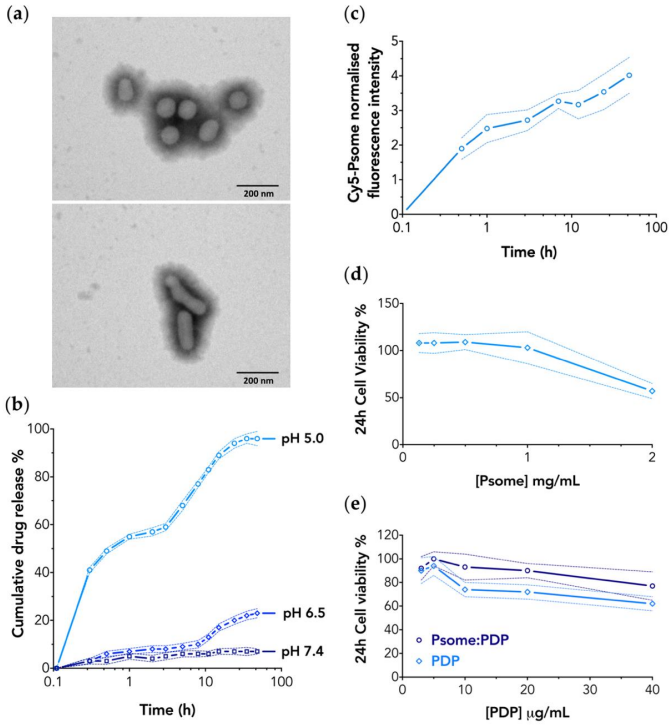

Figure 1. (**a**) Representative TEM images of empty (top) and PDP loaded PMPC–PDPA polymersomes (bottom) produced via film rehydration method (200 nm scale bar). (**b**) PDP cumulative drug release profile in each tested pH condition over 50 h at 37 °C. Data express as mean ± SD (n = 3). (**c**) Cy5–PMPC–PDPA polymersomes normalised fluorescent intensity relative to the nucleus signal measured as a function of time upon uptake by macrophages. Data express the mean ± SD (10 images for n = 2). Cell viability assay after 24 h incubation with increasing concentrations of (**d**) unloaded PMPC–PDPA polymersomes (Psome), (**e**) either free PDP or PDP loaded polymersomes (Psome:PDP). Data express as mean ± SD (n = 3).

An important aspect to take into consideration is the potential effect of polymersomes towards cell viability, because of such an enhanced cell uptake level. Most importantly such a fast entry does not affect cell viability in M0-macrophages. Both 24 and 48 h of incubation time with PMPC–PDPA polymersomes showed (Figure 1d; Figure S3a) no significant effects on cells survival, and no cytotoxicity was observed up to a concentration of 1 mg/mL. Further cytotoxicity investigations were carried out aiming to compare M0-macrophages viability as a function of treatment with either the PDP loaded

PMPC–PDPA polymersomes or the free drug (both tested using the same PDP final concentration), after 24 and 48 h of incubation. M0-macrophages treated with PDP loaded polymersomes exhibited over 80% of cell viability upon 24 h of incubation time (Figure 1e). The cytotoxic effect of the free PDP was comparable to the loaded one only at lower concentrations (<10 µg/mL). In contrast, cells viability was reduced in a concentration-dependent manner after 48 h of incubation for both free and loaded PDP (Figure S3b), resulting in 30% decrease of cell viability at the highest concentration.

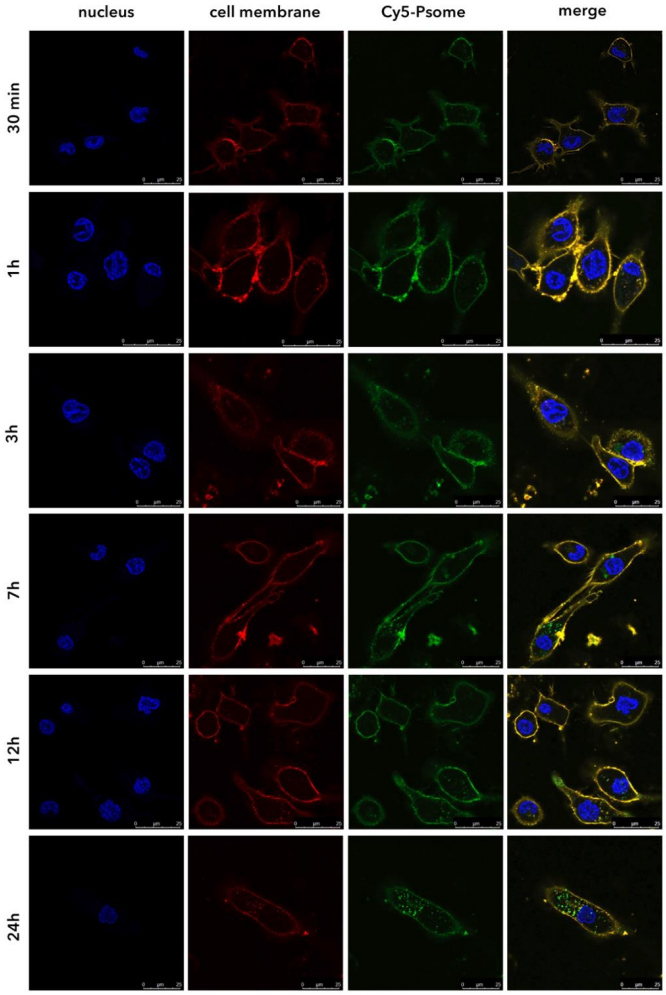

Figure 2. Representative CLSM images of Cy5–PMPC–PDPA polymersomes (green fluorescence intensity signal) cellular uptake overtime (scale bar: 25 µm). Staining of the cell nuclei (blue fluorescence intensity signal) with Hoechst 33342 and cell membrane (red fluorescence intensity signal) with far-red CellMask™. The yellow fluorescence intensity signal corresponds to the co-localisation (merge) of the Cy5–PMPC–PDPA polymersomes and cell membrane fluorescence signals.

3.4. PDP Loaded PMPC–PDPA Polymersomes Promote Inflammation Resolution In Vitro

In vitro cellular studies were carried out to evaluate the anti-inflammatory effect of PDP loaded PMPC–PDPA polymersomes in activated M0-macrophages (also known as M1-macrophages). We stimulated M0- into M1-macrophages by exposing them to LPS and their activation was assessed by checking for the nuclear translocation of the pro-inflammatory transcription factor NF-κB [7,38]. As shown by immunofluorescence microscopy (Figure 3a), the NF-κB transcription factor is mainly cytosolic within M0-macrophages and upon LPS stimulation the NF-κB translocate to the nucleus giving rise to M1-macrophages. Such an assay can be easily quantified by imaging and we measured 80% cells presenting nuclear NF-κB fluorescence intensity in good agreement with previously reported data [38]. The NF-κB activity was also measured using THP-1 genetically modified with a NF-κB reporter that upon translocation secretes in the media alkaline phosphatase [38]. The secreted embryonic alkaline phosphatase (SEAP) assay allows the detection and quantification of NF-κB activation through the quantification of the phosphatase level by colorimetry. Both assays allow for assessing anti-inflammatory activity of free PDP, loaded, and unloaded PMPC–PDPA polymersomes. Quantitative imaging analysis of immunofluorescence macrographs (Figure 3b) revealed a mild anti-inflammatory effect of unloaded polymersomes and a reduction to 60% with the free PDP. While PDP loaded polymersomes significantly reduce ($p < 0.0001$ compared to control) the nuclear translocation of NF-κB by 50% after 24 h incubation. Results plotted in Figure 3c showed that all treatments reduced the amount of SEAP secreted with respect to the M1-macrophages (used as control) either after 6 or 24 h of incubation. Remarkably, both unloaded and PDP loaded PMPC–PDPA polymersomes show a significant reduction on SEAP production after 6 h of incubation. This reduction was much more significant ($p < 0.001$ compared to control) after 24 h of treatment of M1-macrophages with PDP loaded polymersomes. We thus demonstrated that PMPC–PDPA polymersomes mediated intracellular delivery of PDP and enhances its anti-inflammatory effect. The inhibition on the NF-κB transduction signalling pathway is indeed significantly higher ($p < 0.05$ compared to free PDP). In the early stages of the inflammation, Nf-κB translocation from the cytosol to the nucleus occurs, as confirmed by the differences in the CLSM imaging analysis between M0- and M1-macrophages (Figure 3a). The translocation of Nf-κB induces then the upregulation of pro-inflammatory genes, TNFα, IL1β, IL6, and IL8 [7,10,38]. We thus measured such genes mRNA expression by RT-qPCR (Figure 3d) confirming that the transition from M0 to M1 corresponds with upregulation of all these pro-inflammatory genes [6,11]. Further analyses of the RT-qPCR data plotted in Figure 3d revealed that 6 h incubation with any of the treatments significantly decreases gene expression levels of all inflammation-related markers compared to the control. Most notably, all the treatments equally decrease gene expression levels of IL8 (a potent neutrophil chemo-attractant [39]) by 2-fold ($p < 0.0001$ compared to control). Such data suggest that PDP loaded PMPC–PDPA polymersomes can also potentially regulate the activation of neutrophils in vivo, and hence modulate the recruitment of leucocytes to the inflammation site. Both RT-qPCR and ELISA results confirmed the well-known immunosuppressive and anti-inflammatory effect of PDP [8,12]. The free PDP indeed significantly ($p < 0.0001$ compared to control) decreases the gene expression of all the tested pro-inflammatory cytokines (Figure 3d). Likewise, PDP loaded PMPC–PDPA polymersomes significantly downregulate the IL1β and IL6 gene expression levels (more than 10-fold for $p < 0.0001$ compared to control). Particularly, IL6 plays not only an important role in the activation of both innate and adaptive immune system, but it is also involved in the regulation of chronic inflammatory response [10,40]. ELISA analysis plotted in Figure 3e further revealed that IL6 protein secretion levels are significantly decreased ($p < 0.0001$ compared to control) after 24 h of incubation with PDP, either loaded or as free drug. Similar behaviour was observed for TNFα secretion levels (Figure 3e), which significantly decreases ($p < 0.001$ compared to control) upon incubation with any of the treatments. Though, and in agreement with the gene expression studies, ELISA results also show that there was not a significant difference between free and loaded PDP within PMPC–PDPA polymersomes. In conclusion, PDP loaded PMPC–PDPA polymersomes have a significant effect on the inhibition of the NF-κB nuclear translocation (Figure 3c). They also modulate the gene expression profiles of

pro-inflammatory mediators (Figure 3d), and the secretion level of IL6 and TNFα proteins (Figure 3e) by M1-macrophages.

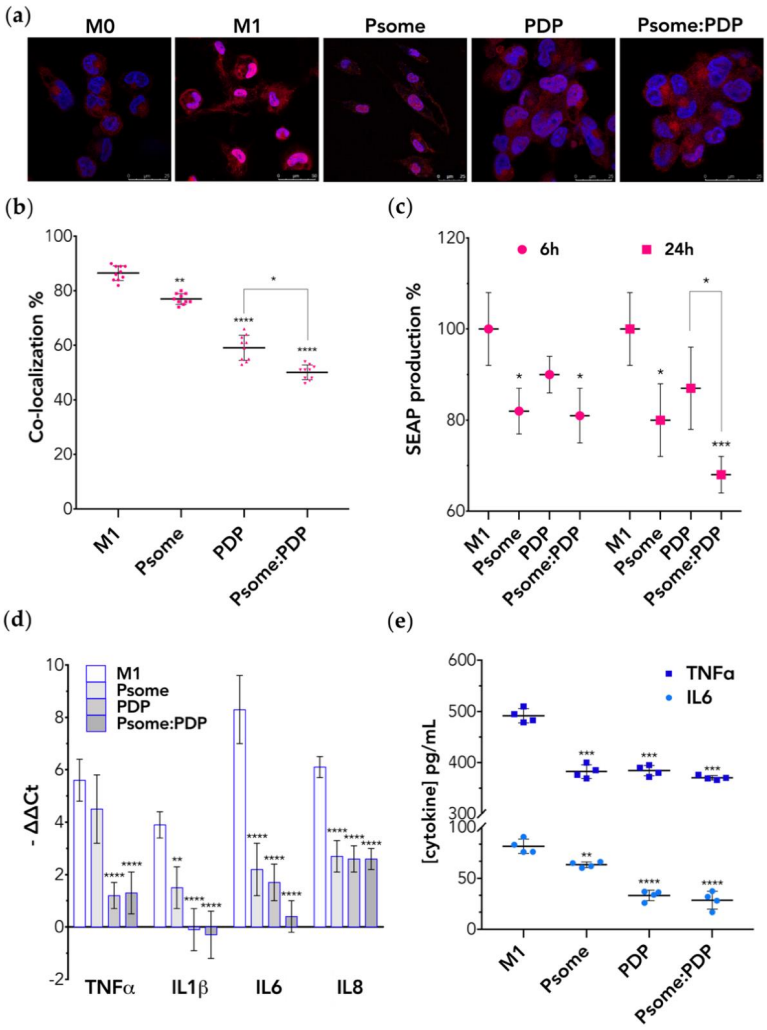

Figure 3. In vitro inflammation-related cellular studies on M1-macrophages after incubation with either PMPC–PDPA polymersomes (Psome), free PDP, or PDP loaded polymersomes (Psome:PDP). (**a**) Representative CLSM images of NFκB (red fluorescence intensity signal) translocation from cytoplasm to the nucleus (blue fluorescence intensity signal) (scale bar: 25 μm). (**b**) Co-localisation analysis of the merged fluorescence signals (pink). Data express as mean ± SD (5 images for $n = 2$). (**c**) SEAP assay for the quantification of Nf-κB nuclear translocation. Data express as mean ± SD ($n = 3$). (**d**) RT-qPCR of pro-inflammatory genes expression levels. Data express as mean ± SD ($n = 3$). (**e**) ELISA for IL6 and TNFα protein secretion levels. Data express as mean ± SD ($n = 4$). In all experiments, the differences were statistically significant when * $p < 0.05$, ** $p < 0.01$, *** $p < 0.001$, and **** $p < 0.0001$.

Remarkably, all the in vitro inflammation-related studies (Figure 3) suggest that unloaded PMPC–PDPA polymersomes inactivated the NF-κB signalling pathway in M1-macrophages and, as consequence, the gene expression of inflammation-related cytokines. We believe that this might be related to the phosphatidylcholine anti-inflammatory properties [41] possibly associated with its ability to target the SRBI cell receptor. It was previously reported [42] that this receptor regulates macrophage inflammation upon ligand binding, as the activation of the NF-κB is reduced and leads to the increase of anti-inflammatory mediators. Still, future studies need to be performed to understand these remarkable evidences. Taken together, with these in vitro studies, we confirm that LPS-activated NF-κB mediates the inflammatory response in macrophages. Moreover, we demonstrate that PDP loaded PMPC–PDPA polymersomes inhibit the NF-κB nuclear translocation pathway and hence reduce inflammation-related expression at molecular level.

4. Conclusions

PMPC–PDPA polymersomes have been demonstrated here to be a suitable drug delivery carrier enabling both drug's protection and stability overtime under mimicking physiologic pH conditions. The drug release study confirmed the pH responsiveness of polymersomes to acidic pH, mimicking the intracellular endosomal compartments. This enables an efficient intracellular and targeted delivery of loaded prednisolone into the cytosol. In vitro cell uptake studies revealed that PMPC–PDPA polymersomes enhance the accumulation of prednisolone within macrophages without affecting their viability. Plus, this increases the intracellular bioavailability of effective low dosage of PDP and hence its anti-inflammatory effect. Indeed, we show that the inflammation-activated NF-κB signalling pathway was shut down in inflamed macrophages treated with PDP loaded within polymersomes, and as consequence the expression of pro-inflammatory genes and proteins is reduced. Overall, pH-responsive PMPC–PDPA polymersomes ensure stability and selectivity towards target cells, as well as promote inflammation resolution in vitro. We prove the therapeutic potential of pH-responsive polymersomes to reduce the well-known deleterious side effects and the resistance that compromises the effectiveness of glucocorticoid therapy in the treatment of inflammatory disorders.

Supplementary Materials: The following are available online at http://www.mdpi.com/1999-4923/11/11/614/s1. Figure S1: Chemical structure of (a) $PMPC_{25}$–$PDPA_{68}$ and (b) Cy5–$PMPC_{25}$–$PDPA_{70}$. Figure S2: (a) DLS data on the hydrodynamic diameter (D_h) and polydispersity index (PDI) values of all formulations of unloaded and PDP loaded PMPC–PDPA polymersomes ($n = 3$). Analysis on the PDI values below 0.2 indicates a formulation of polymersomes with monodisperse and homogeneous size distribution. (b) TEM representative image of Cy5–PMPC–PDPA polymersomes produced via film rehydration method (200 nm scale bar). (c) DLS data on the number of PMPC–PDPA polymersomes as a function of the D_h. Analysis on the drug loading capacity represented as the number of PDP molecules per polymersome as a function of their size. (d) Cryo-TEM representative image of PMPC–PDPA polymersomes produced via pH-switch method (200 nm scale bar). (e) Chemical structure and electrostatic surfaces of prednisolone disodium 21-phosphate (PDP) and respective representation of the electrostatic surfaces. Table S1: Mathematical models for drug-release kinetics. Table S2: Correlation coefficient (r^2) from various drug release mathematical models for each pH profile. Figure S3: Cell viability assay after 48 h incubation with increasing concentrations of (a) unloaded PMPC–PDPA polymersomes, (b) either free PDP or PDP loaded polymersomes (Psome:PDP). Table S3: Forward (Fw) and reverse (Rv) gene sequences of designed primers (PRIMER-BLAS; Sigma-Aldrich) used for gene expression studies.

Author Contributions: Conceptualisation, V.M.G., L.R., C.N., A.O., S.R., and G.B.; Project administration, V.M.G. and L.R.; Investigation, V.M.G., A.P. (polymers synthetises), and L.R.-P. (Cryo-TEM); Formal analysis, V.M.G.; Visualisation, V.M.G.; Validation, L.R. and C.N.; Writing—original draft preparation, V.M.G.; Writing—review and editing, L.R., C.N., S.R., and G.B.; Supervision, G.B., S.R., and A.O.; Resources and funding acquisition, G.B. All authors gave final approval for publication.

Funding: This research was partly funded by the ERC (Grants: StG-MEViC 278793, PoC- AIDViC 543379, and CheSSTAG 769798 and the EPSRC (Grants: EP/N026322/1 and EP/I001697/1).

Acknowledgments: V.M.G. thanks the received financial support from FCT (Fundação para a Ciência e Tencnologia) through the FCT PhD Programmes and by POCH (Programa Operacional Potencial Humano), specifically by the Doctoral Programme on Cellular and Molecular Biotechnology Applied to Health Sciences for the grant (PD/BD/128388/2017). V.M.G. is also grateful to Ciro Lopez for his expertise and technical assistance with TEM. C.N. also thanks FCT for the Investigator grant (IF/00293/2015) and respective exploratory project, which is in the

framework of this work. L.R. sincerely thanks the Marie Skłodowska-Curie actions for supporting his research activities. A.P. gratefully acknowledges the NC3Rs UK for the financial support.

Conflicts of Interest: The authors declare no conflict of interest. The funders had no role in the design of the study; in the collection, analyses, or interpretation of data; in the writing of the manuscript, and in the decision to publish the results.

References

1. Dunster, J. The macrophage and its role in inflammation and tissue repair: Mathematical and systems biology approaches. *Wiley Interdiscip. Rev.-Syst. Biol. Med.* **2016**, *8*, 87–99. [CrossRef]
2. Chen, L.; Deng, H.; Cui, H.; Fang, J.; Zuo, Z.; Deng, J.; Li, Y.; Wang, X.; Zhao, L. Inflammatory responses and inflammation-associated diseases in organs. *Oncotarget* **2018**, *9*, 7204–7218. [CrossRef] [PubMed]
3. Fujiwara, N.; Kobayashi, K. Macrophages in inflammation. *Curr. Drug Targets Inflamm. Allergy* **2005**, *4*, 281–286. [CrossRef] [PubMed]
4. Oishi, Y.; Manabe, I. Macrophages in inflammation, repair and regeneration. *Int. Immunol.* **2018**, *30*, 511–528. [CrossRef] [PubMed]
5. Ginhoux, F.; Jung, S. Monocytes and macrophages: Developmental pathways and tissue homeostasis. *Nat. Rev. Immunol.* **2014**, *14*, 392–404. [CrossRef] [PubMed]
6. Lund, M.E.; To, J.; O'Brien, B.A.; Donnelly, S. The choice of phorbol 12-myristate 13-acetate differentiation protocol influences the response of THP-1 macrophages to a pro-inflammatory stimulus. *J. Immunol. Methods* **2016**, *430*, 64–70. [CrossRef] [PubMed]
7. Liu, T.; Zhang, L.; Joo, D.; Sun, S.C. NF-kappaB signaling in inflammation. *Signal Transduct. Target. Ther.* **2017**, *2*. [CrossRef]
8. Barnes, P.J. Mechanisms and resistance in glucocorticoid control of inflammation. *J. Steroid Biochem. Mol. Biol.* **2010**, *120*, 76–85. [CrossRef]
9. Lühder, F.; Reichardt, H.M. Novel Drug Delivery Systems Tailored for Improved Administration of Glucocorticoids. *Int. J. Mol. Sci.* **2017**, *18*, 1836. [CrossRef]
10. Brasier, A.R. The nuclear factor-kappaB-interleukin-6 signalling pathway mediating vascular inflammation. *Cardiovasc. Res.* **2010**, *86*, 211–218. [CrossRef]
11. Scheller, J.; Chalaris, A.; Schmidt-Arras, D.; Rose-John, S. The pro- and anti-inflammatory properties of the cytokine interleukin-6. *Biochim. Biophys. Acta* **2011**, *1813*, 878–888. [CrossRef] [PubMed]
12. Hayashi, R.; Wada, H.; Ito, K.; Adcock, I.M. Effects of glucocorticoids on gene transcription. *Eur. J. Pharmacol.* **2004**, *500*, 51–62. [CrossRef] [PubMed]
13. Colley, H.E.; Hearnden, V.; Avila-Olias, M.; Cecchin, D.; Canton, I.; Madsen, J.; MacNeil, S.; Warren, N.; Hu, K.; McKeating, J.A.; et al. Polymersome-mediated delivery of combination anticancer therapy to head and neck cancer cells: 2D and 3D in vitro evaluation. *Mol. Pharm.* **2014**, *11*, 1176–1188. [CrossRef] [PubMed]
14. Murdoch, C.; Reeves, K.J.; Hearnden, V.; Colley, H.; Massignani, M.; Canton, I.; Madsen, J.; Blanazs, A.; Armes, S.P.; Lewis, A.L.; et al. Internalization and biodistribution of polymersomes into oral squamous cell carcinoma cells *in vitro* and *in vivo*. *Nanomedicine (Lond.)* **2010**, *5*, 1025–1036. [CrossRef]
15. Massignani, M.; Canton, I.; Sun, T.; Hearnden, V.; Macneil, S.; Blanazs, A.; Armes, S.P.; Lewis, A.; Battaglia, G. Enhanced fluorescence imaging of live cells by effective cytosolic delivery of probes. *PLoS ONE* **2010**, *5*, e10459. [CrossRef] [PubMed]
16. Rizzello, L.; Robertson, J.D.; Elks, P.M.; Poma, A.; Daneshpour, N.; Prajsnar, T.K.; Evangelopoulos, D.; Canseco, J.O.; Yona, S.; Marriott, H.M.; et al. Targeting mononuclear phagocytes for eradicating intracellular parasites. *bioRxiv* **2017**. [CrossRef]
17. Contini, C.; Pearson, R.; Wang, L.; Messager, L.; Gaitzsch, J.; Rizzello, L.; Ruiz-Perez, L.; Battaglia, G. Bottom-Up Evolution of Vesicles from Disks to High-Genus Polymersomes. *iScience* **2018**, *7*, 132–144. [CrossRef]
18. Wang, L.; Chierico, L.; Little, D.; Patikarnmonthon, N.; Yang, Z.; Azzouz, M.; Madsen, J.; Armes, S.P.; Battaglia, G. Encapsulation of biomacromolecules within polymersomes by electroporation. *Angew. Chem. Int. Ed. Engl.* **2012**, *51*, 11122–11125. [CrossRef]

19. Lomas, H.; Du, J.; Canton, I.; Madsen, J.; Warren, N.; Armes, S.P.; Lewis, A.L.; Battaglia, G. Efficient encapsulation of plasmid DNA in pH-sensitive PMPC-PDPA polymersomes: Study of the effect of PDPA block length on copolymer-DNA binding affinity. *Macromol. Biosci.* **2010**, *10*, 513–530. [CrossRef]
20. Massignani, M.; LoPresti, C.; Blanazs, A.; Madsen, J.; Armes, S.P.; Lewis, A.L.; Battaglia, G. Controlling cellular uptake by surface chemistry, size, and surface topology at the nanoscale. *Small* **2009**, *5*, 2424–2432. [CrossRef]
21. Pegoraro, C.; Cecchin, D.; Gracia, L.S.; Warren, N.; Madsen, J.; Armes, S.P.; Lewis, A.; Macneil, S.; Battaglia, G. Enhanced drug delivery to melanoma cells using PMPC-PDPA polymersomes. *Cancer Lett.* **2013**, *334*, 328–337. [CrossRef] [PubMed]
22. Guan, L.; Rizzello, L.; Battaglia, G. Polymersomes and their applications in cancer delivery and therapy. *Nanomedicine (Lond.)* **2015**, *10*, 2757–2780. [CrossRef] [PubMed]
23. Lardner, A. The effects of extracellular pH on immune function. *J. Leukoc. Biol.* **2001**, *69*, 522–530. [PubMed]
24. Du, J.; Tang, Y.; Lewis, A.L.; Armes, S.P. pH-sensitive vesicles based on a biocompatible zwitterionic diblock copolymer. *J. Am. Chem. Soc.* **2005**, *127*, 17982–17983. [CrossRef] [PubMed]
25. Gaitzsch, J.; Delahaye, M.; Poma, A.; Du Prez, F.; Battaglia, G. Comparison of metal free polymer-dye conjugation strategies in protic solvents. *Polym. Chem.* **2016**, *7*, 3046–3055. [CrossRef]
26. Robertson, J.D.; Yealland, G.; Avila-Olias, M.; Chierico, L.; Bandmann, O.; Renshaw, S.A.; Battaglia, G. pH-sensitive tubular polymersomes: Formation and applications in cellular delivery. *ACS Nano* **2014**, *8*, 4650–4661. [CrossRef]
27. Battaglia, G.; Ryan, A.J. The evolution of vesicles from bulk lamellar gels. *Nat. Mater.* **2005**, *4*, 869–876. [CrossRef]
28. Fetsch, C.; Gaitzsch, J.; Messager, L.; Battaglia, G.; Luxenhofer, R. Self-Assembly of Amphiphilic Block Copolypeptoids - Micelles, Worms and Polymersomes. *Sci. Rep.* **2016**, *6*, 33491. [CrossRef]
29. Robertson, J.D.; Rizzello, L.; Avila-Olias, M.; Gaitzsch, J.; Contini, C.; Magoń, M.S.; Renshaw, S.A.; Battaglia, G. Purification of Nanoparticles by Size and Shape. *Sci. Rep.* **2016**, *6*, 27494. [CrossRef]
30. Ruiz-Pérez, L.; Messager, L.; Gaitzsch, J.; Joseph, A.; Sutto, L.; Gervasio, F.L.; Battaglia, G. Molecular engineering of polymersome surface topology. *Sci. Adv.* **2016**, *2*, e1500948. [CrossRef]
31. Gouveia, V.M.; Lopes-de-Araujo, J.; Costa Lima, S.A.; Nunes, C.; Reis, S. Hyaluronic acid-conjugated pH-sensitive liposomes for targeted delivery of prednisolone on rheumatoid arthritis therapy. *Nanomedicine (Lond.)* **2018**, *13*, 1037–1049. [CrossRef] [PubMed]
32. Zhu, Y.; Poma, A.; Rizzello, L.; Gouveia, V.M.; Ruiz-Perez, L.; Battaglia, G.; Williams, C.K. Metabolically Active, Fully Hydrolysable Polymersomes. *Angew. Chem. Int. Ed. Engl.* **2019**, *58*, 4581–4586. [CrossRef] [PubMed]
33. Robertson, J.D.; Ward, J.R.; Avila-Olias, M.; Battaglia, G.; Renshaw, S.A. Targeting Neutrophilic Inflammation Using Polymersome-Mediated Cellular Delivery. *J. Immunol.* **2017**, *198*, 3596–3604. [CrossRef] [PubMed]
34. Blanco, E.; Shen, H.; Ferrari, M. Principles of nanoparticle design for overcoming biological barriers to drug delivery. *Nat. Biotechnol.* **2015**, *33*, 941–951. [CrossRef]
35. Canton, I.; Battaglia, G. Endocytosis at the nanoscale. *Chem. Soc. Rev.* **2012**, *41*, 2718–2739. [CrossRef]
36. Mircioiu, C.; Voicu, V.; Anuta, V.; Tudose, A.; Celia, C.; Paolino, D.; Fresta, M.; Sandulovici, R.; Mircioiu, I. Mathematical Modeling of Release Kinetics from Supramolecular Drug Delivery Systems. *Pharmaceutics* **2019**, *11*, 140. [CrossRef]
37. Mhlanga, N.; Ray, S.S. Kinetic models for the release of the anticancer drug doxorubicin from biodegradable polylactide/metal oxide-based hybrids. *Int. J. Biol. Macromol.* **2015**, *72*, 1301–1307. [CrossRef]
38. Chanput, W.; Mes, J.J.; Wichers, H.J. THP-1 cell line: An in vitro cell model for immune modulation approach. *Int. Immunopharmacol.* **2014**, *23*, 37–45. [CrossRef]
39. Skov, L.; Beurskens, F.J.; Zachariae, C.O.; Reitamo, S.; Teeling, J.; Satijn, D.; Knudsen, K.M.; Boot, E.P.; Hudson, D.; Baadsgaard, O.; et al. IL-8 as antibody therapeutic target in inflammatory diseases: Reduction of clinical activity in palmoplantar pustulosis. *J. Immunol.* **2008**, *181*, 669–679. [CrossRef]
40. Tanaka, T.; Narazaki, M.; Kishimoto, T. IL-6 in inflammation, immunity, and disease. *Cold Spring Harb. Perspect. Biol.* **2014**, *6*, a016295. [CrossRef]

41. Treede, I.; Braun, A.; Sparla, R.; Kuhnel, M.; Giese, T.; Turner, J.; Anes, E.; Kulaksiz, H.; Fullekrug, J.; Stremmel, W.; et al. Anti-inflammatory effects of phosphatidylcholine. *J. Biol. Chem.* **2007**, *282*, 27155–27164. [CrossRef] [PubMed]
42. Linton, M.F.; Tao, H.; Linton, E.F.; Yancey, P.G. SR-BI: A Multifunctional Receptor in Cholesterol Homeostasis and Atherosclerosis. *Trends Endocrinol. Metab.* **2017**, *28*, 461–472. [CrossRef] [PubMed]

Supplementary information

pharmaceutics

MDPI

Supplementary Materials: Macrophage Targeting pH Responsive Polymersomes for Glucocorticoid Therapy

Virgínia M. Gouveia, Loris Rizzello, Claudia Nunes, Alessandro Poma, Lorena Ruiz-Perez, António Oliveira, Salette Reis and Giuseppe Battaglia

Polymers synthesis and characterization 2

Polymersomes characterization study 4

Drug release study 5

Cell viability study 6

Gene expression study 7

Polymer Synthesis and Characterization

PMPC-*b*-PDPA was prepared by loading a round bottom flask (equipped with a magnetic stir bar) with 2-methacryloyloxyethyl phosphorylcholine (MPC, 25 eq.), 2-(4-morpholino)ethyl 2-bromoisobutyrate (ME-Br) initiator (1 eq.) and ethanol (final [MPC] = 2.8M), and this solution was deoxygenated by purging N_2 for at least 1 h under stirring at room temperature. Then, 2,2'-bipyridine (bpy) ligand (2 eq.) and Cu(I)Br (1 eq.) were added as solids whilst maintaining the flask under a mild positive N_2 pressure. The reaction was carried out under a N_2 atmosphere at 30 °C. After 90 min (MPC conversion > 99% from ^{1}H-NMR), an ethanolic solution of 2-(diisopropylamino) ethyl methacrylate (DPA, 85 eq., [DPA] = 3.8 M), previously deoxygenated by purging N_2, was injected into the flask. After 48 h, the reaction solution was opened to air, diluted with ethanol and left stirring for 1 h. The solution was then passed through a silica column to remove the copper catalyst. After this step, the filtrate was concentrated by rotary evaporation and dialysed using a 3.5 kDa MWCO dialysis membrane (Spectrum Labs, Netherland) against chloroform/methanol 2:1 (*v*/*v*) (2–3 × 500 mL), methanol (2 – 3 × 500 mL), and double-distilled water (4 – 6 × 2 L). After dialysis the copolymer was isolated by freeze-drying.

^{1}H-NMR [$CDCl_3$/CD_3OD 3:1 (*v*/*v*), 600 MHz, H given in number per monomer unit, all broad signals]: $PMPC_{25}$-$PDPA_{68}$, δ = 4.24 (2H, PMPC); 4.14 (2H, PMPC) 3.98 (2H, PDPA), 3.84 (2H, PMPC), 3.69 (2H, PMPC), 3.24 (9H, PMPC) 3.00 (2H, PDPA), 2.64 (2H, PDPA), 1.87–1.78 (2H, PMPC and 2H, PDPA), 1.01 (12H, PDPA), 0.89 (3H, PMPC and 3H, PDPA). GPC (H_2O + 0.25% TFA as eluent): $PMPC_{25}$-$PDPA_{68}$, M_n = 21.0 kDa, M_w/M_n = 1.39.

Cy5-labelled PMPC-*b*-PDPA was prepared as above but using bis[2 -(2-bromoisobutyryloxy)ethyl] disulfide as initiator [1]. After purification and isolation, an aliquote of the obtained polymer was reacted with Cyanine5 maleimide (1.1 eq.) and PPh_3 (2 eq.) in degassed chloroform/methanol [2:1 (*v*/*v*)]. The final polymer concentration was 1.6 mM, and the reaction was kept stirring under N_2 and in the dark at room temperature for 48 h. After this time, the reaction solution was opened to the air, filtered onto a silica column and dialysed using a 3.5 kDa MWCO dialysis membrane (Spectrum Labs, Netherland) against chloroform/methanol 2:1 (*v*/*v*) (2 – 3 × 500 mL), methanol (4 – 6 × 500 mL), and double-distilled water (4 – 6 × 2 L). After dialysis the copolymer was isolated by freeze-drying.

GPC (H_2O + 0.25% TFA as eluent): Cy5-$PMPC_{25}$-$PDPA_{70}$, M_n = 23.0 kDa, M_w/M_n = 1.35.

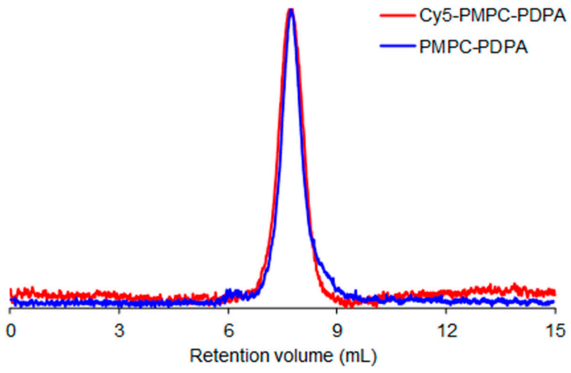

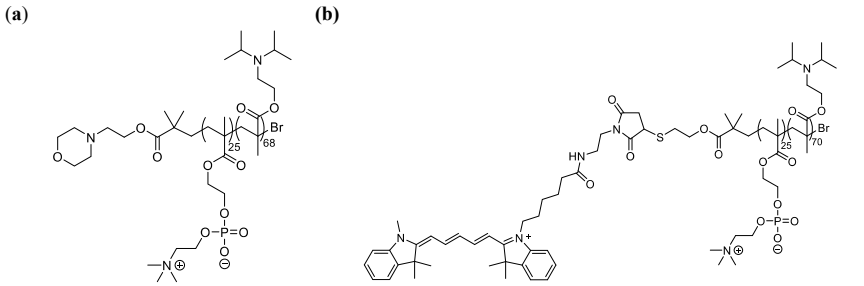

Figure S1: Chemical structure of (**a**) $PMPC_{25}$-$PDPA_{68}$ and (**b**) Cy5-$PMPC_{25}$-$PDPA_{70}$.

Polymersomes Characterization

Regarding the characterization study, HPLC analyses resulted in the drug encapsulation and loading efficiencies within PMPC-PDPA polymersomes. The drug encapsulation efficiency (EE) was calculated as the ratio between the final and initial mass of loaded prednisolone disodium 21-phosphate (PDP). The drug loading efficiency (LE) was determined according to a previously reported method [2] represented as the number of PDP molecules loaded within the total lumen volume of PMPC-PDPA polymersomes (which is related with the size of the vesicle and the actual amount of loaded drug).

(**a**)

	D_h (nm)	PDI
Psome	117 ± 5	0.098 ± 0.01
Psome:PDP	178 ± 4	0.166 ± 0.10

(**b**)

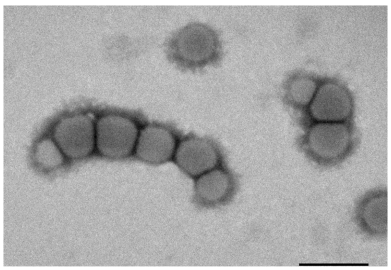

(**c**)

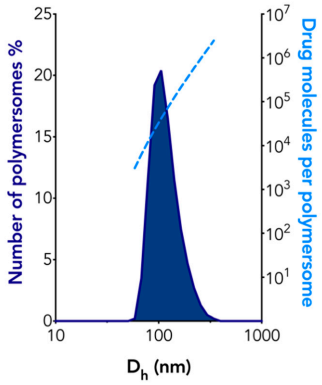

(**d**)

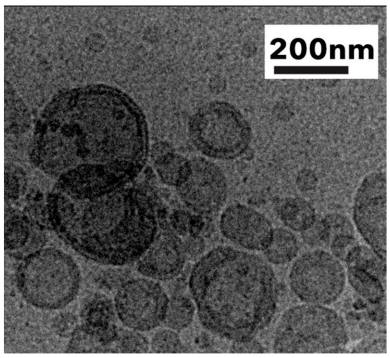

(**e**)

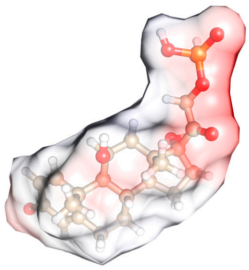

Figure S2: (**a**) DLS data on the hydrodynamic diameter (D_h) and polydispersity index (PDI) values of all formulations of unloaded and PDP loaded PMPC-PDPA polymersomes (n = 3). Analysis on the PDI values below 0.2 indicates a formulation of polymersomes with monodisperse and homogeneous size distribution [3]. (**b**) TEM representative image of Cy5-PMPC-PDPA polymersomes produced via film rehydration method (200 nm scale bar). (**c**) DLS data on the number of PMPC-PDPA polymersomes as a function of the D_h. Analysis on the drug loading capacity represented as the number of PDP molecules per polymersome as a function of their size. (**d**) Cryo-TEM representative image of PMPC-PDPA polymersomes produced via pH-switch method (200 nm scale bar). (**e**) Chemical structure and electrostatic surfaces of prednisolone disodium 21-phosphate (PDP) and respective representation of the electrostatic surfaces.

Drug Release study

To examine the kinetics and mechanism of PDP release from the PMPC-PDPA polymersomes, the data obtained from the in vitro drug release studies of each pH profile was analyzed using various models, including the zero and first order, Higuchi, Hixson-Crowell and Korsmeyer-Peppas models [4,5].

Table S1. Mathematical models for drug-release kinetics.

Release Model	Equation [1]	Information
Zero–Order	$Q = Q_0 + K_0 t$	refers to the process of constant drug release from a drug delivery device
First–Order	$\text{Log } C = \text{Log } C_0 - k_1 t / 2.303$	represents a system where the release rate of the drug depends on the concentration of the drug in the system
Hixson–Crowell	$Q_0 1/3 - Q_t 1/3 = K_{HC}\, t$	describes the release from systems where there is a change in surface area and diameter of particles
Higuchi	$Qt = k_H\, (t)^{0.5}$	assumes that the drug's release is caused primarily by a diffusion mechanism
Korsmeyer–Peppas	$F = M_t/M\ N = Kt^n$	provides insight into the type of drug release mechanism taking place from swellable devices

[1] Q is the amount of drug released or dissolved; Q_0 is initial amount of drug in solution; C_0 is the initial concentration of drug; t is the time in hours; F is the fraction of drug release at time t; M_t/M is the fraction of drug released at time t; K are the rate constants for each models.

Table S2. Correlation coefficient (r^2) from various drug release mathematical models for each pH profile.

	Zero–Order	First–Order	Hixson–Crowell	Higuchi	Korsmeyer–Peppas
pH 5.0	0.935	0.635	0.643	0.995	0.172
pH 6.5	0.984	0.657	0.757	0.959	0.503
pH 7.4	0.636	0.419	0.410	0.758	0.348

Cell Viability Study

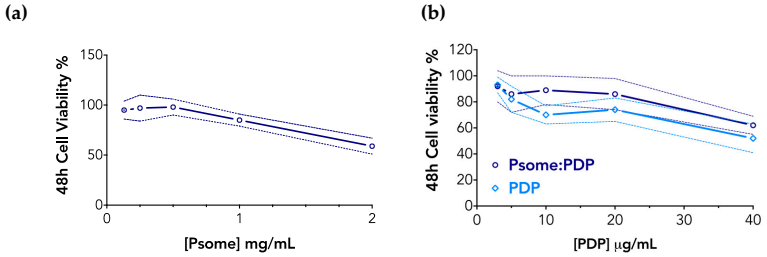

Figure S3: Cell viability assay after 48 h incubation with increasing concentrations of (**a**) unloaded PMPC-PDPA polymersomes, (**b**) either free PDP or PDP-loaded polymersomes (Psome:PDP).

Gene Expression Study

For the RT-qPCR experiments, the ribosomal protein L13A (RPL13A) was used as reference gene, because it was stably expressed in THP-1, both in stimulated and unstimulated cells (data not shown).

Table S3. Forward (Fw) and reverse (Rv) gene sequences of designed primers (PRIMER-BLAS; Sigma-Aldrich) used for gene expression studies.

Gene		Primers	Classification
RPL13A	Fw	CTTCCTTTCCAGTTTGCTGC	ribosomal protein
	Rv	TCTCGCAGTCCACTTCCTTT	
TNFα	Fw	GGAGAAGGGTGACCGACTCA	tumor necrosis
	Rv	CTGCCCAGACTCGGCAA	factor
IL8	Fw	TCCAAACCTTTCCACCCCAAA	chemokine
	Rv	ACCCTCTGCACCCAGTTTTC	
IL6	Fw	TGCAATAACCACCCCTGACC	interleukin
	Rv	AGCTGCGCAGAATGAGATGA	
IL1β	Fw	CCAAAGAAGAAGATGGAAAAGGC	interleukin
	Rv	GGGAACTGGGCAGACTCAAA	

RT-qPCR data was analysed using the comparative cycle threshold (Ct) method, also known as the ΔΔCt method. The Ct value of each target gene (TNFα, IL1β, IL6 and IL8) was normalized to the reference gene (RPL13A), obtaining the ΔCt value (Equation 1) of treatment and control (i.e., non-treated). Then, the change in Ct is compared against the control to obtain the ΔΔCt value (Equation 2) using the following equations:

$$\Delta Ct = Ct\ (\text{target gene}) - Ct\ (\text{RPL13A}) \quad (1)$$

$$\Delta\Delta Ct = \Delta Ct\ (\text{treated}) - \Delta Ct\ (\text{non-treated}) \quad (2)$$

Then, the – ΔΔCt values corresponds to the folds in gene expression change of the treated compared to the non-treated group.

References

1. Gaitzsch, J.; Delahaye, M.; Poma, A.; Du Prez, F.; Battaglia, G. Comparison of metal free polymer-dye conjugation strategies in protic solvents. *Polym. Chem.* **2016**, *7*, 3046–3055, doi:10.1039/c6py00518g.
2. Wang, L.; Chierico, L.; Little, D.; Patikarnmonthon, N.; Yang, Z.; Azzouz, M.; Madsen, J.; Armes, S.P.; Battaglia, G. Encapsulation of biomacromolecules within polymersomes by electroporation. *Angew Chem. Int. Ed. Engl.* **2012**, *51*, 11122–11125, doi:10.1002/anie.201204169.
3. Blanco, E.; Shen, H.; Ferrari, M. Principles of nanoparticle design for overcoming biological barriers to drug delivery. *Nat. Biotechnol.* **2015**, *33*, 941–951, doi:10.1038/nbt.3330.
4. Mircioiu, C.; Voicu, V.; Anuta, V.; Tudose, A.; Celia, C.; Paolino, D.; Fresta, M.; Sandulovici, R.; Mircioiu, I. Mathematical Modeling of Release Kinetics from Supramolecular Drug Delivery Systems. *Pharmaceutics* **2019**, *11*, doi:10.3390/pharmaceutics11030140.
5. Mhlanga, N.; Ray, S.S. Kinetic models for the release of the anticancer drug doxorubicin from biodegradable polylactide/metal oxide-based hybrids. *Int. J. Biol. Macromol.* **2015**, *72*, 1301–1307, doi:10.1016/j.ijbiomac.2014.10.038.

Chapter 3

III. pH-responsive polymersomes in the control of arthritic inflammation *in vitro*

Virgínia M. Gouveia [1,2,3,4], Loris Rizzello [3,4,5], Cláudia Nunes [1], Edoardo Scarpa [3,4], Alessandro Poma [3,4,6], António Oliveira [2], Salette Reis [1] and Giuseppe Battaglia [3,4,5,7,8]

[1] LAQV, REQUIMTE, Department of Chemical Sciences, Faculty of Pharmacy, University of Porto, 4050-313 Porto, Portugal

[2] Abel Salazar Biomedical Sciences Institute, University of Porto, 4050-313 Porto, Portugal

[3] Department of Chemistry, University College London, London WC1H 0AJ, UK

[4] Institute of Physics of Living Systems, University College London, London WC1H 0AJ, UK

[5] Institute for Bioengineering of Catalonia (IBEC), The Barcelona Institute of Science and Technology, 08028 Barcelona, Spain

[6] Division of Biomaterials and Tissue Engineering, UCL Eastman Dental Institute, University College London, London WC1X 8LD, UK

[7] EPSRC/JEOL Centre for Liquid Phase Electron Microscopy, University College London, London WC1H 0AJ, UK

[8] Catalan Institution for Research and Advanced Studies (ICREA), 08010 Barcelona, Spain

---

Original research article.

Abstract

Rheumatoid arthritis (RA) is a chronic inflammatory joint disorder characterised by progressive synovial inflammation. Methotrexate (Mtx) is a well-known anti-rheumatic drug used as a first line therapy in RA. Although it is still hampered by deleterious side-effects, despite its proven therapeutic efficacy. In this study, we present promising *in vitro* data using pH-responsive polymersomes, made of poly(2-methacryloyloxyethyl phosphorylcholine)–poly(2-(diisopropylamino)ethyl methacrylate) (PMPC–PDPA), as suitable drug delivery nanocarriers for the treatment of RA. The great advantages of this nanomedicine are based on the physicochemical properties of its building blocks. The PMPC endows targeting ability to enable the selective delivery of the loaded Mtx to the macrophages and synoviocytes found within the synovium. Whereas, the PDPA pH responsiveness allows the controlled intracellular release of Mtx along the endocytic pathway. Thereby, pH-responsive PMPC-PDPA polymersomes have the potential to improve the therapeutic efficacy of loaded Mtx in resolving synovial inflammation, while minimizing its off-target toxicity.

Keywords

rheumatoid arthritis, chronic inflammation, methotrexate, pH-responsive polymersome, macrophages, synoviocytes, cytokines, chemokines, metalloproteases

Highlights

pH-responsive PMPC-PDPA polymersomes:

- are suitable as drug delivery nanomedicine
- are not cytotoxic
- enable rapid drug delivery within activated macrophages and synoviocytes
- enable the intracellular drug-controlled release
- enhance the immuno-anti-inflammatory therapeutic effect of loaded drug

1. Introduction

Rheumatoid arthritis (RA) is a chronic immune-mediated inflammatory disease associated with the enduring synovial inflammation of joints [1, 2]. Severe disease progression can lead to the synovial tissue damage and further irreversible destruction of joints [2, 3]. Although, seen as an autoimmune disease, RA etiology remains still ambiguous, as several environmental, genetic and other risk factors seem to be involved in its origin [3, 4]. A better understanding of the RA pathogenesis has led to the identification of molecules and cells involved in the initiation of the autoimmune response, perpetuation of synovial inflammation and hence disease destructive progression [1, 2].

RA pathogenesis involves the interplay of both innate and adaptive immune responses [1, 2, 5]. The influx of immune cells to the synovium and subsequent interacting cascades of pro-inflammatory cytokines causes synovitis [1, 2, 5]. The inflammation of the synovium leads to an increased vascular permeability, which in turn leads to synovial hyperplasia and formation of pannus tissue [6, 7]. Additionally, local synovial cellular interactions initiate and maintain the inflammatory process through the activation of macrophages and synovial fibroblasts (also known as synoviocytes) [1, 2, 5]. Both of these cells are found in abundance in the synovium of joints and play a central role in RA pathogenesis by actively driving the perpetuation of immune and inflammatory responses and further damage of joint synovial tissue [1, 2, 8, 9]. Synovial macrophages induce the secretion of several pro-inflammatory cytokines, such as tumour necrosis factorα (TNFα), interleukin (IL)1β and IL6, and chemokines, such as CXCL8 (*i.e.* IL8) and CCL3 (also known as macrophage inflammatory protein 1α) [1, 2, 5, 9]. Through cascades of cytokine-mediated signalling pathways, synovial macrophages activate other cells found within the synovium that are involved in the disease progression [1, 2, 5, 8, 9]. Among them, the synoviocytes inflammatory phenotype activation stimulates the production of more pro-inflammatory cytokines and chemokines, thus perpetuating synovial inflammation. These cells are important in the maintenance of the normal stromal synovial environment of joints through the secretion of a range of extracellular matrix components [2, 8, 10-12]. Although, under synovitis, activated synoviocytes increase the secretion of tissue-degrading enzymes, such as the matrix metalloproteinases (MMPs) that are involved in the degradation of cartilage [2, 8, 10-12]. In addition, the synoviocytes secrete the receptor activator of nuclear factor-κB (NF-κB) ligand (RANKL), which, in

turn, induce the differentiation and proliferation of osteoclasts that are mainly responsible for bone erosion [2, 8, 10-12]. Moreover, synoviocytes play an important disease-promoting role through the secretion of vascular endothelial growth factors associated with angiogenesis [6, 7, 12-15]. The enhanced synovial vascularization and prominent angiogenesis endures synovitis and facilitates the access of synoviocytes to the bloodstream, hence increasing the dissemination of arthritis to other unaffected joints [6, 12-14, 16].

The management of RA treatment relies on the use of disease-modifying anti-rheumatic drugs (DMARDs) for both symptomatic relief and cease of synovial inflammation progression [3, 17-19]. Thereby, early treatment intervention is crucial to slow-down the irreversible joint damage [20]. Methotrexate (Mtx) is a well-known DMARD used currently in clinic as a potent and effective therapy for RA, and other autoimmune diseases [17-19]. Different mechanisms of action are involved in the therapeutic effectiveness of this DMARD [21-23]. Namely, Mtx adenosine-mediated anti-inflammatory and immunosuppressive effects regulate the production of cellular adhesion and pro-inflammatory molecules involved in synovial and systemic inflammation [21-23]. Despite the therapeutic efficacy of Mtx in RA treatment, up to 16% of patients discontinue the therapy, mostly due to deleterious side effects [17, 18, 24-26]. This fact is particularly an important issue in RA, because the long-term use of this drug allied with its widespread off-site biodistribution, causes liver damage, often leading to hepatitis [17, 18, 24-26]. Therefore, there is the urgent need to create novel nanomedicines for delivering Mtx to the target diseased synovial tissue and hence overcome the limitations of this DMARD in the treatment of RA. The vital role of both synovial macrophages and synoviocytes in RA pathogenesis, makes them the target for the delivery of Mtx, and, ultimately, enhance its therapeutic effect, while minimising off-site cytotoxicity. Here, we developed an innovative polymer based nanotherapy – polymersomes loading Mtx – with the potential to target and treat synovial inflammation. Polymersomes are formed by the self-assembly of amphiphilic block copolymers into vesicles [27-29]. Thereby, polymersomes enable the encapsulation of both hydrophilic, amphiphilic and hydrophobic drug molecules in the aqueous core or in the hydrophobic membrane [28, 30]. In addition, the macromolecular and synthetic nature of polymersomes building blocks facilitate the tailored design of their physicochemical properties, including size, shape, surface ligands, permeability and mechanical stability [27-32]. As well as, the control of their self-

assembly/disassembly mechanism using environmental stimuli responsiveness, for example to pH, temperature, hydrolysis, oxidation, light or enzymes [27-32].
In this study, pH-responsive polymersomes are made using the highly biocompatible hydrophilic block – poly(2-methacryloyloxyethyl phosphorylcholine) (PMPC) – and the hydrophobic poly(2-(diisopropylamino)ethyl methacrylate) (PDPA) block. This amphiphilic di-block copolymer is designed to self-assemble into vesicles only in aqueous conditions at pH above 6.2 (the PDPA pKa) [29] [33, 34] [35]. Thereby, the PDPA block confers the pH responsiveness of polymersomes to disassemble at pH lower than 6.2 [28, 29, 33-42]. This pH responsiveness-trigger mechanism is particularly useful as polymersomes, upon cellular internalisation, experience a drop in pH within the endosomes (pH~6 to 5.5), which bestows their rapid disassembling [28, 29, 37, 43]. This, in turn, provokes an osmotic shock in the endosome and the consequent membrane poration [28, 29, 37, 43]. Thus, enabling the intracellular release of the loaded Mtx to the cytosol. In addition, this feature can be further exploited as a targeting strategy for RA, as the cellular acidosis within the synovium leads to the pH drop [15, 44, 45], thus allowing the release of loaded Mtx in the target inflamed synovial tissues. Another advantage of using PMPC-PDPA polymersomes is that PMPC block has an inherent binding affinity to the family of class B scavenger receptors, including type B1 and B3 [36, 38, 40, 41]. These surface cell receptors are expressed by macrophages and synoviocytes [46-49], which play a critical role in RA pathogenesis, and that can be therefore targeted by these polymersomes. In addition, the biocompatible hydrophilic nature of the PMPC block avoids the protein fouling, which might delay the mononuclear phagocyte system recognition and rapid clearance of polymersomes from blood circulation [36, 38, 40, 41].
Here, *in vitro* studies support the potential of PMPC-PDPA polymersomes to grant the stability and targeting ability of loaded Mtx towards inflamed synovium. Hence, enabling the intracellular drug bioavailability and on-site therapeutic efficacy. Therefore, pH-responsive PMPC-PDPA polymersomes loading Mtx have a high impact in the progression of inflammatory arthritis and potentially in the treatment of RA.

2. Materials and Methods

2.1. Preparation of PMPC-PDPA polymersomes

The $PMPC_{25}$-$PDPA_{68}$ diblock copolymer was synthesised as previously reported [35, 50] by atom-transfer radical polymerization. Polymersomes were prepared by pH-driven self-assembly of the $PMPC_{25}$-$PDPA_{68}$ copolymers using a previously reported method [42, 51] with some modifications. Briefly, under sterile conditions, $PMPC_{25}$-$PDPA_{68}$ copolymer was dissolved in acidic phosphate-buffered saline (PBS 0.1 M, Sigma-Aldrich) up to a concentration of 10 mg/mL, and the pH solution was adjusted to pH 2.0 by addition of hydrochloric acid (HCL 2 M). The self-assembly process was controlled by increasing the solution pH from 2.0 to approximately neutral pH 7.4, through needle injection system (2 μL/minute), with sodium hydroxide (NaOH 0.5 M). Formulations of PMPC-PDPA polymersomes loading methotrexate (Mtx, $C_{20}H_{22}N_8O_5$, MW 454.44, λ (300 nm), Sigma-Aldrich) were prepared also using the above-mentioned pH-switch method by injecting the Mtx (3 mg/mL) dissolved together in the NaOH solution. Additionally, for fluorescence imaging *in vitro* studies, Cyanine5-labelled PMPC-PDPA polymersomes were prepared using the solvent-switch method as previously reported [52] with some modifications. Here, 10% (w/w) Cy5-$PMPC_{25}$-$PDPA_{68}$ copolymer, previously synthesised by atom-transfer radical polymerization [53], was dissolved together with the $PMPC_{25}$-$PDPA_{68}$ in an organic solution of 3:1 (v/v) methanol:tetrahydrofuran (Sigma-Aldrich) for a final copolymer concentration of 20 mg/mL. Then, PBS at neutral pH was injected at the rate of 2 μL/minute into the organic solution under constant stirring at 42ºC, until a 0.6% (w/v) PBS content was reached. Afterwards, any remaining organic solvent was removed using dialysis (3.5 kD MWCO tubing membrane, Spectrum Labs) against PBS for 2 days, with solvent changes occurring every 3 hours or longer. In the end, after preparation, all formulations of PMPC-PDPA polymersomes were purified as previously described by size exclusion chromatography [51].

2.2. Characterization Studies

2.2.1. Size and morphology study

All produced formulations of PMPC-PDPA polymersomes were characterised in term of size, size distribution and morphology. Dynamic light scattering (DLS) was used for the hydrodynamic diameter (D_h) measurement in the Zetasizer Nano ZS

(Zen1600, Malvern Instruments), equipped with a 633 nm HeNe laser in a scattering angle of 173º. Transmission electronic microscopy (TEM) imaging analysis was conducted on a JEOL 2100 operating at 200 kV, equipped with an Orius SC2001CCD Gatan camera. Prior to DLS and TEM characterization, samples were respectively prepared as previously reported [35, 54].

2.2.2. Polymer and drug quantification study

The amount of $PMPC_{25}$-$PDPA_{68}$ copolymer and loaded drug after purification process was determined by high-performance liquid chromatography (HPLC) using a Dionex Ultimate®3000. This instrument is equipped with a variable wavelength detector and a C18 analytical column (Jupiter Phenomenex 300A, 150x4.6 mm, 5 μm). The samples, previously diluted in DPBS at pH 2.0, were run according to a ramp gradient of eluent A [0.05% (v/v) trifluoroacetic acid (TFA, Thermo-Fisher) in Milli-Q filtered H_2O] and eluent B [0.05% (v/v) TFA in methanol]: for 10 minutes from 5% to 100%; keep constant for 15 minutes and return within 1 minute to initial condition. By using the Chomeleon software, the peak area was integrated at respective elution time and wavelength (λ) on the HPLC system to analyse the UV absorption of $PMPC_{25}$-$PDPA_{68}$ at λ(220 nm) and Mtx at λ(300 nm). Then, the amount of $PMPC_{25}$-$PDPA_{68}$ copolymer and Mtx was quantified using their respective previously accessed calibration curves. Further analysis on the drug encapsulation and loading efficiencies were determined using a previously reported method [34, 35] (details in Supplementary Information).

2.2.3. Drug-polymer interaction study

The drug-polymer interaction study was performed by determining the partition coefficient (expressed as K_p and log D) of Mtx in a polymersomes/water system. A previously reported method of derivative spectrophotometry [55], was used with some modifications, to determine the K_p of Mtx with the PMPC-PDPA membrane at pH 7.4 and 37ºC. Briefly, samples with increasing concentrations of PMPC-PDPA polymersomes (0 - 120 μM) and a fixed concentration of Mtx (25 μM) at pH 7.4 were prepared and incubated for 1 hour. The absorption spectra (220 - 370 nm) were obtained at 37ºC using a UV-Vis microplate spectrophotometer (Synergy HT, Biotek). The obtained experimental data were mathematically analysed using a previously reported *Kp calculator* [55]. The second-derivative spectra were used to eliminate the light scattering effect caused by the polymersomes and improve

bands resolution. Hence, by plotting the second-derivative values, at a wavelength where the scattering was eliminated (λ_{min}~255 nm), as function of the PMPC-PDPA molar concentrations, the K_p (M^{-1}) was determined by fitting the experimental data using a nonlinear least-squares regression method. Results on the drug interaction with the water/polymer system is expressed as log *D* (details in Supplementary Information; Figure S1).

2.2.4. Drug release study

The drug release study was performed using the dialysis method under sink conditions. As previously described [35], 1 mL of Mtx loaded PMPC-PDPA polymersomes or free Mtx (at the same concentration of the loaded one) was filled in a cellulose ester dialysis membrane tube (3.5-5 kDa MWCO, Float-a-Lyzer G2, Spectrum Laboratories Inc.). These dialyses were carried out against 10 mL of three different outer buffer pH conditions (PBS solution at pH 7.4; acetate-buffered solution at pH 6.5 and 5.0) for 50 hours under continuous magnetic stirring at 37ºC (RT15 power, IKA-Werke GmbH & Co. KG). At regular time points, aliquots (200 µL) were withdrawn and the same volume of respective fresh outer buffer solution replaced in order to maintain the sink conditions. The quantification of permeated drug aliquots throughout the 50 hours was determined by measuring the UV absorbance of Mtx at λ (300 nm) using the UV-Vis microplate spectrophotometer (Synergy HT, Biotek).

Mathematical models for drug-release kinetics, including zero-order and first-order equations, Higuchi and Hixson–Crowell models, were applied to each drug release profile to evaluate the mechanism of drug release (details in Supplementary Information; Table S1). The fitting of each model was evaluated based on the correlation coefficient (r^2) values.

2.3. In vitro cellular studies

2.3.1. Cell culture and activation

Human leukemic monocytes (THP-1) were cultured and maintained in RPMI-1640, 2 mM L-glutamine, 25 mM Hepes (Sigma-Aldrich) supplemented with 10% (v/v) heat-inactivated fetal bovine serum (FBS, Sigma-Aldrich), 1% (v/v) penicillin-streptomycin (Sigma-Aldrich) and 0.1% (v/v) amphotericin B (Sigma-Aldrich). Human fibroblast like synoviocytes (HFLS) purchase from Sigma-Aldrich were cultured and maintained in synoviocytes growth medium (Sigma-Aldrich) supplemented with 10

% (v/v) FBS, 1% (v/v) penicillin-streptomycin, 1% (v/v) L-glutamine (Sigma-Aldrich) and 0.1% (v/v) amphotericin B. Prior to all *in vitro* cellular studies, THP-1 cells differentiation into mature macrophages-like state was induced through incubation with 10 ng/mL of phorbol 12-myristate 13-acetate (PMA, Sigma-Aldrich) for 48 hours [35, 56] in a humidified atmosphere, 95% air, 5% CO_2 at 37ºC. Moreover, unless stated otherwise, macrophages inflammatory phenotype (*i.e.* activated) was induced with 600 ng/mL of lipopolysaccharide (LPS, Sigma-Aldrich) [35, 56]; while, inflammatory synoviocytes were induced with 20 ng/mL of TNFα (Sigma-Aldrich) [57]. Follow by 24 hours incubation in a humidified atmosphere, 95% air, 5% CO_2 at 37ºC.

2.3.2. Cell uptake imaging study

The cell uptake imaging was performed using confocal laser scanning microscopy (CLSM, Leica SP8). First, macrophages and synoviocytes were seeded at a concentration of $5{\cdot}10^4$ cells per glass-bottom petri dish (Ibidi) and then activated as above mentioned. Then, cells were incubated with 0.5 mg/mL of Cy5-labelled PMPC-PDPA polymersomes for 0.5, 1, 2, 4, 6, 12, 24 and 48 hours, in a humidified atmosphere, 95% air, 5% CO_2 at 37ºC. After each incubation time point, followed by 3 steps of DPBS washing, cells were stained for CLSM live imaging. Respectively, for nuclear and cell membrane staining, Hoesh 33342 (Sigma-Aldrich) and far-red Cell Mask™ (Life Technologies) were incubated for 10 minutes at room temperature, before visualization under CLSM. At least 10 different regions of the petri dishes were captured and analysed using the Fiji ImageJ software (version 2.0). For the quantification of Cy5-labelled PMPC-PDPA polymersomes within stimulated macrophages and synoviocytes, their fluorescent intensity signal was normalized relative to the nuclear intensity signal.

2.3.3. Cell surface receptors study

The cell scavenger receptor (SR)B1 and SRB3 (commonly known as CD36) proteins expression levels in either non- or activated cells were detected by Western blotting assay. First, macrophages and synoviocytes were seeded at a concentration of 10^6 cells per well in 6-well plate (CytoOne) and then activated to the inflammatory state as above mentioned. After 24 hours incubation in a humidified atmosphere, 95% air, 5% CO_2 at 37ºC, cells then washed with DPBS and lysed using radioimmunoprecipitation (RIPA) buffer (containing 50 mM Tris-HCl, pH 8.0, 1%

Nonidet P-40, 150 mM NaCl, 0.5% sodium deoxycholate, 0.1% sodium dodecyl sulfate, 2 mM ethylenediaminetetraacetic acid and 1 mM dithiothreitol) supplemented with protease and phosphatase inhibitor cocktails. Followed by centrifugation (12,000 g) at 4ºC for 10 minutes to remove the nuclei and any insoluble cell debris. The post-nuclear extracts were collected and used as total cell lysates. The protein concentration from these lysates was then determined following the Bradford assay kit protocol (Bio-Rad). Western blotting was performed as previously described with minor modifications [58]. Briefly, the cell lysates were first denatured in 4x Laemmli sample buffer (Bio-Rad) at 95ºC for 5 minutes. Then, 10 μg of total cell lysates proteins were separated by electrophoresis on 10% SDS polyacrylamide gels (previously prepared following the Bio-Rad protocol) and transferred to a polyvinylidene difluoride (PVDF) membrane (Bio-Rad). The PVDF membranes were then blocked with 5% milk in Tris-buffered saline with 0.1% Tween-20 (TBST) for 1 hour at room temperature. For the immunodetection of SRB1 and CD36 protein expression, the PVDF membranes were first incubated, overnight at 4ºC, with 1:1000 dilution of each specific primary antibody (Novus Biologicals NB400-144 and NB400-131) in 1% milk/TBST. And then, after several washes with TBST, the PVDF membranes were incubated with the secondary antibodies (1:20000) in 1% milk/TBST for 1 hour at room temperature. The signals of the goat anti-rabbit and anti-mouse IgG DyLight 800 (Invitrogen) were detected using the Odyssey CLx imaging system. The densitometry analyses were performed using Fiji ImageJ software (version 2.0), and the obtained values represent the ratio between the immunodetected protein and the glyceraldehyde 3-phosphate dehydrogenase (GAPDH, Abcam) loading control. Then, the fold change expression was determined by normalisation to the non-activated control.

2.3.4. Cell viability study

The thiazolyl blue tetrazolium bromide (MTT, Sigma-Aldrich) assay was used, as previously reported [59], to evaluate the cytotoxicity of PMPC-PDPA polymersomes, unloaded and loaded Mtx. Briefly, for MTT assay, cells were seeded at a density of $5{\cdot}10^3$ cell per well in 96-well plates (CytoOne). After seeding and activation, increasing concentrations of each treatment were incubated for 24 hours in a humidified atmosphere, 95% air, 5% CO_2 at 37ºC. Control wells were incubated with equivalent volumes of corresponding cell culture medium and/or a solution of 10% (v/v) dimethyl sulfoxide (DMSO, Sigma-Aldrich) in DPBS. Follow by 24 hours incubation, 0.5 mg/mL of MTT solution was added to each well, and 2 hours later

the MTT solution was replaced by the same volume of DMSO per well to dissolve the formed formazan crystals. Then, the optical density of solubilized blue crystals was read by measuring UV absorbance at 590 nm and 630 nm using a UV-Vis microplate spectrophotometer (SynergyTM HT, Biotek). The cell viability was determined as the percentage of the metabolic activity of treated cells normalised to the control wells.

2.3.5. NF-κB signalling imaging study

Nuclear factor-κB (NF-κB) signalling imaging was performed using CLSM. Firstly, cells were seeded at a concentration of $5 \cdot 10^4$ cells per glass-bottom petri dish (Ibidi) and activated as above mentioned. Then, M1-macrophages were incubated with 10 µg/mL of either free Mtx or Mtx loaded PMPC-PDPA polymersomes for 24 hours in a humidified atmosphere, 95% air, 5% CO_2 at 37ºC. Following treatment, cells were washed with DPBS and fixed using 3.7% formaldehyde (Sigma-Aldrich) for 10 minutes at room temperature. After fixation step, followed by DPBS washing for the membrane permeabilization step, cells were incubated with 0.2% Triton-X (Sigma-Aldrich) for a further 10 minutes at room temperature. Then, the immunostaining blocking was performed using 5% bovine serum albumin (BSA) (Sigma-Aldrich), to prevent unspecific antibody binding. After 1 hour at room temperature, cells were incubated with NFκB p65 Antibody (F-6) Alexa Fluor® 647 (SantaCruz Biotechnology) 1:500 diluted in 1% BSA overnight in a humidified chamber at 4ºC. The following day, cells were washed with DPBS and the nucleus was stained with Hoescht 33342 (Thermo Fisher) for 10 minutes at room temperature, before visualisation under CLSM. At least 10 different regions of the petri dishes were acquired and the NF-κB nuclear translocation imaging analysis was evaluated by co-localisation (Pierce's coefficient values) of the NF-κB and nucleus fluorescence intensity signals using Fiji ImageJ software (version 2.0).

2.3.6. Enzyme linked immunosorbent assay

IL6 and TNFα protein levels were determined using an enzyme linked immunosorbent assay (ELISA). Firstly, macrophages and synoviocytes were seeded at a concentration of 10^6 cells per well in 6-well plate (CytoOne) and activated to the inflammatory state as above mentioned. Followed by 24 hours treatment with 10 µg/mL of either free Mtx or Mtx loaded PMPC-PDPA polymersomes. Cells

supernatants were then collected and the ELISA (Invitrogen) was carried following the manufacturer protocol.

2.3.7. RNA extraction, reverse transcription and real-time quantitative polymerase chain reaction

Analyses on the gene expression of inflammation-related markers, including TNFα, IL1β, IL6, IL8, CCL3 and MMP13 was assessed using real-time quantitative polymerase chain reaction (RT-qPCR). Firstly, cells were seeded at a concentration of 10^6 cells/well in 6-well plate (CytoOne) and activated as above mentioned. Followed treatment with 10 μg/mL of free Mtx or Mtx loaded PMPC-PDPA polymersomes, for 6 and 20 hours, respectively for macrophages and synoviocytes. Cells were then lysed and the RNA was extracted following the RNeasy mini kit (Qiagen) protocol pre-installed in the QIAcube (Qiagen). The total ribonucleic acid (RNA) concentration was measured with NanoDrop spectrophotometer (ThermoScientific). Complementary deoxyribonucleic acid (cDNA) was synthesised from every 1 μg of total mRNA in 20 μL volume with QuantiTect Reverse Transcription Kit (Qiagen) according to the manufacture protocol. This procedure provided a fast and efficient cDNA synthesis with integrated removal of genomic DNA contamination. Briefly, the sample of RNA is incubated at 42°C for 2 minutes to effectively remove containing genomic DNA, then the reaction occurred for another 15 minutes at 42ºC and then inactivated at 95ºC. RT-qPCR reaction was performed on yield cDNA synthetized from each sample using QuantiTec® Rotor-Gene™ SYBR Green RT-PCR kit (Qiagen) using the Qiagility instrument software (Qiagen). This software enables rapid and high-precision system of sample preparation for RT-qPCR analysis, providing a step-by-step guidance for automatic calculation of all primers, cDNA template and Rotor-Gene SYBR Green master mixes need for the reaction. For the RT-qPCR experiments, the ribosomal protein L13A (RPL13A) and glyceraldehyde 3-phosphate dehydrogenase (GADPH) were used as reference genes, respectively for macrophages and synoviocytes. The list of designed primers of each target gene and reference gene are detailed in the Table S3 in Supplementary Information. Following sample preparation, the PCR mixtures are placed in the Rotor-Gene Q cycler (Qiagen) and amplification process starts using the following protocol steps: initial cycling step at 95ºC during 5 minutes for the DNA polymerase activation; followed by 40 cycles of 95ºC during 5 seconds for denaturation; and 60ºC during 10 seconds for combined annealing and extension

for all primers. RT-qPCR data analysis of folds-changes in gene expression levels normalized to the non-activated cells was determined by the -ΔΔCt method (details in Supplementary Information), using cycle threshold (Ct) values acquired from the amplification curve using the Rotor-Gene Q instrumentation software (Qiagen).

2.4. Data statistical analysis

Differences using GraphPad Prism. Statistical analyses were performed using GraphPad Prism (version 8.2.1). Differences between groups were assessed by one-way or two-way ANOVA with Tukey multiple comparison test. The differences were statistically significant for * $p < 0.05$, ** $p < 0.01$, *** $p < 0.001$ and **** $p < 0.0001$.

3. Results

3.1. Physicochemical characterisation

Formulations of unloaded and Mtx-loaded PMPC-PDPA polymersomes were successfully produced via the pH-switch method; and then characterised in terms of size, size distribution and morphology. TEM micrograph demonstrated that PMPC-PDPA polymersomes have a spherical morphology with a small size (60-70 nm) and homogeneous distribution (Figure 1A). Similar size regarding the hydrodynamic diameter (D_h) were measured by DLS (Figure 1B). In recent years, PMPC-PDPA polymersomes were designed and investigated for efficient loading of various pharmaceutical molecules, including drugs, proteins and siRNA [28, 29, 33-42]. PMPC-PDPA polymersomes showed efficient encapsulation of Mtx, reaching high levels of drug loading contents up to 18 wt% (Figure 1B). This value was achieved mostly because of the method used for the encapsulation of Mtx. As calculated by the MarvinSketch calculator (Chemaxon), the solubility of the drug in aqueous media was found to increase as a function of the pH; due to the deprotonation of the two carboxylic acids present in the chemical structure of Mtx at pH above 7.1 (Figure S1A). This encouraged the idea of preparing Mtx-loaded PMPC-PDPA polymersomes through a modified pH-switch method. Whereby, the drug is solubilised in a NaOH solution, rather than in the polymer solution at pH 2.0, before the self-assembly. This approach enabled a higher loading and encapsulation efficiency, possibly due to the affinity of Mtx for the polymer during the self-assembly process. In fact, drug-polymer partition studies showed that the

experimentally obtained log D at pH 7.4 is 2.2 ± 0.1 (Figure S1B), confirming the affinity of Mtx with the polymeric phase of the water/polymersome system.

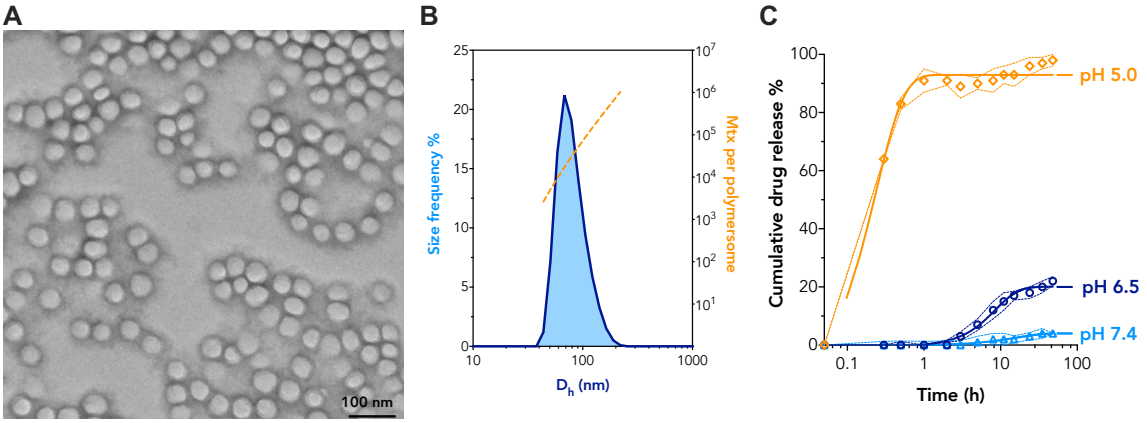

Figure 1. (A) TEM micrograph of Mtx-loaded PMPC-PDPA polymersomes (100 nm scale bar). **(B)** Analysis on the drug loading capacity represented as the number of Mtx molecules per polymersome as a function of their hydrodynamic diameter (D_h) measured by DLS. **(C)** Drug release profiles of Mtx from PMPC-PDPA polymersomes in pH 5.0, 6.5 and 7.4 buffer solutions at 37ºC for 50 hours (n = 3).

In vitro release studies confirm the pH-responsiveness of PMPC-PDPA polymersomes to acidic pH mimicking the intracellular endosomal compartments; thus, resulting in a burst drug release profile at pH 5.0 (Figure 1C). While the Mtx release was practically complete within 1 hour at pH 5.0, under pH 6.5 conditions, meant to mimic the extracellular acidosis environment, it is observed a sustained drug released overtime (up to only 20%; Figure 1C). Drug release kinetics analyses based on the regression coefficient (r^2) revealed that the best fitting model for pH 5.0 and pH 6.5 was obtained by the Zero-Order and Higuchi models (Table S2). These models suggest a controlled diffusion mechanism of Mtx release from the PMPC-PDPA polymersomes. In addition, as expected, practically negligible drug release was observed throughout 50 hours under pH neutral conditions at 37ºC (pH 7.4; Figure 1C). This was also confirmed by analysing the r^2 for the drug release profile at pH 7.4, as there was no best-fitted model (Table S2).

3.2. In vitro cell uptake and viability studies

The *in vitro* cellular uptake of Cy5-PMPC-PDPA polymersomes either by non- or activated macrophages and synoviocytes was assessed using confocal laser scanning microscopy (CLSM). CLSM imaging analysis of macrophages revealed that the normalised fluorescence intensity signal of Cy5-PMPC-PDPA polymersomes

constantly increases in a time-dependent manner up to 10-hours after incubation, followed by a plateau (Figure 2A and B).

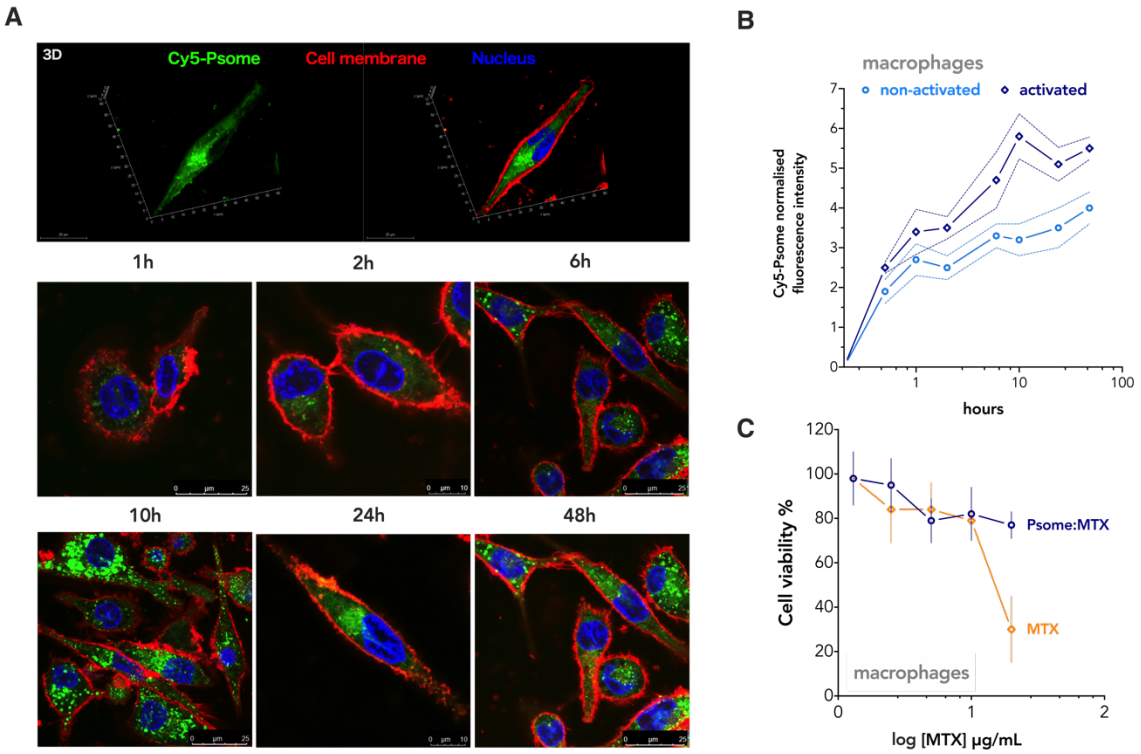

Figure 2. (A) CLSM images of Cy5-PMPC-PDPA polymersome (green fluorescence intensity signal) uptake by LPS-activated macrophages overtime. 3D image corresponds to the 24-hour time point. Staining of the cell nuclei (blue fluorescence intensity signal) with Hoechst 33342 and cell membrane (red fluorescence intensity signal) with far-red CellMask™. **(B)** Cell uptake profile of Cy5-PMPC-PDPA polymersomes normalised fluorescent intensity relative to the nucleus signal measured as a function of time. Data express the mean ± SEM (10 images for n=2). **(C)** Cell viability assay in LPS-activated macrophages after 24 hours incubation with increasing concentrations of either free Mtx or Mtx loaded PMPC-PDPA polymersomes. Data express as mean ± SD (n=3).

Conversely, CLSM imaging analysis of normalised Cy5-PMPC-PDPA polymersomes fluorescence intensity signal on activated synoviocytes resulted in a triphasic cell uptake profile (Figure 3A and B). First, there was an increase on the internalisation of Cy5-PMPC-PDPA polymersomes, followed by a plateau of 5 hours and, then again, an increase of Cy5 fluorescence intensity signal to the double (Figure 3B). Oppositely, the uptake profile by non-activated synoviocytes suggest a slow internalisation of Cy5-PMPC-PDPA polymersomes overtime reaching a plateau after 1 hour of incubation. Overall, cell uptake profiles suggest that there is a rapid and higher internalisation of PMPC-PDPA polymersomes by inflammation activated

macrophages and synoviocytes comparing with the non-activated ones over the 48 hours period (Figure 2B and 3B).

Additional CLSM imaging analysis suggest that the fluorescence intensity of Cy5-labelled polymersomes in activated macrophages was higher than in synoviocytes (Figure 2B and 3B). This is not only due to the intrinsic professional phagocytic nature of macrophages [60, 61], but also possibly to the high affinity of the PMPC moiety towards the cell scavenger receptor SRB1 and CD36 [36, 38, 40, 41].

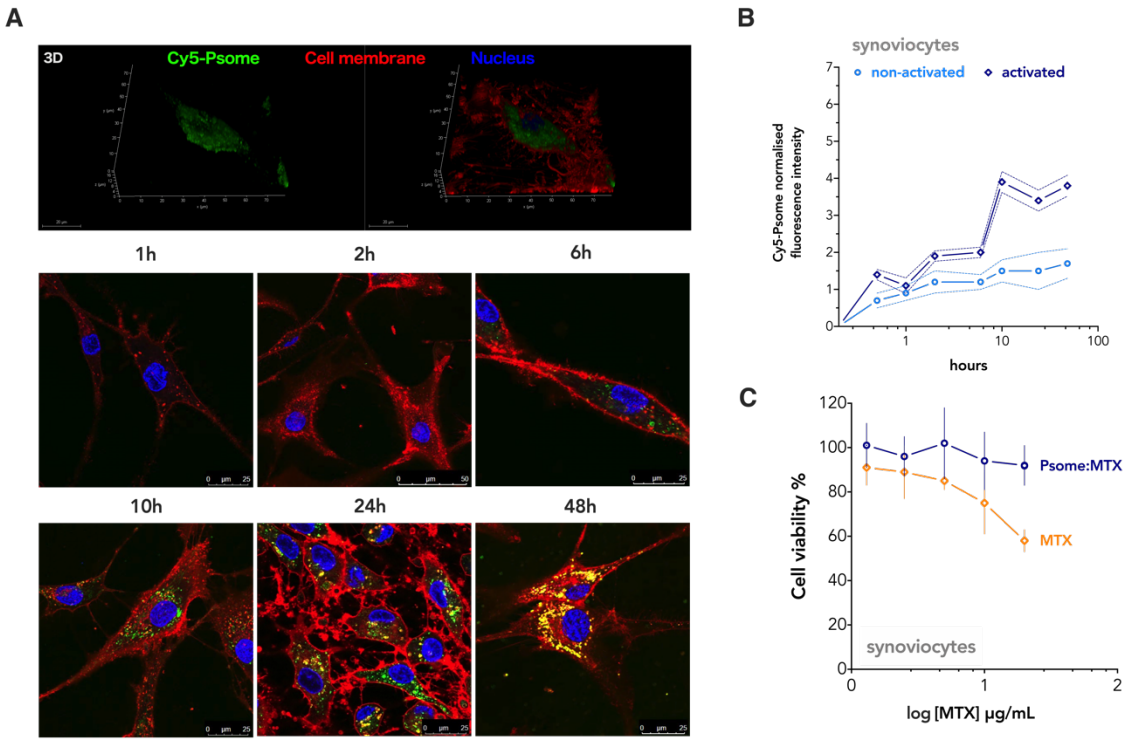

Figure 3. (A) CLSM images of Cy5-labelled PMPC-PDPA polymersome (green fluorescence intensity signal) uptake by TNFα-activated synoviocytes over time. 3D image corresponds to the 10-hour time point. Staining of the cell nuclei (blue fluorescence intensity signal) with Hoechst 33342 and cell membrane (red fluorescence intensity signal) with far-red CellMask™. **(B)** Cell uptake profile of Cy5-PMPC-PDPA polymersomes normalised fluorescent intensity relative to the nucleus signal measured as a function of time. Data express the mean ± SEM (10 images for n=2). **(C)** Cell viability assay in TNFα-activated synoviocytes after 24 hours incubation with increasing concentrations of either free Mtx or Mtx loaded PMPC-PDPA polymersomes. Data express as mean ± SD (n=3).

Thereby, protein expression levels of these cell surface receptors were then investigated followed by activation of cells using western blot analysis (Figure 4A). Results revealed that the SRBI and CD36 expression levels in activated macrophages increased by 2- and 4-fold, respectively, comparing with non-

activated control ($p<0.05$ and $p<0.01$; Figure 4B). Additionally, the activation of synoviocytes significantly boosts the expression of CD36 ($p<0.0001$ *versus* the non-activated control; Figure 4B). Though, the expression of SRBI was only slightly increased by these cells (Figure 4B). Thereby, superior uptake of PMPC-PDPA polymersomes by activated cells possibly occurs due to the high binding affinity of PMPC to the overexpressed SRBI and CD36 cell surface receptors. In turn, these surface cell receptors bestow the internalisation of PMPC-PDPA polymersomes via endocytosis and phagocytosis [30, 43, 46, 47].

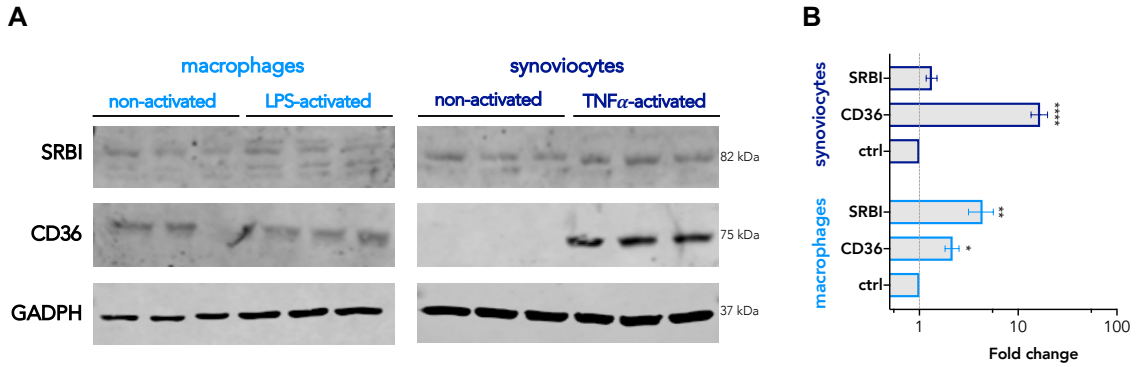

Figure 4. (A) SRBI and CD36 cell surface proteins expression levels in non- and activated macrophages and synoviocytes detected by western blot assay (n=3). The SRBI and CD36 were revealed using specific antibodies and glyceraldehyde 3-phosphate dehydrogenase (GAPDH) was used as the loading control. **(B)** Fold change expression normalised to non-activated control. Data express as mean ± SD (n=3). The differences relative to the non-activated control were statistically significant for *p<0.05, **p<0.01, ***p<0.001 and ****p<0.0001.

In addition, *in vitro* cytotoxicity studies were performed to evaluate if such increased cellular uptake of PMPC-PDPA polymersomes by activated cells might be affecting their viability. To this end, the MTT assay was carried out on both activated macrophages and synoviocytes 24 hours after incubation with either free Mtx, unloaded- or Mtx-loaded PMPC-PDPA polymersomes. Results confirm the biocompatibility of unloaded PMPC-PDPA polymersomes, as both cell types did not show any considerable sign of cytotoxicity for concentrations up to 0.6 mg/mL (Figure S3). MTT results revealed that Mtx-loaded PMPC-PDPA polymersomes did not show relevant cytotoxicity towards activated macrophages and synoviocytes, up to a concentration of 20 µg/mL of loaded drug (Figure 2C and 3C). Whereas, free Mtx treatment displayed concentration dependent-cytotoxicity on both cell types, resulting in a sharp decrease on cell viability at the highest concentration (Figure 2C and 3C). Considering these MTT results, any Mtx treatment presented

henceforth, either as free form or loaded, will be referring to a concentration of 10 μg/mL, if not otherwise specified.

3.3. In vitro inflammation studies

In vitro inflammation cellular studies were carried out in activated macrophages and synoviocytes to evaluate the anti-inflammatory effect of Mtx-loaded PMPC-PDPA polymersomes and compare it with free drug treatment.

The inflammatory state of the cells can be confirmed by assessing the cellular localisation of the inflammatory transcription factor NF-κB using CLSM. As shown on Figure 5A and C, macrophages and synoviocytes activation with LPS and TNFα, respectively, trigger the translocation of NF-κB (red fluorescence intensity signal) found mainly distributed within cytosol on non-activated cells, to the nucleus (blue fluorescence intensity signal). Thereby, once inflammation is induced, in turn, the NF-κB translocation signalling pathway is activated. Indeed, CLSM imaging analysis on the co-localisation fluorescence intensity signal (pink), demonstrate a 2-fold increase of the NF-κB nuclear translocation in comparison to non-activated cells ($p<0.0001$; Figure 5B).

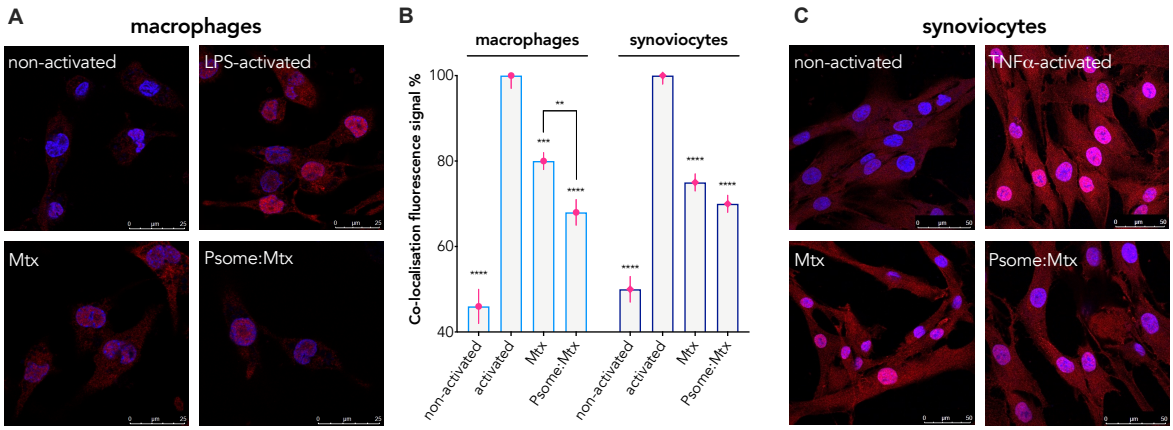

Figure 5. CLSM images of NFκB (red fluorescence intensity signal) translocation from cytoplasm to the nucleus (blue fluorescence intensity signal) in **(A)** LPS-activated macrophages and **(C)** TNFα-activated synoviocytes. **(B)** Quantitative imaging co-localisation (pink fluorescence intensity signal) analysis after 24 hours treatment with either free Mtx or Mtx-loaded PMPC-PDPA polymersomes. Data express as mean ± SEM (5 images for n=2). The differences relative to activated cells control were statistically significant when *$p<0.05$, **$p<0.01$, ***$p<0.001$ and ****$p<0.0001$.

NF-κB is a key regulator of gene transcription in RA pathogenesis, with an important role in the production of pro-inflammatory mediators [1, 2, 9]. Thereby, inhibiting the activation of the NF-κB signalling pathway is a crucial step to regulate the synovial inflammatory process.

CLSM imaging analysis on activated macrophages and synoviocytes demonstrate that Mtx-loaded PMPC-PDPA polymersomes 24 hours treatment resulted in a significant reduction on the nuclear translocation of NF-κB ($p<0.0001$ compared to activated control; Figure 5B). Nonetheless, activated macrophages and synoviocytes treated with free Mtx also decrease the NF-κB nuclear translocation by 20 and 25%, respectively ($p<0.0001$ and $p<0.001$ compared to activated control).

Having demonstrated that both treatments inhibit the activation of the NF-κB signalling pathway, it was important to evaluate their efficacy related to the production of pro-inflammatory cytokines involved in the perpetuation of synovial inflammatory response.

To this end, protein expression of TNFα and IL6 was analysed by ELISA 24 hours after treatment of activated macrophages and synoviocytes with increasing concentrations of either free or loaded Mtx. Results revealed that both treatments reduce cytokine secretion levels in a concentration-dependent manner on activated macrophages (Figure 6 A and B). Though, Mtx-loaded polymersomes show a strong effect in reducing the secretion level of both cytokines, which could be possibly due to their enhanced uptake by activated cells. This suggests that the intracellular availability of Mtx could be increased by the PMPC-PDPA polymersomes. In fact, even lower concentrations of loaded Mtx (2.5 μg/mL) reduced TNFα levels by 1.5-fold comparing with the free drug treatment (Figure 6A). IL6 concentration was reduced to almost undetectable levels when activated macrophages were treated with a Mtx-loaded PMPC-PDPA polymersomes at concentrations higher than 2.5 μg/mL; while equal concentrations of the free drug results in a ~5-fold higher levels of the same cytokine (Figure 6B).

ELISA results on activated synoviocytes also revealed that both treatments have the same effect in the secretion of TNFα, decreasing its concentration by nearly 1-fold compared to the non-treated control (*i.e.* 0 μg/mL of Mtx; Figure 6D). IL6 secretion levels in activated synoviocytes treated with Mtx-loaded PMPC-PDPA polymersomes, were decreased in a concentration-dependent down to 10 μg/mL; oppositely to free drug treatment that were maintained (Figure 6E).

Additionally, RT-qPCR was carried out on both activated synoviocytes and macrophages 24 hours after treatment with loaded or free Mtx to further investigate the expression profile of a set of inflammation-related genes.

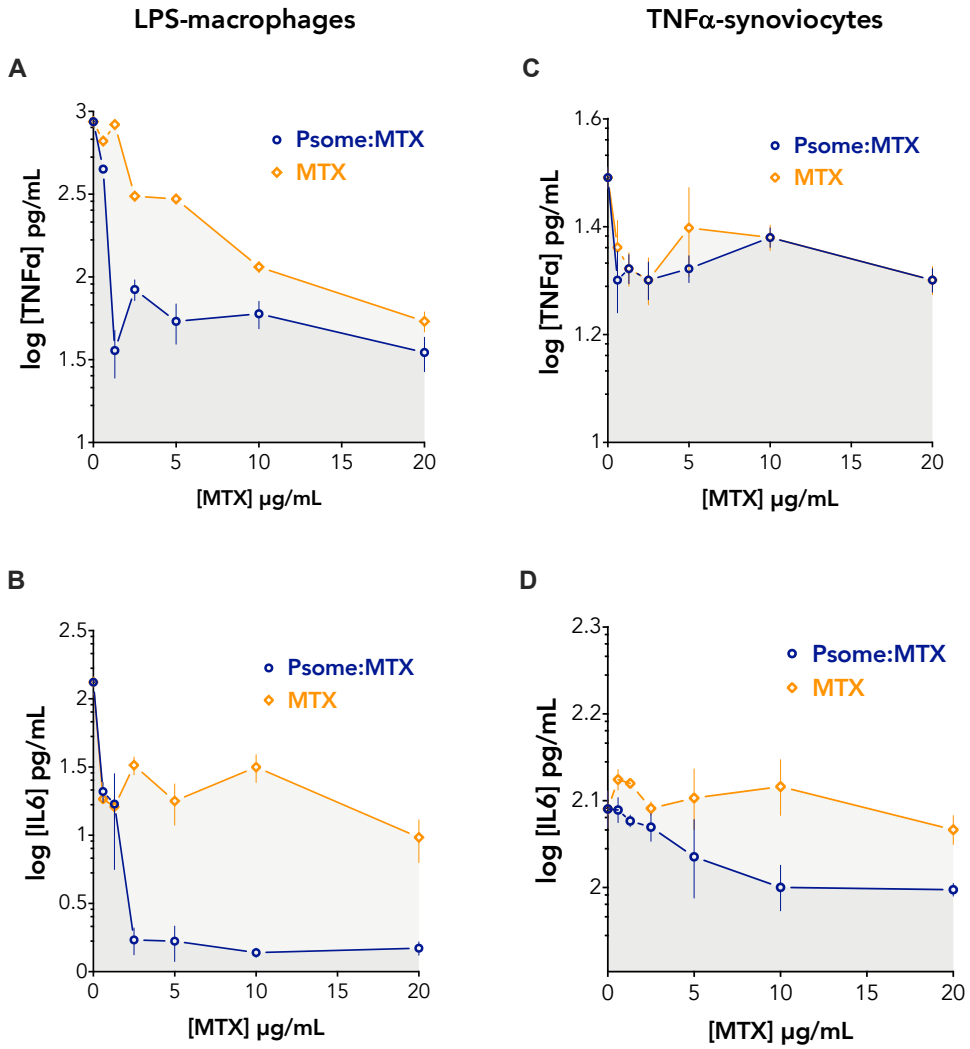

Figure 6. ELISA analysis on the TNFα and IL6 protein secretion levels in **(A, B)** LPS-activated macrophages and **(C, D)** TNFα-activated synoviocytes after 24 hours incubation with increasing concentrations of either free Mtx or Mtx-loaded PMPC-PDPA polymersomes. Data express as mean ± SD (n=3).

Results confirmed that activation of macrophages and synoviocytes induces the up-regulation of all tested pro-inflammatory genes (Figure 7). Treatment of activated macrophages with Mtx-loaded PMPC-PDPA polymersomes significantly inhibit the up-regulation of all tested pro-inflammatory cytokines and chemokines expression levels (Figure 7A). Similarly, free Mtx treatment also significantly reduced the expression levels of all these genes, except for the TNFα (Figure 7A).

RT-qPCR analyses on synoviocytes revealed that both treatments significantly reduce the IL1β, IL6 and MMP13 gene expression levels (Figure 7B). Particularly, IL6 gene expression was significantly decreased on both cell types when treated with Mtx-loaded PMPC-PDPA polymersomes ($p<0.01$ and $p<0.0001$ comparing with the free drug treatment, for macrophages and synoviocytes, respectively; Figure 7).

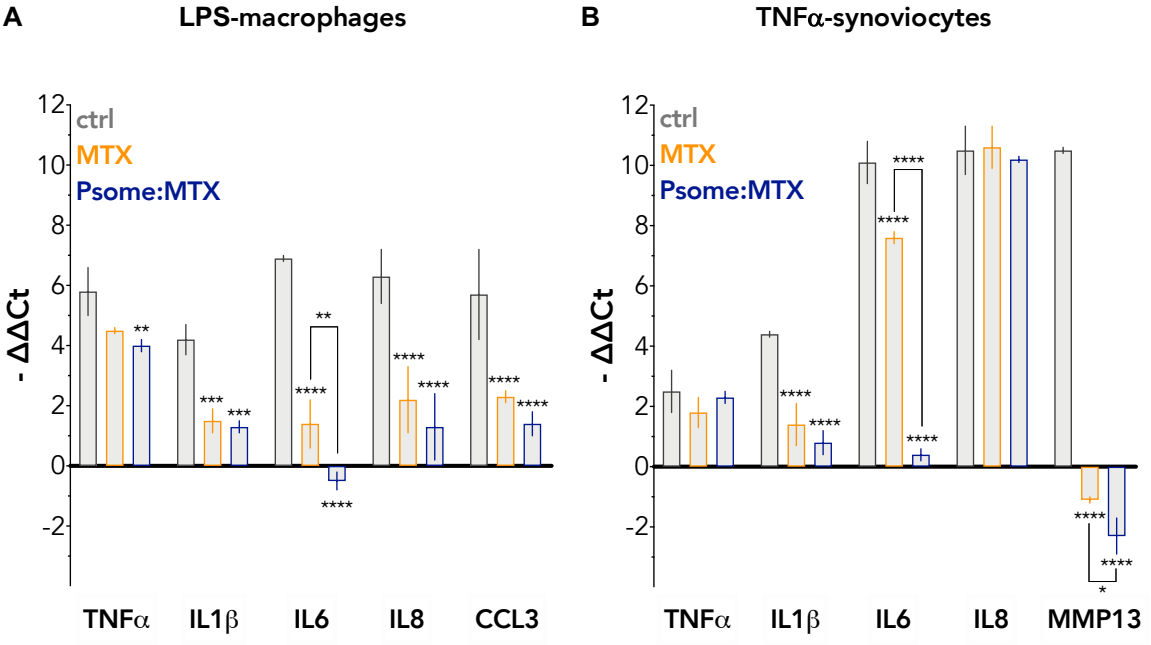

Figure 7. RT-qPCR on the gene expression levels in **(A)** LPS-activated macrophages and **(B)** TNFα-activated synoviocytes after 24 hours incubation with either free Mtx or Mtx-loaded PMPC-PDPA polymersomes. Data express as mean ± SD (n=3). The differences relative to non-treated control were statistically significant for *p<0.05, **p<0.01, ***p<0.001 and ****p<0.0001.

Taken together, *in vitro* inflammation studies demonstrate that Mtx-loaded PMPC-PDPA polymersomes have strong effect on the inhibition of the NF-κB nuclear translocation (Figure 5), as well as, on the modulation of the pro-inflammatory genes and on the protein expression profiles (Figure 6 and 7).

4. Discussion

RA is characterised by a chronic immune-mediated inflammatory process in synovial joint tissues [1, 2]. Local synovial cellular interactions, namely between synovial macrophages and fibroblast, are key in the perpetuation of synovial inflammation, as well as in the processes that drives cartilage damage and further

bone erosion [1, 2, 5, 9, 11]. Thereby, both macrophages and synoviocytes become attractive targets for drug delivery within inflamed tissues due to their importance in RA pathogenesis.

The use of Mtx is the golden standard for the treatment of RA, however often associated with several off-site cytotoxicity. In this study we present a novel approach whereby pH-responsive PMPC-PDPA polymersomes loaded with Mtx have been developed for the treatment of RA.

Characterisation studies confirm the effectiveness of PMPC-PDPA polymersomes as a nanomedicine that ensures the loading of Mtx and its release on-site when required. The obtained small size and spherical morphology of PMPC-PDPA polymersomes (Figure 1A) are key features that enable to predict their stability *in vivo,* for instance, under circulation in the bloodstream [62]. The nanometric size facilitate the passive accumulation of polymersomes through the enhanced permeation and retention effect, by taking advantage of the prominent angiogenesis and enhanced vascularisation of inflamed synovial tissues [28, 31, 39, 43, 62]. In addition, these features increase the surface area relatively to the volume of the polymersome, thus allowing higher biologic interactions and hence endorsing the cell binding affinity and uptake [28, 31, 32, 39, 43, 62]. *In vitro* cell uptake studies demonstrated that PMPC-PDPA polymersomes rapidly accumulate within inflammation activated macrophages and synoviocytes without affecting their viability (Figure 2 and 3). This enhanced internalisation is possibly granted by the polymersomes nanometric size [31, 32] together with the high ligand affinity of PMPC towards SRBI and CD36 cell scavenger receptors, which are highly expressed in these activated cells (Figure 4).

Drug release studies confirm the acidic pH responsiveness of PMPC-PDPA polymersomes to bestow their rapid disassemble along the endocytic pathway (pH 5.0 at 37ºC; Figure 1C). As the Mtx mechanism of action occurs intracellularly [21-23], this feature is key to enable the efficient intracellular delivery of loaded drug within endosomes and ultimately its release to the cytosol. Thereby, pH-responsive PMPC-PDPA polymersomes enable the efficient delivery of loaded Mtx within target synovial cells.

As mentioned before, synovial macrophages and synoviocytes have a highly active role in the maintenance and perpetuation of the synovial inflammatory process in RA pathogenesis, mainly through the secretion of high levels of pro-inflammatory cytokines and chemokines [1, 2, 5, 8, 9, 11]. Under synovitis, these inflammatory mediators strongly contribute for synovial cells activation since the early disease

stages [1, 2, 9]. Particularly, synoviocytes take on a more aggressive and invasive phenotype that eventually drive to irreversible joint destruction [2, 8, 10-12]. The activation of the inflammatory phenotype in both macrophages and synoviocytes has been shown as result of the NF-κB signalling pathway activation (Figure 5) and the increased gene expression of key pro-inflammatory mediators (Figure 7).

In vitro inflammation cellular studies gave insight into the anti-inflammatory action of low dose Mtx in mediating the secretion of metalloproteases and in the regulation of cytokines and chemokines expression profiles [9, 21-23]. Mtx-loaded PMPC-PDPA polymersomes showed an anti-inflammatory effect in inhibiting the NF-κB nuclear translocation on both activated macrophages and synoviocytes (Figure 5). Moreover, by inhibiting the NFκB nuclear translocation on activated synoviocytes (Figure 5), Mtx-loaded PMPC-PDPA also might have an impact on bone erosion, because RANK, which induces osteoclast differentiation, is regulated by NFκB-dependent signalling [1, 2, 8-12].

Additionally, the inactivation of the NF-κB signalling pathway in turn results in the decreased expression of pro-inflammatory cytokines and chemokines involved in the progression of immune and inflammatory responses associated with RA pathogenesis (Figure 6 and 7). Among these, IL6 mediates both innate and adaptive immune system activation, together with TNFα and IL1β, since the early acute inflammatory state of the disease [1, 2, 9, 63, 64]. Therefore, the down-regulation of IL6 and IL1β observed on both cell types (Figure 6 and 7) are crucial for treatment efficacy, due to their importance in driving chronic synovial inflammation.

Moreover, the immunosuppressive effect followed by Mtx-loaded PMPC-PDPA polymersomes treatment was further demonstrated with the reduce expression levels of IL8 and CCL3 genes on macrophages (Figure 7A). These chemokines are involved in the acute inflammation phase of RA mediating the recruitment and activation of immune cells to the synovium [1, 2, 9, 65]. Further confirmation of the potential efficacy of Mtx-loaded PMPC-PDPA polymersomes in in shutting down the joint destructive process in RA was results from the down-regulation of MMP13 gene expression on synoviocytes (Figure 7B). During synovial inflammation, synoviocytes activation induces the production of these metalloproteases, which are responsible for the cartilage and bone erosion [1, 2, 9-12].

In summary, all the performed *in vitro* cellular studies prove: *(i)* the enhanced targeting ability of PMPC-PDPA polymersomes to be internalised by inflammation-activated macrophages and synoviocytes; *(ii)* the effective intracellular drug delivery and release on-site; *(iii)* the enhanced efficacy in inhibiting inflammation-

activated signalling pathways and *(iv)* the down-expression of pro-inflammatory cytokines and chemokines. Thus, PMPC-PDPA polymersomes loading Mtx promote synovial inflammation resolution *in vitro*.

5. Conclusion

The PMPC-PDPA polymersomes selective delivery of low dose of Mtx within activated macrophages and synoviocytes exerts anti-inflammatory effects by acting at different levels of the pathophysiological cascade. In particular, the modulation of pro-inflammatory expression profiles seems to be crucial for shutting down synovial inflammation and further control disease progression. Thereby, pH-responsive PMPC-PDPA polymersomes improve the therapeutic efficacy of loaded Mtx in resolving synovial arthritic inflammation, while minimizing its off-target toxicity.

In conclusion, it is possible to recognise the potential of PMPC-PDPA polymersomes loading Mtx as a promising nanotherapy to target and treat RA. Future studies need to focus on the evaluation of the therapeutic efficacy of PMPC-PDPA polymersomes *in vivo* using relevant animal models of arthritis.

References

1 McInnes IB, Schett G. The pathogenesis of rheumatoid arthritis. N Engl J Med 2011;365(23):2205-19.

2 Müller-Ladner U, Pap T, Gay RE, Neidhart M, Gay S. Mechanisms of disease: the molecular and cellular basis of joint destruction in rheumatoid arthritis. Nat Clin Pract Rheumatol 2005;1(2):102-10.

3 Gouveia V, Lima S, Nunes C, Reis S. Non-Biologic Nanodelivery Therapies for Rheumatoid Arthritis. Journal of Biomedical Nanotechnology 2015;11(10):1701-21.

4 Cooles FA, Isaacs JD. Pathophysiology of rheumatoid arthritis. Curr Opin Rheumatol 2011;23(3):233-40.

5 Kinne RW, Stuhlmüller B, Burmester GR. Cells of the synovium in rheumatoid arthritis. Macrophages. Arthritis Res Ther 2007;9(6):224.

6 Szekanecz Z, Besenyei T, Szentpétery A, Koch AE. Angiogenesis and vasculogenesis in rheumatoid arthritis. Curr Opin Rheumatol 2010;22(3):299-306.

7 Maracle CX, Kucharzewska P, Helder B, et al. Targeting non-canonical nuclear factor-κB signalling attenuates neovascularization in a novel 3D model of rheumatoid arthritis synovial angiogenesis. Rheumatology (Oxford) 2017;56(2):294-302.

8 Karouzakis E, Neidhart M, Gay RE, Gay S. Molecular and cellular basis of rheumatoid joint destruction. Immunol Lett 2006;106(1):8-13.

9 Choy E. Understanding the dynamics: pathways involved in the pathogenesis of rheumatoid arthritis. Rheumatology (Oxford) 2012;51 Suppl 5:v3-11.

10 Hardy RS, Hülso C, Liu Y, et al. Characterisation of fibroblast-like synoviocytes from a murine model of joint inflammation. Arthritis Res Ther 2013;15(1):R24.

11 Bustamante MF, Garcia-Carbonell R, Whisenant KD, Guma M. Fibroblast-like synoviocyte metabolism in the pathogenesis of rheumatoid arthritis. Arthritis Res Ther 2017;19(1):110.

12 Bartok B, Firestein GS. Fibroblast-like synoviocytes: key effector cells in rheumatoid arthritis. Immunol Rev 2010;233(1):233-55.

13 Tas SW, Maracle CX, Balogh E, Szekanecz Z. Targeting of proangiogenic signalling pathways in chronic inflammation. Nat Rev Rheumatol 2016;12(2):111-22.

14 Bartok B, Hammaker D, Firestein GS. Phosphoinositide 3-kinase δ regulates migration and invasion of synoviocytes in rheumatoid arthritis. J Immunol 2014;192(5):2063-70.

15 Leblond A, Allanore Y, Avouac J. Targeting synovial neoangiogenesis in rheumatoid arthritis. Autoimmun Rev 2017;16(6):594-601.

16 Lefèvre S, Knedla A, Tennie C, et al. Synovial fibroblasts spread rheumatoid arthritis to unaffected joints. Nat Med 2009;15(12):1414-20.

17 Smolen JS, Landewé R, Breedveld FC, et al. EULAR recommendations for the management of rheumatoid arthritis with synthetic and biological disease-modifying antirheumatic drugs: 2013 update. Ann Rheum Dis 2014;73(3):492-509.

18 Smolen JS, Steiner G. Therapeutic strategies for rheumatoid arthritis. Nat Rev Drug Discov 2003;2(6):473-88.

19 Singh JA, Saag KG, Bridges SL, et al. 2015 American College of Rheumatology Guideline for the Treatment of Rheumatoid Arthritis. Arthritis Rheumatol 2016;68(1):1-26.

20 Upchurch KS, Kay J. Evolution of treatment for rheumatoid arthritis. Rheumatology (Oxford) 2012;51 Suppl 6:vi28-36.

21 Brown PM, Pratt AG, Isaacs JD. Mechanism of action of methotrexate in rheumatoid arthritis, and the search for biomarkers. Nat Rev Rheumatol 2016;12(12):731-42.

22 Tian H, Cronstein BN. Understanding the mechanisms of action of methotrexate: implications for the treatment of rheumatoid arthritis. Bull NYU Hosp Jt Dis 2007;65(3):168-73.

23 Wessels JA, Huizinga TW, Guchelaar HJ. Recent insights in the pharmacological actions of methotrexate in the treatment of rheumatoid arthritis. Rheumatology (Oxford) 2008;47(3):249-55.

24 Khan ZA, Tripathi R, Mishra B. Methotrexate: a detailed review on drug delivery and clinical aspects. Expert Opin Drug Deliv 2012;9(2):151-69.

25 Visser K, Katchamart W, Loza E, et al. Multinational evidence-based recommendations for the use of methotrexate in rheumatic disorders with a focus on rheumatoid arthritis: integrating systematic literature research and expert opinion of a broad international panel of rheumatologists in the 3E Initiative. Ann Rheum Dis 2009;68(7):1086-93.

26 Visser K, van der Heijde DM. Risk and management of liver toxicity during methotrexate treatment in rheumatoid and psoriatic arthritis: a systematic review of the literature. Clin Exp Rheumatol 2009;27(6):1017-25.

27 Battaglia G, Ryan AJ. The evolution of vesicles from bulk lamellar gels. Nat Mater 2005;4(11):869-76.

28 Guan L, Rizzello L, Battaglia G. Polymersomes and their applications in cancer delivery and therapy. Nanomedicine (Lond) 2015;10(17):2757-80.

29 Contini C, Pearson R, Wang L, et al. Bottom-Up Evolution of Vesicles from Disks to High-Genus Polymersomes. iScience 2018;7:132-44.

30 Messager L, Gaitzsch J, Chierico L, Battaglia G. Novel aspects of encapsulation and delivery using polymersomes. Curr Opin Pharmacol 2014;18:104-11.

31 Massignani M, LoPresti C, Blanazs A, et al. Controlling cellular uptake by surface chemistry, size, and surface topology at the nanoscale. Small 2009;5(21):2424-32.

32 LoPresti C, Massignani M, Fernyhough C, et al. Controlling polymersome surface topology at the nanoscale by membrane confined polymer/polymer phase separation. ACS Nano 2011;5(3):1775-84.

33 Lomas H, Du J, Canton I, et al. Efficient encapsulation of plasmid DNA in pH-sensitive PMPC-PDPA polymersomes: study of the effect of PDPA block length on copolymer-DNA binding affinity. Macromol Biosci 2010;10(5):513-30.

34 Wang L, Chierico L, Little D, et al. Encapsulation of biomacromolecules within polymersomes by electroporation. Angew Chem Int Ed Engl 2012;51(44):11122-5.

35 Gouveia VM, Rizzello L, Nunes C, et al. Macrophage Targeting pH Responsive Polymersomes for Glucocorticoid Therapy. Pharmaceutics 2019;11(11).

36 Massignani M, Canton I, Sun T, et al. Enhanced fluorescence imaging of live cells by effective cytosolic delivery of probes. PLoS One 2010;5(5):e10459.

37 Pegoraro C, Cecchin D, Gracia LS, et al. Enhanced drug delivery to melanoma cells using PMPC-PDPA polymersomes. Cancer Lett 2013;334(2):328-37.

38 Colley HE, Hearnden V, Avila-Olias M, et al. Polymersome-mediated delivery of combination anticancer therapy to head and neck cancer cells: 2D and 3D in vitro evaluation. Mol Pharm 2014;11(4):1176-88.

39 Robertson JD, Ward JR, Avila-Olias M, Battaglia G, Renshaw SA. Targeting Neutrophilic Inflammation Using Polymersome-Mediated Cellular Delivery. J Immunol 2017;198(9):3596-604.

40 Rizzello L, Robertson JD, Elks PM, et al. Targeting mononuclear phagocytes for eradicating intracellular parasites. 2017.

41 Murdoch C, Reeves KJ, Hearnden V, et al. Internalization and biodistribution of polymersomes into oral squamous cell carcinoma cells in vitro and in vivo. Nanomedicine (Lond) 2010;5(7):1025-36.

42 Canton I, Massignani M, Patikarnmonthon N, et al. Fully synthetic polymer vesicles for intracellular delivery of antibodies in live cells. FASEB J 2013;27(1):98-108.

43 Canton I, Battaglia G. Endocytosis at the nanoscale. Chem Soc Rev 2012;41(7):2718-39.

44 Lardner A. The effects of extracellular pH on immune function. J Leukoc Biol 2001;69(4):522-30.

45 Fukamachi T, Wang X, Mochizuki Y, Maruyama C, Saito H, Kobayashi H. Acidic environments enhance the inhibitory effect of statins on proliferation of synovial cells. Int Immunopharmacol 2013;17(1):148-53.

46 El Khoury JB, Moore KJ, Means TK, et al. CD36 mediates the innate host response to beta-amyloid. J Exp Med 2003;197(12):1657-66.

47 Park YM. CD36, a scavenger receptor implicated in atherosclerosis. Exp Mol Med 2014;46:e99.

48 Farnaghi S, Crawford R, Xiao Y, Prasadam I. Cholesterol metabolism in pathogenesis of osteoarthritis disease. Int J Rheum Dis 2017;20(2):131-40.

49 Linton MF, Tao H, Linton EF, Yancey PG. SR-BI: A Multifunctional Receptor in Cholesterol Homeostasis and Atherosclerosis. Trends Endocrinol Metab 2017;28(6):461-72.

50 Du J, Tang Y, Lewis AL, Armes SP. pH-sensitive vesicles based on a biocompatible zwitterionic diblock copolymer. J Am Chem Soc 2005;127(51):17982-3.

51 Robertson JD, Rizzello L, Avila-Olias M, et al. Purification of Nanoparticles by Size and Shape. Sci Rep 2016;6:27494.

52 Fetsch C, Gaitzsch J, Messager L, Battaglia G, Luxenhofer R. Self-Assembly of Amphiphilic Block Copolypeptoids - Micelles, Worms and Polymersomes. Sci Rep 2016;6:33491.

53 Gaitzsch J, Delahaye M, Poma A, Du Prez F, Battaglia G. Comparison of metal free polymer-dye conjugation strategies in protic solvents. Polymer Chemistry 2016;7(17):3046-55.

54 Ruiz-Pérez L, Messager L, Gaitzsch J, et al. Molecular engineering of polymersome surface topology. Sci Adv 2016;2(4):e1500948.

55 Magalhães LM, Nunes C, Lúcio M, Segundo MA, Reis S, Lima JL. High-throughput microplate assay for the determination of drug partition coefficients. Nat Protoc 2010;5(11):1823-30.

56 Lund ME, To J, O'Brien BA, Donnelly S. The choice of phorbol 12-myristate 13-acetate differentiation protocol influences the response of THP-1 macrophages to a pro-inflammatory stimulus. J Immunol Methods 2016;430:64-70.

57 Lin HC, Lin TH, Wu MY, et al. 5-Lipoxygenase inhibitors attenuate TNF-α-induced inflammation in human synovial fibroblasts. PLoS One 2014;9(9):e107890.

58 Matias D, Dubois LG, Pontes B, et al. GBM-Derived Wnt3a Induces M2-Like Phenotype in Microglial Cells Through Wnt/β-Catenin Signaling. Mol Neurobiol 2019;56(2):1517-30.

59 Gouveia VM, Lopes-de-Araújo J, Costa Lima SA, Nunes C, Reis S. Hyaluronic acid-conjugated pH-sensitive liposomes for targeted delivery of prednisolone on rheumatoid arthritis therapy. Nanomedicine (Lond) 2018;13(9):1037-49.

60 Fujiwara N, Kobayashi K. Macrophages in inflammation. Curr Drug Targets Inflamm Allergy 2005;4(3):281-6.

61 Oishi Y, Manabe I. Macrophages in inflammation, repair and regeneration. Int Immunol 2018;30(11):511-28.

62 Blanco E, Shen H, Ferrari M. Principles of nanoparticle design for overcoming biological barriers to drug delivery. Nat Biotechnol 2015;33(9):941-51.

63 Narazaki M, Tanaka T, Kishimoto T. The role and therapeutic targeting of IL-6 in rheumatoid arthritis. Expert Rev Clin Immunol 2017;13(6):535-51.

64 Fonseca JE, Santos MJ, Canhão H, Choy E. Interleukin-6 as a key player in systemic inflammation and joint destruction. Autoimmun Rev 2009;8(7):538-42.

65 Skov L, Beurskens FJ, Zachariae CO, et al. IL-8 as antibody therapeutic target in inflammatory diseases: reduction of clinical activity in palmoplantar pustulosis. J Immunol 2008;181(1):669-79.

66 Mircioiu C, Voicu V, Anuta V, et al. Mathematical Modeling of Release Kinetics from Supramolecular Drug Delivery Systems. Pharmaceutics 2019;11(3).

67 Mhlanga N, Ray SS. Kinetic models for the release of the anticancer drug doxorubicin from biodegradable polylactide/metal oxide-based hybrids. Int J Biol Macromol 2015;72:1301-7.

Supplementary Information

- *Drug quantification study*

The drug encapsulation efficiency was calculated as the ratio between the final and initial mass of loaded methotrexate (Mtx) in solution after the injection process. The drug loading efficiency was determined according to a previously reported method represented as the number of Mtx molecules loaded within the total lumen volume of PMPC-PDPA polymersomes (which is related with the size of the vesicle and the actual amount of loaded drug) [34, 35].

- *Drug-polymer interaction study*

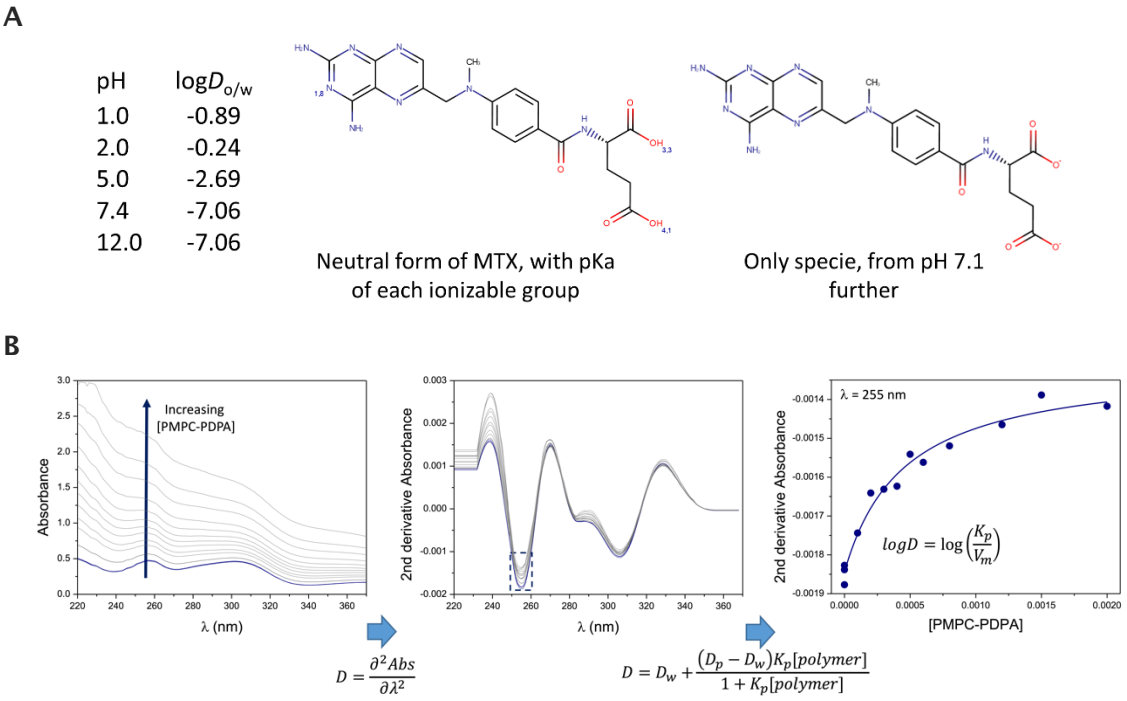

Figure S1. (A) Log $D_{o/w}$ calculations for Mtx at different pH conditions using the MarvinSketch calculator (Chemaxon). **(B)** Absorption spectra and second-derivative spectra of Mtx at pH 7.4 (25 μM) (blue lines) incubated in with increasing concentrations of PMPC-PDPA polymersomes at 37ºC (gray lines) (0 – 120 μM). Graphic represents the fitting curve of the experimental second-derivative spectrophotometric data using a nonlinear least squares regression method at wavelength 255 nm where the scattering is eliminated [55]. The partition coefficients are then calculated by fitting the equation to experimental derivative spectrophotometric data through a nonlinear regression method, where the adjustable parameters are D_p and K_p [55]. D, D_w and D_p correspond to the second derivative of total, aqueous and polymer absorbance of Mtx, respectively; K_p is the partition coefficient (M^{-1}), *[polymer]* the PMPC-PDPA concentration ($mol.L^{-1}$) and $V\varphi$ the polymer molar volume ($L.mol^{-1}$).

- *Drug release study*

To examine the kinetics and mechanism of Mtx release from the PMPC-PDPA polymersomes, the data obtained from the *in vitro* drug release studies of each pH profile was analysed using various models, including the zero and first order, Higuchi, and Hixson-Crowell models [66, 67].

Table S1: Mathematical models for drug-release kinetics.

Release Model	Equation [1]	Information
Zero-Order	$Q = Q_0 + K_0 t$	refers to the process of constant drug release from a drug delivery device
First-Order	$\text{Log } C = \text{Log } C_0 - k_1 t / 2.303$	represents a system where the release rate of the drug depends on the concentration of the drug in the system
Hixson-Crowell	$Q_0 1/3 - Q_t 1/3 = K_{HC}\, t$	describes the release from systems where there is a change in surface area and diameter of particles
Higuchi	$Qt = k_H\, (t)^{0.5}$	assumes that the drug´s release is caused primarily by a diffusion mechanism

[1] Q is the amount of drug released or dissolved; Q_0 is initial amount of drug in solution; C_0 is the initial concentration of drug; t is the time in hours; F is the fraction of drug release at time t; M_t/M is the fraction of drug released at time t; K are the rate constants for each models.

Table S2: Correlation coefficient (r^2) from various drug release mathematical models for each pH profile.

	Zero-Order	First-Order	Hixson-Crowell	Higuchi
pH 5.0	0.890	0.348	0.648	0.994
pH 6.5	0.957	0.561	0.708	0.962
pH 7.4	0.676	0.462	0.573	0.684

- *Gene expression study*

For the RT-qPCR experiments, the ribosomal protein L13A (RPL13A) and glyceraldehyde 3-phosphate dehydrogenase (GADPH) were used as reference genes, respectively for THP1 and HFLS cells.

Table S3: Forward (Fw) and reverse (Rv) gene sequences of designed primers (PRIMER-BLAS from Sigma-Aldrich) used for gene expression studies.

Gene	Primers			
RPL13A	Fw	CTTCCTTTCCAGTTTGCTGC	Rv	TCTCGCAGTCCACTTCCTTT
GADPH	Fw	CAGCCTCAAGATCATCAGCA	Rv	GTCTTCTGGGTGGCAGTGAT
TNFα	Fw	GGAGAAGGGTGACCGACTCA	Rv	CTGCCCAGACTCGGCAA
IL8	Fw	TCCAAACCTTTCCACCCCAAA	Rv	ACCCTCTGCACCCAGTTTTC
IL6	Fw	TGCAATAACCACCCCTGACC	Rv	AGCTGCGCAGAATGAGATGA
IL1β	Fw	CCAAAGAAGAAGATGGAAAAGGC	Rv	GGGAACTGGGCAGACTCAAA
CCL3	Fw	GCTCTCTGCAACCAGTTCTCT	Rv	CACTGGCTGCTCGTCTCAAA
MMP13	Fw	TTGAGCTGGACTCATTGTCG	Rv	TCTCGGAGCCTCTCAGTCAT

RT-qPCR data was analysed using the comparative cycle threshold (Ct) method, also known as the ΔΔCt method. The Ct value of each target gene was normalized to the reference gene, obtaining the ΔCt value (eq. 1) of treatment and non-treated control. Then, the change in Ct is compared against the control to obtain the ΔΔCt value (eq. 2). Then, the – ΔΔCt values corresponds to the folds in gene expression change of the treated compared to the non-treated group.

$$\Delta Ct = Ct\ (target\ gene) - Ct\ (reference\ gene) \quad (1)$$

$$\Delta\Delta Ct = \Delta Ct\ (treated) - \Delta Ct\ (non\text{-}treated) \quad (2)$$

- *Characterisation study*

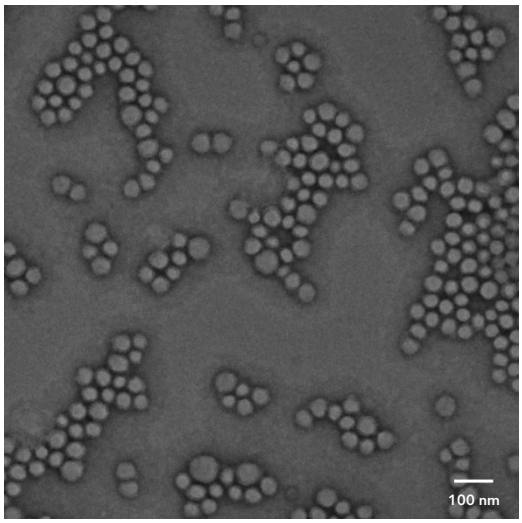

Figure S2. TEM micrograph of Cy5-PMPC-PDPA polymersomes produced by solvent-switch method (100 nm scale bar).

- *Cell viability study*

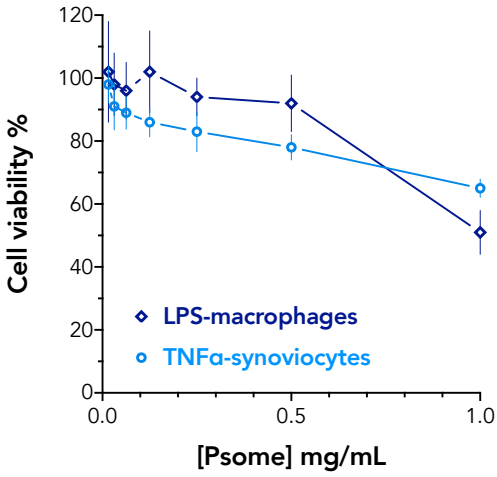

Figure S3. Cell viability of 24 hours treatment with unloaded PMPC-PDPA polymersomes in activated macrophages and synoviocytes.

Chapter 3

IV. pH-NITRA: pH-responsive nano immune therapy for rheumatoid arthritis

Virgínia M. Gouveia [1,2,3,4], Loris Rizzello [3,4,5], Bruno Vidal [6], Edoardo Scarpa [3,4], Claudia Nunes [1], Alessandro Poma [3,4,7], António Oliveira [2], João E. Fonseca [6,8], Salette Reis [1] and Giuseppe Battaglia [3,4,5,9,10]

[1] LAQV, REQUIMTE, Department of Chemical Sciences, Faculty of Pharmacy, University of Porto, 4050-313 Porto, Portugal
[2] Abel Salazar Biomedical Sciences Institute, University of Porto, 4050-313 Porto, Portugal
[3] Department of Chemistry, University College London, London WC1H 0AJ, UK
[4] Institute of Physics of Living Systems, University College London, London WC1H 0AJ, UK
[5] Institute for Bioengineering of Catalonia (IBEC), The Barcelona Institute of Science and Technology, 08028 Barcelona, Spain
[6] Rheumatology Research Unit, Institute of Molecular Medicine (IMM – João Lobo Antunes), Faculty of Medicine, University of Lisbon, 1649-028 Lisboa, Portugal
[7] Division of Biomaterials and Tissue Engineering, UCL Eastman Dental Institute, University College London, London WC1X 8LD, UK
[8] Serviço de Reumatologia e Doenças Ósseas Metabólicas, Hospital de Santa Maria, CHLN
[9] EPSRC/JEOL Centre for Liquid Phase Electron Microscopy, University College London, London WC1H 0AJ, UK
[10] Catalan Institution for Research and Advanced Studies (ICREA), 08010 Barcelona, Spain

---

Original research article.

Abstract

Rheumatoid arthritis (RA) is a systemic immune-mediated chronic inflammatory disease. It is characterised by inflammation of joint synovial tissues, followed by a progressive and irreversible joint structural destruction. Current gold-standard treatment of RA includes conventional disease-modifying anti-rheumatic drugs, such as methotrexate (Mtx). Despite being a highly effective drug, severe side effects and intolerance issues often limits its therapeutic potential. Here, we present a pH-responsive nano-immune therapy for rheumatoid arthritis – pH-NITRA – with the aim to overcome the therapeutic drawbacks of Mtx. *In vivo* studies were carried out in an established adjuvant-induced arthritis animal model to evaluate the biodistribution, biocompatibility and therapeutic efficacy of pH-NITRA. First, we demonstrate the selective accumulation of pH-NITRA within the synovial inflammation site and possibly reduced off-target action in other organs. Second, we show the beneficial therapeutic effect of pH-NITRA loading Mtx in preventing both inflammatory arthritic manifestations and destruction of joints after 15 days of treatment. With this study, we prove the therapeutic potential of pH-NITRA in the complete abrogation of arthritis progression, which makes it a promising anti-inflammatory nanotherapy in the treatment of RA.

Key words

rheumatoid arthritis, methotrexate, nanotherapy, polymersomes, *in vivo,* AIA model, biodistribution, therapeutic efficacy

Highlights

- pH-NITRA accumulated in areas of synovial inflammation.
- pH-NITRA resolve arthritic inflammation.
- pH-NITRA abrogate the joint destructive process.
- Mtx-loaded pH-NITRA showed similar efficacy as the free Mtx.
- pH-NITRA remarkably showed anti-inflammatory efficacy.

1. Introduction

Rheumatoid arthritis (RA) is chronic inflammatory immune mediated disease affecting nearly 1% of the population [1-3]. Arthritic disorders are characterised by progressive inflammation of the synovial tissue of multiple body joints, causing progressive loss of joint functionality [2-5]. At an early stage, the disease manifestations include synovitis, erythema and joint swelling [2, 5-11]. As the disease progresses, cellular interactions and cascades of pro-inflammatory cytokines in the synovium results in the formation of pannus tissue, causing joint stiffness [2, 4-7, 10-14]. At later disease stages, the chronic synovial inflammation leads to cartilage damage and then eventually the bone erosion [4-7]. Therefore, the stage of synovial inflammation of joints is a key hallmark to measure the disease progression and severity [6, 7, 15].

Although not regarded as lethal, RA is a serious health condition with no resolutive cure so far, despite the advances of treatment modalities focused mostly towards the treatment of inflammation manifestations [16-18]. During the first half of the 20th century, the progression of RA from synovial inflammation to the major joint disability was often inevitable [6, 9, 17, 18]. The European League Against Rheumatism (EULAR) and the American College of Rheumatology (ACR) endorse that an early intervention is crucial for treatment success in the remission of arthritic inflammation and in preventing the irreversible joint destruction [9, 17, 18]. The current treatment guidelines of EULAR and ACR include the use of methotrexate (Mtx) as a monotherapy or in a combination therapy with glucocorticoids [2, 9, 16-18]. Despite being a highly effective disease-modifying anti-rheumatic drug used in clinic for RA treatment, several adverse effects (hepatotoxicity, ulcerative colitis, nephrotoxicity) and intolerance issues frequently limit its therapeutic potential [2, 19-21].

In the last 15 years, several nanomedicines have been developed to improve the Mtx selectivity and on-site delivery in inflamed synovial tissues, in order to overcome the drawbacks that this drug entails [3, 22, 23]. Our recent findings (Gouveia, V. M. *et al.*, unpublished) encourage the use of Mtx-loaded pH-responsive polymersomes made of poly(2-(methacryloyloxy) ethyl phosphorylcholine – poly(2-(diisopropylamino)ethyl methacrylate (PMPC–PDPA), as a promising nanomedicine to target and treat RA. This *in vitro* study demonstrates PMPC-PDPA polymersomes ability to enable the selective and increase uptake by activated synovial cells and to control the intracellular release of loaded Mtx. Hence, to improve the on-site

drug therapeutic activity and reduce the immune-mediated inflammatory response *in vitro*. Based on these very recent findings, we propose a promising pH-responsive nano immune therapy for rheumatoid arthritis – pH-NITRA. The aim in this *in vivo* study was to investigate pH-NITRA safety and therapeutic effectiveness in established adjuvant-induced arthritis (AIA) animal model. The AIA animal model for arthritis has been extensively used for testing a variety of anti-arthritic and biologic therapies, as it shares key features with human RA [24, 25]. Comparing with other arthritis animal models, the AIA exhibits the greatest magnitude of disease symptoms as measured by erythema, cellular infiltration, synovial hyperplasia and high cytokine levels within the synovial joint [24, 25]. Other important arthritic hallmarks of advanced disease stages, such as cartilage damage and bone erosions, are also present in this model [25, 26].

The pH-NITRA nanotherapy was evaluated for its anti-inflammatory and anti-arthritic efficacy by assessing (*i*) the arthritis inflammation score, (*ii*) the serum level of pro-inflammatory cytokines and (*iii*) the histopathological features of paw ankle joints of AIA rats. With this *in vivo* study, we demonstrate the ability of pH-NITRA to accumulate within inflamed joints of AIA rats, to decrease the synovial inflammation and to completely abrogate arthritis progression, while reducing deleterious off-site effects that compromises the effectiveness of RA treatment.

2. Methods

2.1. Preparation and characterization of pH-NITRA

The pH-responsive poly(2-methacryloyloxyethyl phosphorylcholine)–poly(2-(diisopropylamino)ethyl methacrylate) (PMPC-PDPA) polymersomes were prepared using the previously reported pH-switch method with some modifications [27, 28]. Briefly, under sterile conditions, $PMPC_{25}$-$PDPA_{68}$ copolymer, previously synthesised by atom-transfer radical polymerization [29], was dissolved in acidic phosphate-buffered saline (PBS 0.1 M, Sigma-Aldrich) up to a concentration of 10 mg/mL, and the pH solution was adjusted to pH 2.0 by addition of hydrochloric acid (HCL 2 M). The pH-driven self-assembly process was controlled by increasing the solution pH from 2.0 to approximately neutral pH 7.4, through needle injection system (2 μL/minute), with sodium hydroxide (NaOH 0.5 M). Formulations of pH-NITRA (i.e. PMPC-PDPA polymersomes loading methotrexate (Mtx, $C_{20}H_{22}N_8O_5$, MW 454.44, λ (300 nm), Sigma-Aldrich)) were prepared also using the above-mentioned pH-switch

method by injecting the Mtx (3 mg/mL) dissolved together in the NaOH solution. Additionally, for fluorescence imaging purposes Cyanine7-labelled PMPC-PDPA polymersomes were prepared using the solvent-switch method as reported with some modifications [30]. Briefly, 10% (w/w) Cy7-$PMPC_{25}$-$PDPA_{68}$ copolymer was dissolved together with the $PMPC_{25}$-$PDPA_{68}$ in an organic solution of 3:1 (v/v) methanol:tetrahydrofuran (Sigma-Aldrich) for a final copolymer concentration of 20 mg/mL. Then, PBS at neutral pH was added into the copolymer solution under constant stirring at 42ºC, through needle injection system at the rate of 2 μL/minute, until a 0.6% (w/v) PBS content was reached. Finally, any remained organic solvent was removed by dialysis (3.5 kD MWCO tubing membrane, Spectrum Labs) against PBS for 2 days. Afterwards, all formulations of PMPC-PDPA polymersomes were purified, as previously described by size exclusion chromatography, and characterised in terms of size, size distribution and morphology [28]. Dynamic light scattering (DLS) technique was used for the hydrodynamic size measurements in the Zetasizer Nano ZS (Zen1600, Malvern Instruments), equipped with a 633 nm HeNe laser in a scattering angle of 173º. Additionally, the morphology was accessed by transmission electronic microscopy (TEM) using a JEOL 2100 operating at 200 kV, equipped with an Orius SC2001CCD Gatan camera. Prior to DLS and TEM characterization, all samples were respectively prepared as previously reported [31, 32]. Follow the purification process, the pH-NITRA drug loading capacity, estimated as the number of Mtx molecules per PMPC-PDPA polymersome, was determined using a previously reported method [32, 33], after measurement on the amount of $PMPC_{25}$-$PDPA_{68}$ copolymer and loaded Mtx by high-performance liquid chromatography (HPLC, Dionex Ultimate®3000, Thermo Scientific).

2.2. *In vivo* pH-NITRA therapeutic efficacy

2.2.1. *Animal experimental design*

Adjuvant induced arthritis (AIA) 8-week-old female Wistar rats purchased from Charles River laboratories international (Spain) were housed in European type II standard filter top cages (Tecniplast) at the Specific Pathogen Free animal facility at the Institute of Molecular Medicine at the Faculty of Medicine, University of Lisbon. Here, the animals were individually identified and randomly housed in experimental groups of n=5, as follows: *(i)* AIA treated with Mtx (0.223 mg/kg body weight by daily intraperitoneal (i.p.) administration); *(ii)* AIA treated with Mtx-

loaded PMPC-PDPA polymersomes (0.223 mg/kg/day via i.p.); *(iii)* AIA treated with unloaded PMPC-PDPA polymersomes (10 mg/kg body weight corresponding to the an equal mass of polymer injected in the *(ii)* group); the respective *(iv)* AIA and *(v)* non-arthritic healthy vehicle groups (received an equal volume of PBS). Daily i.p. injections in treated and vehicle groups started 4 days after disease induction, when the AIA Wistar rats already presented clinical signs of arthritis [34-36]. Experiments were approved by the Animal User and Ethical Committees, at the Institute of Molecular Medicine according to Portuguese law and European recommendations.

2.2.2. *Arthritic inflammatory signs evaluation*

Arthritic inflammation signs in rats' paws and body weight were evaluated on a daily basis during the 15 days period of treatment. Inflammation scores were recorded following standard protocols and criteria established [34-36] by counting the score of each joint in a scale of 0 – 3, where: 0 = absence, 1 = erythema; 2 = erythema and joint swelling; 3 = deformities and functional impairment of the entire paw. The total inflammation score of each animal was defined as the sum of the partial scores of each affected joint. Additionally, the swelling of the hind paws was evaluated by measuring the ankle perimeter. In the end, all animals were then sacrificed 19 days post disease induction (15 days after treatment was started) where a maximum disease activity and severity occurs [25]. At the sacrifice time animals were anesthetised with pentobarbital (100 mg/kg body weight) administrated intraperitoneally. Here, the blood samples were collected by cardiac puncture and then processed (centrifugation 2000 rcf for 10 minutes at 4ºC) for further serum subsequent analysis. Afterwards, the animal was perfused transcardially with PBS for vascular and organs haemoglobin release. The main organs (kidney, spleen, liver and heart) and all paws were also collected and wet weight for further analysis.

2.2.3. *Hind paws histopathological evaluation*

Left hind paw samples were collected at the time of sacrifice and fixed immediately in 10% (v/v) neutral buffered formalin solution and then decalcified in 10% (v/v) formic acid. Samples were then dehydrated and embedded in paraffin, serially sectioned at a thickness of 4 μm. Sections were stained with haematoxylin and eosin (H&E) for histological analysis and were scanned using Hamamatsu

NanoZoomerSQ slide scanner. The histopathological evaluation of structural changes and cellular infiltration was performed following previously reported [34-36] criteria in a blind fashion using 5 semi-quantitative scores: Sublining layer infiltration score (0 = none to diffuse infiltration, 1 = lymphoid cell aggregate, 2 = lymphoid follicles, 3 = lymphoid follicles with germinal center formation); Lining layer cell number score (0 = fewer than three layers, 1 = three to four layers, 2 = five to six layers, 3 = more than six layers); Bone erosion score (0 = no erosions, 1 = minimal, 2 = mild, 3 = moderate; 4 = severe); Cartilage surface (0 = normal, 1 = irregular, 2 = clefts, 3 = clefts to bone); Global severity score (0 = no signs of inflammation, 1 = mild, 2 = moderate, 3 = severe).

2.2.4. *Serum inflammation-related cytokines*

Serum levels of TNFα, IL1β and IL6 were quantified using a specific rat enzyme linked immunosorbent assay (ELISA, Invitrogen, Thermo Scientific) following the manufacturer protocol.

2.3. *In vivo* pH-NITRA pharmacokinetics and biodistribution

Animals from both healthy and arthritic vehicle groups were injected intraperitoneally (i.p.) with Cy7-labelled pH-NITRA polymersomes (10 mg/Kg body weight) at 24 hours prior sacrifice. For pharmacokinetics analysis, blood samples were collected from the rat tail at several timepoints (0.5, 2, 4, 8 and 24 hours) and immediately processed (centrifugation 2000 rcf for 10 minutes at 4ºC) for plasma separation from the blood cells. The plasma concentration of near infrared (NIR) fluorescence of Cy7-labelled pH-NITRA was measured using a multimode microplate fluorometer (Spark, Tecan, Switzerland). For the biodistribution study, 24 hours post i.p. injection., the main organs (kidney, spleen, liver and heart) were collected and wet weight and further NIR fluorescence analysis of Cy7-labelled pH-NITRA was accessed. Briefly, a part of the organ tissue was weight and homogenised following the protocol of the Precellys soft tissue lysing kit (CK14, Bertin Instruments, VWR, UK). The fluorescence of Cy7-labelled pH-NITRA was measured in using a multimode microplate fluorometer (Spark, Tecan, Switzerland). Additionally, an *in vivo* imaging system (IVIS, Perkin Elmer) was used to evaluate the biodistribution of Cy7-labelled pH-NITRA in the front and right hind paws of both healthy and AIA Wistar rats.

2.4. Data statistical analysis

Statistical analyses were performed using GraphPad Prism (version 8.2.1). Differences between groups were assessed by one-way or two-way ANOVA with Tukey multiple comparison test. The differences were statistically significant when * $p < 0.05$, ** $p < 0.01$, *** $p < 0.001$ and **** $p < 0.0001$.

3. Results and Discussion

3.1. pH-NITRA physicochemical characterisation

Formulations of pH-NITRA (*i.e.* PMPC-PDPA polymersomes) either unloaded or Mtx-loaded were successfully produced by pH-switch self-assembling methodology as previously mentioned (Gouveia V. M. *et al.*, unpublished).

Transmission electron microscopy (TEM) characterisation confirm the spherical morphology of pH-NITRA polymersomes with a uniform size distribution of about 90 nm (Figure 1A). Dynamic light scattering (DLS) measurements showed that both Mtx-loaded and unloaded pH-NITRA polymersomes presented unimodal size distribution profiles with hydrodynamic diameters (D_h, Figure 1B) of 93.2 ± 12.7 nm and 96.4 ± 11.5 nm, respectively.

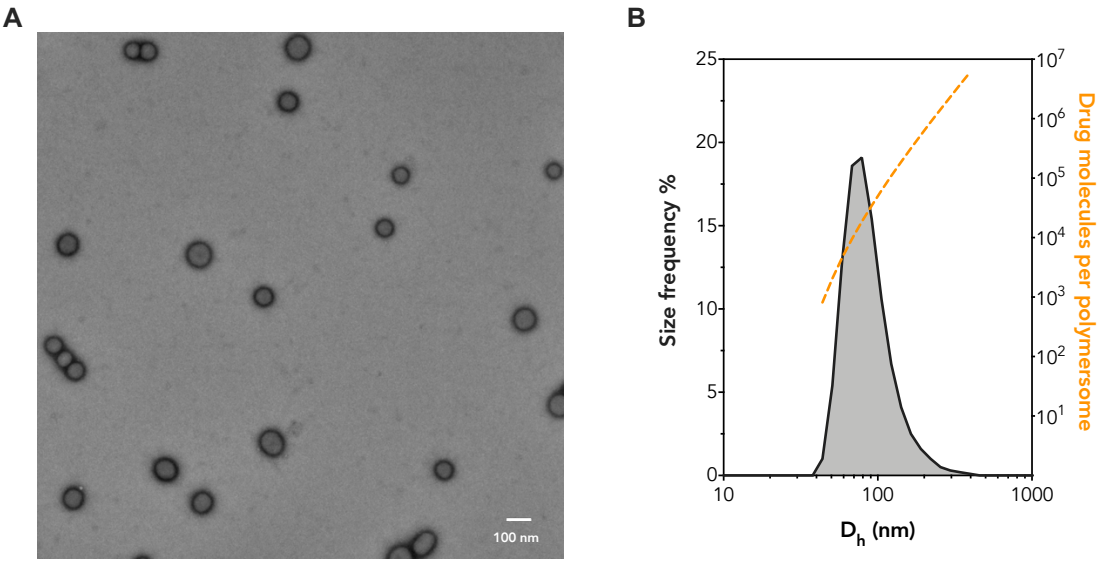

Figure 1. (A) Representative TEM image of Mtx-loaded pH-NITRA polymersomes (100 nm scale bar). **(B)** Analysis on the drug loading capacity represented as the number of Mtx molecules per PMPC-PDPA polymersome as a function of their hydrodynamic diameter (D_h) measured by DLS.

High performance liquid chromatography quantifications revealed the final amount of Mtx in the pH-NITRA:Mtx formulation was of 5.1 mg. More importantly, the drug loading capacity of pH-NITRA polymersomes guarantees the required dose of loaded Mtx to be injected in the animals throughout the *in vivo* experiments (Figure 1B).

3.2. pH-NITRA *in vivo* pharmacokinetics and biodistribution

In order to understand the behaviour and stability of pH-NITRA polymersomes *in vivo*, were carried out a pharmacokinetic study of 24 hours. Two experimental groups of rats (n=3), one healthy and other with adjuvant-induced arthritis (AIA), were intraperitoneally (i.p.) injected with Cy7-labelled pH-NITRA polymersomes (10 mg/kg body weight). Blood samples were collected by tail vein puncture at 0.5, 2, 4, 8 and 24 hours. The plasma concentration profiles over-time of the injected Cy7-labelled pH-NITRA polymersomes in both healthy and arthritic animal models indicates a two phases profile typical of i.p. administration (Figure 2A). It also reveals similarities between healthy and AIA rats in terms of absorption and elimination phases. The absorption phase occurred immediately after the i.p. injection, reaching a maximum peak of concentration in the plasma after 2 hours in both experimental groups (70 ± 23 μg/ml; Figure 2A). The terminal half-life ($t_{1/2}$) of Cy7-labelled pH-NITRA in the plasma of healthy and arthritic animals were calculated by a one phase decay analysis starting from the elimination phase (dot lines in Figure 2A and B). The results suggest a longer $t_{1/2}$ in the AIA group of animals, although the difference with the healthy group was not statistically significant (Figure 2B). In addition, the elimination rate (K_e) in healthy rats was 2.5 times faster than in AIA group (Figure 2B). Despite the similarity of the plasma concentration-time profiles, the area under the plasma concentration-time curve (AUC, determined by the trapezoid rule during the 24 hours of the experiment) for the AIA profile was greater than for healthy one (Figure 2B). These results suggest longer blood circulation time of pH-NITRA polymersomes in the arthritic animal model.

Biodistribution studies of pH-NITRA polymersomes in the main organs were assessed in both healthy and arthritic animal models. After 24 hours from the i.p. injection of Cy7-labelled pH-NITRA, all animals were euthanised and various organs, including the spleen, kidneys, liver and heart, were removed and wet weighed.

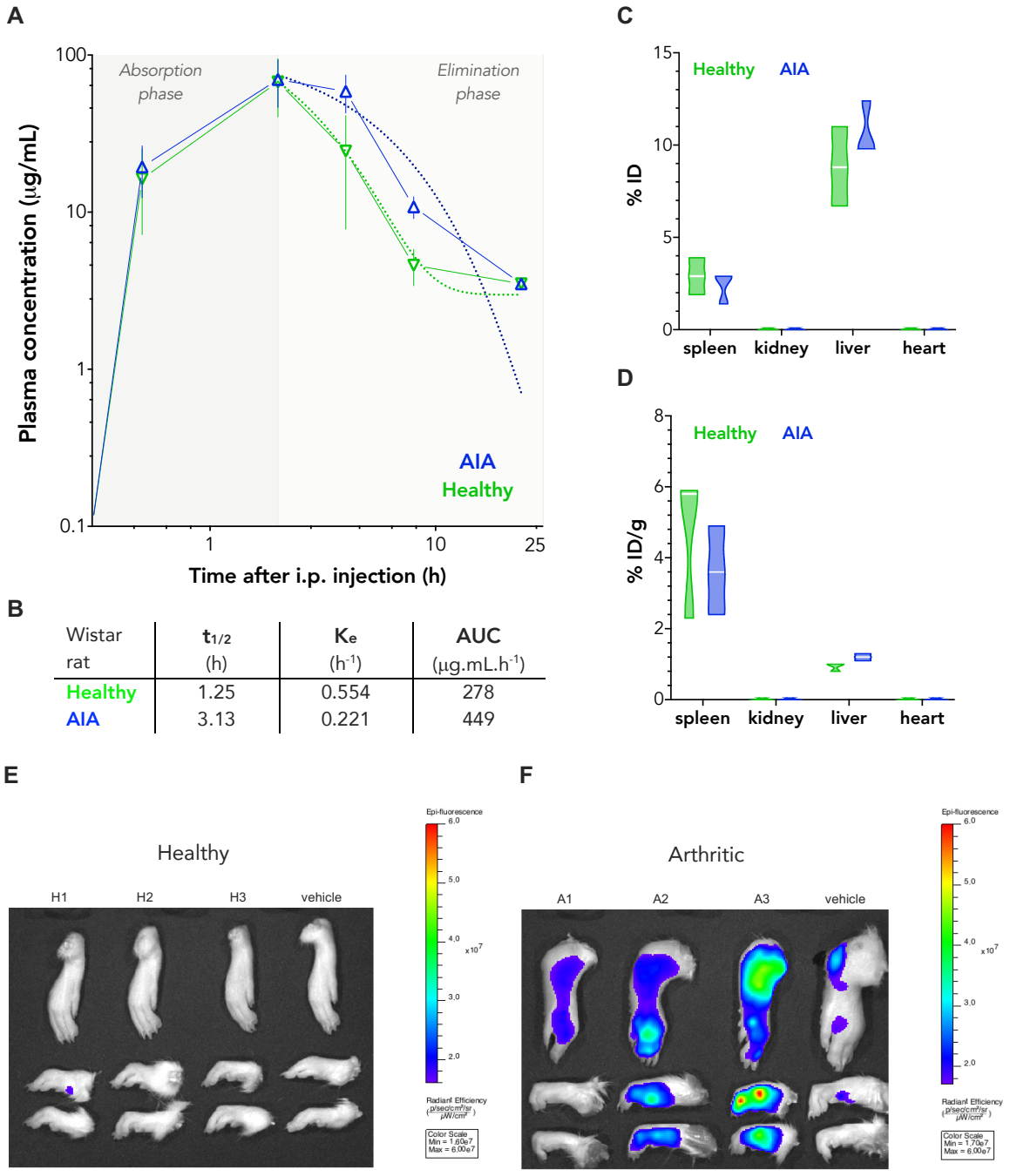

Wistar rat	$t_{1/2}$ (h)	K_e (h^{-1})	AUC ($\mu g.mL.h^{-1}$)
Healthy	1.25	0.554	278
AIA	3.13	0.221	449

Figure 2. (A) The blood plasma concentration-time profiles of Cy7-labelled pH-NITRA after intraperitoneal injection in healthy and AIA Wistar rats. The plasma concentrations of Cy7-labelled pH-NITRA are expressed in µg/mL. **(B)** Pharmacokinetic parameters – terminal half-life ($t_{1/2}$), elimination rate (K_e), area under the curve (AUC) – regarding the plasma concentration-time profiles of Cy7-labelled pH-NITRA after intraperitoneal injection of healthy and AIA Wistar rats. **(C)** The injected dose of Cy7-labelled pH-NITRA (% ID) in the spleen, kidney, liver, heart, after 24 hours intraperitoneal injection in healthy and AIA Wistar rats. **(D)** The % ID of Cy7-labelled pH-NITRA per gram of organ tissue weight. **(E, F)** IVIS images of the right hind and front paws of healthy and AIA Wistar rats. Data express the mean ± SEM (n=3).

The percentage of injected dose per gram of tissue (%ID/g) was then calculated correlating the measured intensity of fluorescence of Cy7-labelled pH-NITRA to the total weight of each organ. The results revealed that high amounts of Cy7-labelled pH-NITRA were found in the spleen of both groups of animals (4.7 ± 1.2 and 3.0 ± 1.2 % for healthy and AIA rats, respectively; Figure 2D). Conversely, that the injected dose of Cy7-labelled pH-NITRA per gram of liver was only of 1.0 ± 0.1 and 1.2 ± 0.1 % for healthy and AIA rats, respectively (Figure 2D). Additionally, the amount of Cy7-labelled pH-NITRA polymersomes determined in the heart and kidneys was negligible (Figure 2C and 2D). Still, there are no significant differences between the healthy and arthritic rats (Figure 2C and D).

Besides the distribution in the main organs, it was important to assess the distribution of pH-NITRA in the paws in order to assess their ability to target areas of inflammation. Thus, IVIS imaging was performed in all rat paws 24 hours after i.p. injection of Cy7-labelled pH-NITRA polymersomes. Results show that no epi-fluorescence intensity signal was detected in the paws of healthy rats (used as control group; Figure 2E). While, the paws of AIA rats exhibited a much higher epi-fluorescence intensity signal (Figure 2F). Interestingly, we noticed that the fluorescence intensity detected in the paws of AIA rats was dependent of the degree of joint swelling. For instance, as observed on Figure 2F, paws of the rat A1 were scored with 2, oppositely to A2 and A3 that were with 3. Overall, IVIS imaging analysis confirm that pH-NITRA accumulated in inflamed paws of AIA rats.

3.3. pH-NITRA *in vivo* therapeutic efficacy

The AIA rat model has a rapid and severe disease progression, following the administration of a foreign antigen of mycobacterial origin [24, 25]. The ankle swelling of the hind paws, monitored by the inflammation score and by measuring the ankle perimeter, is indicate of disease progression and severity [24, 25]. The rapid symptomatic escalation was observed in the AIA vehicle-treated group overtime (Figure 3A). At day 4 post disease induction, the arthritis was developed in all paws as evidenced by the presence erythema and the visible swelling of the joint (Figure 3B and C). In comparison to the healthy animals (which the inflammation score is 0), the AIA vehicle control group showed a significant increase in the ankle swelling ($p<0.0001$; Figure 3C). Additionally, as shown on Figure 3D, there was an increase of the ankle swelling by 15% relative to the first day before treatment starts (which also corresponds to the fourth day post disease

induction). Moreover, AIA rats lost weight by the end of the 19 days post disease induction (6% since the beginning of vehicle-treatment; Figure 3E and F).

In this animal model, the severity of the disease increases over time, reaching the acute inflammation phase by day 13 post induction [34-36]. Indeed, as shown in Figure 3, all the arthritic inflammatory clinical signs are severely increased up to day 13 after the induction of inflammation in the AIA vehicle-treated group of animals ($p<0.001$ comparing with the healthy control group). Also, the results confirmed the continuous disease progression between day 13 and 19 in AIA animals, as observed by their body weight loss, the increase in swelling of the hind paws and the arthritic inflammation score. The maximal swelling of the paws, that is generally observed in this model, occurs by day 19 post induction before reaching a plateau phase [34-36]. Taking this into consideration, the experiment was completed within this time frame.

Having established the accumulation of pH-NITRA to inflamed synovial tissue, the therapeutic efficacy and ability of pH-NITRA nanotherapy to control the progression of arthritic inflammation was evaluated for 15 days of treatment (starting at the fourth day post disease induction) in the AIA rat model. To this end, the different groups of AIA rats were daily intraperitoneally (i.p.) injected with free Mtx, Mtx-loaded pH-NITRA (*i.e.* pH-NITRA:Mtx) and unloaded pH-NITRA polymersomes. The therapeutic efficacy of all these treatments in the arthritic animal model were investigated by measurement of animals' body weight, hind paw swelling, and inflammation clinical scores of all paws throughout 15 days. Result analysis revealed that vehicle-treated control group of AIA rats present a progressive arthritis inflammatory score (Figure 3A). By the end of the treatment, paw volumes increased by an average of 15% (Figure 3D) and the rats lost over 4% of their body weight (Figure 3F). All the other treatments resulted in the decrease of the clinical inflammatory arthritic signs in the rats paws comparing with AIA vehicle-treated group (Figure 3A and C). Indeed, AIA animals treated with either pH-NITRA:Mtx or Mtx exhibited a significantly lower arthritic inflammation score than the unloaded pH-NITRA treatment group especially in the last 5 days of treatment ($p<0.0001$; Figure 3A). The average paw swelling of the pH-NITRA:Mtx- and Mtx-treated groups was significantly reduced by 22% and 19% respectively ($p<0.0001$ versus the AIA vehicle-group; Figure 3D). Although, the paw swelling in AIA rats from the pH-NITRA treatment group was reduced only by 4% still when comparing with the AIA control group there was a striking difference by the end of 15 days ($p<0.0001$, Figure 3D).

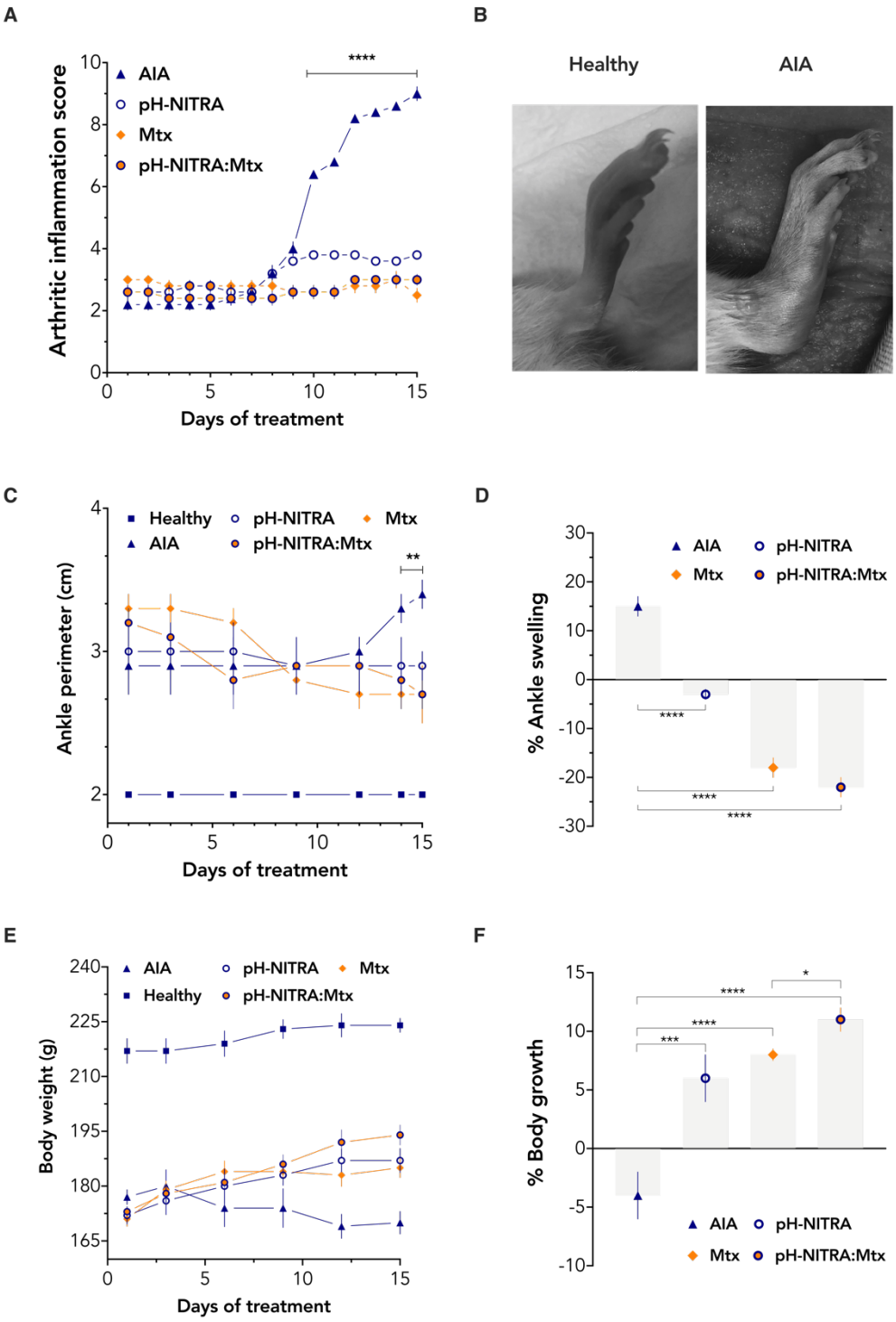

Figure 3. (A) Paws arthritic inflammation score over the 15 days period of treatment. Data defined as the mean ± SEM of the sum of the partial scores of each affected joint. **(B)** Representative images of the left hind paw of a healthy and adjuvant-induced arthritis (AIA) Wistar rat. **(C)** Ankle perimeter of hind paws over the 15 days of treatment. **(D)** Variation of the ankle swelling percentage of the hind paws after the 15 days of treatment. **(E)** Body weight of all animals over the 15 days of treatment. **(F)** Variation of the body growth percentage of animals after the 15 days of treatment. Data express the mean ± SEM (n=5 per experimental group). Statistical analysis for * $p \leq 0.05$, ** $p \leq 0.01$, *** $p \leq 0.001$ and **** $p \leq 0.0001$.

AIA rats receiving either Mtx or pH-NITRA:Mtx treatment resulted in the same degree of paw inflammation score and hind paws swelling (Figure 3A and D, respectively). Furthermore, we observed that oppositely to the arthritic animals, by the end of 15 days, as a consequence of the pH-NITRA:Mtx treatment the body weight increased by 11% ($p<0.0001$; Figure 3F). Overall, results revealed that daily treatment of AIA rats with pH-NITRA:Mtx effectively hinder arthritic inflammation.

3.3.1. *Histological evaluation of the hind paws*

Inflammation affects local joints and promotes bone damage in AIA rats since the early stage of arthritis [15, 24, 25]. The therapeutic effect of the different treatments in the joint of left hind paws was assessed using hematoxylin & eosin (H&E) histological analysis.

The H&E images of the AIA vehicle-treated animals show signs of the early inflammatory process, such as immune cellular infiltration and proliferation, followed by formation of pannus (Figure 4A, B and C). Histological analyses using semi-quantitative scores were performed to identify signs of cartilage degradation and bone erosion, also revealing that both scores were significantly increased in the AIA vehicle-treated group comparing with the healthy one ($p<0.0001$; Figure 4D and E). Conversely, histological analysis of the AIA animal joints from either Mtx or pH-NITRA:Mtx treatment groups resulted in a reduction of the sublining layer infiltration score (Figure 4B) and number of lining layer of cells score compared to the arthritic group ($p<0.01$; Figure 4C). As a consequence of no apparent pannus formation, histological analyses of arthritic rats treated with pH-NITRA:Mtx showed a smooth cartilage surface and a reduced subchondral bone leukocyte infiltration (Figure 4E). Consistent with these results, treatment with pH-NITRA:Mtx was more efficient in reducing the bone damage (Figure 4D; $p<0.1$ versus Mtx-treated group). Hence, negligible differences on the global disease severity score were observed in AIA rats administrated with the pH-NITRA:Mtx compared with the healthy rats (Figure 4F). Interestingly, i.p. injection of empty pH-NITRA also demonstrated to have a significant therapeutic effect in the arthritic animals, particularly in preventing bone and cartilage degradation ($p<0.001$ and $p<0.0001$ versus AIA vehicle-treated animals respectively). Additionally, as expected there was no visible inflammation in the paws for all the other treatments with respect to the AIA group (Figure 4A). Overall, H&E results analysis suggest that pH-NITRA completely abrogate arthritic inflammation hence preventing joint destruction.

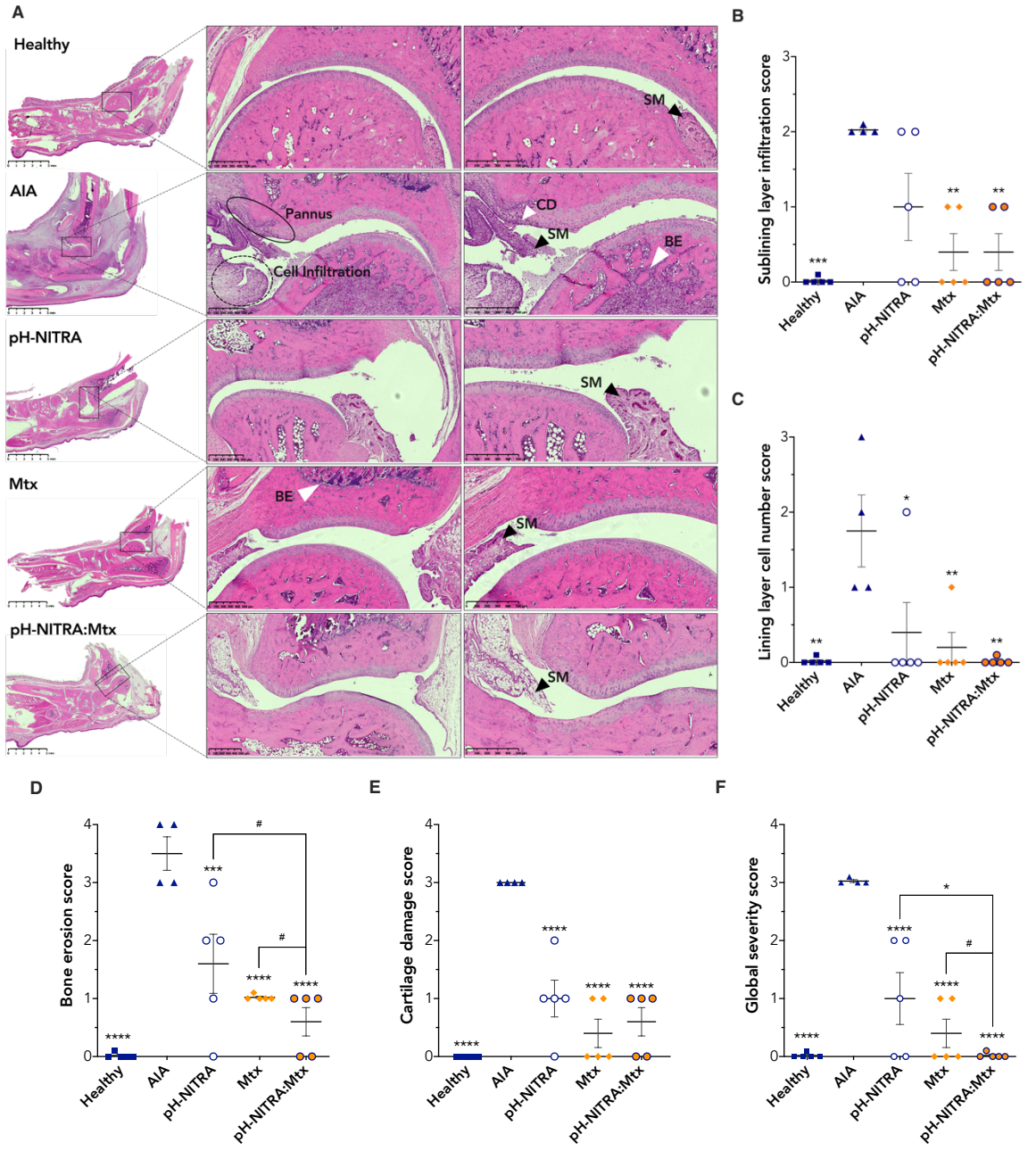

Figure 4. (A) H&E histological representative images of the left hind paw of each experimental animal group (scale bar: 500 μm; SM: synovial membrane; CD: cartilage damage; BE: bone erosion). Histological evaluation: **(B)** Sublining layer infiltration score (0 = none to diffuse infiltration, 1 = lymphoid cell aggregate, 2 = lymphoid follicles, 3 = lymphoid follicles with germinal centre formation); **(C)** Lining layer cell number score (0 = fewer than three layers, 1 = three to four layers, 2 = five to six layers, 3 = more than six layers); **(D)** Bone erosion score (0 = no erosions, 1 = minimal, 2 = mild, 3 = moderate, 4 = severe); **(E)** Cartilage damage score (0 = normal, 1 = irregular, 2 = clefts, 3 = clefts to bone); **(F)** Global severity score (0 = no signs of inflammation, 1 = mild, 2 = moderate, 3 = severe). Data express the mean ± SEM. Statistical analysis versus the AIA experimental group (* $p \leq 0.05$, ** $p \leq 0.01$, *** $p \leq 0.001$ and **** $p \leq 0.0001$) and the pH-NITRA:Mtx experimental group ($^{\#}$ $p \leq 0.1$ and * $p \leq 0.05$).

3.3.2. *Serum inflammation-related cytokines analyses*

Increased levels of TNFα, IL1β and IL6 in the serum of AIA rat animals are associated with disease activity [5, 10, 15, 24, 25, 37]. The levels of these pro-inflammatory cytokines in all animals were quantified in serum by ELISA. ELISA results revealed that vehicle-treated AIA rats exhibited high serum levels of TNFα, IL1β and IL6, in comparison with the healthy control group ($p<0.0001$, $p<0.0001$ and $p<0.01$ respectively; Figure 5). Thereby, as expected, the arthritic group of rats present systemic inflammatory manifestations reflected by hyperplasia and synovial inflammation. In contrast, all tested inflammation-related cytokines decreased to a different extent in the three arthritic groups daily administrated with pH-NITRA, Mtx and pH-NITRA:Mtx. Both Mtx and pH-NITRA:Mtx treatments significantly decreased TNFα concentration in the serum by 5-fold ($p<0.001$ versus AIA vehicle-treated group; Figure 5A). The serum levels of IL1β also decreased in both Mtx- and pH-NITRA:Mtx-treated AIA rats when compared with the vehicle-treated groups (respectively, $p<0.001$ and $p<0.0001$; Figure 5B).

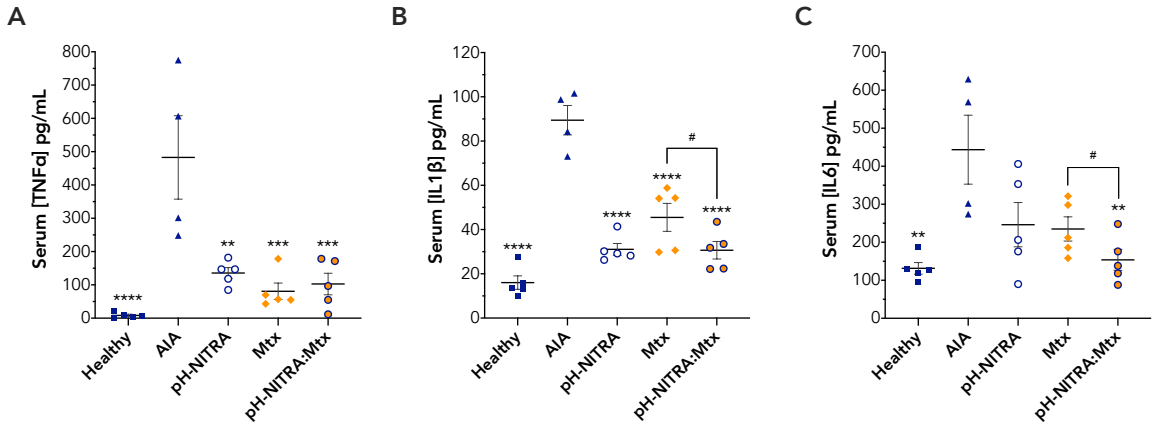

Figure 5. Inflammation-related cytokine analysis in the serum of animals after the 15 days of treatment. Data express the mean ± SEM (n=5 per experimental group). Statistical analysis versus the AIA experimental group (* $p \leq 0.05$, ** $p \leq 0.01$, *** $p \leq 0.001$ and **** $p \leq 0.0001$) and the pH-NITRA:Mtx experimental group ($^{\#}$ $p \leq 0.1$).

Remarkably, pH-NITRA also had similar therapeutic effect at reducing the serum pro-inflammatory cytokine levels, particularly for TNFα and IL1β ($p<0.01$ and $p<0.0001$ respectively when compared with vehicle-treated arthritic rats). The serum concentration levels of IL1β were similar and with negligible differences for both pH-NITRA treatments when compared with the healthy control group. We had shown in a previous *in vitro* study that PMPC-PDPA polymersomes (i.e. pH-NITRA)

effectively inhibit inflammatory pathways signalling and supress the production of TNFα, IL1β and IL6 by activated macrophages [32]. Moreover, pH-NITRA:Mtx was more effective ($p<0.1$) in reducing the IL1β and IL6 levels in serum than conventional Mtx-treatment (Figure 5B and C). Increased values of serum IL6 were also observed in the vehicle-treated AIA group, which have shown bone loss evidence in the histological analyses (Figure 4A and D). By the end of 15 days, the IL6 concentration of the pH-NITRA:Mtx-treated group was significantly reduced to 154 $\pm$ 28 pg/mL ($p<0.01$ versus AIA vehicle-treated group; Figure 5C), which was similar to the healthy vehicle-treated rats (131 $\pm$ 15 pg/mL).

4. Discussion

Arthritis severity is characterised by synovial hyperplasia, due to the infiltration of immune cells and formation of pannus, which invades joint cartilage surface and leads to bone erosion [5, 10]. This *in vivo* study demonstrates the therapeutic potential of pH-NITRA loading Mtx in the complete abrogation of arthritis inflammation progression and hence in improving RA treatment.

In vivo pharmacokinetic studies of 24 hours in the AIA rats are indicative of the pH-NITRA polymersomes ability to enable their late recognition and elimination by the reticuloendothelial system, hence avoiding their rapid clearance from blood circulation. Thus, we confirm that the PMPC building block ensures the pH-NITRA with stealth properties upon administration *in vivo*, as well as, stability in physiologic fluids until reaching the synovial disease-inflamed tissue.

Biodistribution studies indeed prove the pH-NITRA polymersomes ability to selectively accumulate within inflamed joints of arthritic animals. This accumulation is facilitated most likely ascribed to the small size of the polymersomes plus the enhanced vascular permeability and prominent angiogenesis of synovial inflamed tissues [13, 14, 38-41].

Additional biodistribution studies the organs of AIA rats revealed that high amounts of pH-NITRA polymersomes were found in the liver and spleen (Figure 2C and D). Accumulation of pH-NITRA polymersomes within these organs is mostly due to the fact that these are the main routes of excretion for nanomedicines upon administration [42]. And also the fact that most of the i.p. injected substances enter the portal vein and pass through the liver before entering the systemic circulation [42, 43]. Still, a surprisingly low fluorescence intensity was detected in the liver of

both healthy and AIA groups of animals. Nevertheless, *in vivo* biodistribution studies are indicative of pH-NITRA polymersomes ability to improve the on-target bioavailability of loaded Mtx, while potentially decreasing off-target systemic exposure and the well-known deleterious hepatotoxic side effects [21]. Indeed, the safety and biocompatibility of pH-NITRA polymersomes in prolonged administration must be guarantee, as they should not cause any cytotoxic, inflammatory or immunogenic effects. In this study, we showed the biocompatibility of pH-NITRA polymersomes *in vivo,* as no apparent subacute systemic toxicity was observed after 15 days of daily treatment. Although, in order to confirm the extent of any tissue damage and cytotoxic effect related to the treatment of AIA rats, further histopathological analysis need to be performed on the spleen and liver.

The *in vivo* studies on the therapeutic efficacy of pH-NITRA nanotherapy included clinical arthritic signs and inflammation-related histologic analyses on AIA treated animals. Treatment of arthritic animals with Mtx-loaded pH-NITRA resulted in the suppression arthritic synovial inflammation. Also, in the complete abrogation of joint synovial hyperplasia and hence preventing cartilage and bone damages. The enhanced on-site bioavailability of loaded Mtx is fundamental for its therapeutic efficacy. Hereby, the anti-rheumatic and -inflammatory therapeutic effect of pH-NITRA nanotherapy is mostly result of their facilitated accumulation within synovial tissues of inflamed joints. However, also free Mtx treatment had similar beneficial therapeutic effect in the inhibition of the inflammatory arthritic signs (Figure 3 and 4). The timing and dosing of Mtx administrated are also key parameters for treatment efficacy, due to the drug's rapid clearance. It should be noted that the same dose of Mtx (0.223 mg/kg/day) was used in this study either free or loaded. In this sense, in further *in vivo* studies, it would be interesting to lower the administrated dosage of loaded Mtx to evaluate then whether the same (or even better) therapeutic effect would be achieve compared to conventional Mtx treatment. Additionally, it would be also interesting to double the treatment time, as Mtx-loaded pH-NITRA polymersomes might have a long-time effect until complete disease remission.

Further serum levels of pro-inflammatory cytokines analysis demonstrated the efficacy of Mtx-loaded pH-NITRA treatment to inhibit systemic inflammation in arthritic animals. In RA, synovial inflammation progresses through interacting cascades of pro-inflammatory cytokines [5, 10, 15, 44]. In particular, TNFα, IL1β and IL6 are reported to be inherently associated to systemic and local

inflammations in patients with RA [5, 10, 15, 44]. TNFα and IL1β are believed to play an important role since the early phase of the disease as they directly stimulate the infiltration of leucocytes, neutrophils and macrophages into the synovium [5, 10, 15, 44]. IL6 is involved in the perpetuation of synovial inflammation together with IL1β and TNFα, but it plays also a key role in the progressive damage of joints [5, 10, 15, 44-46]. IL6 activates the synoviocytes to release metalloproteases proteases and reactive oxygen species, leading to the destruction of the cartilage tissue [5, 10, 12, 15, 44, 45]. This cytokine is also involved in the osteoclast differentiation and activation, which are mostly responsible for bone erosion [5, 10, 12, 15, 44, 45]. Thereby, the demonstrated reduction on the secretion levels of these inflammation-mediated cytokines show the potential of pH-NITRA nanotherapy to control the progression of systemic inflammation, as well as, to abrogate the disease destructive process.

Remarkably, unloaded pH-NITRA polymersomes show to be also effective in supressing arthritic and systemic inflammatory signs in AIA model of arthritis. Previous reports ascribed the anti-inflammatory action of PMPC-PDPA polymersomes, to the enhanced internalisation of phosphatidylcholine (in the polymeric chain of PMPC block) through the cell scavenger receptor class B type 1, which, in turn, is involve in the regulation of intracellular inflammatory pathways [32, 47, 48].

In summary, the Mtx-loaded pH-NITRA nanotherapy exhibit an effective anti-arthritic and -inflammatory therapeutic effect with significant amelioration of synovial inflammation and complete abrogation of arthritis progression *in vivo*.

5. Conclusion

In vivo studies prove that pH-NITRA polymersomes selectively reach the arthritic inflamed joints, with reduced accumulation in secretion organs. The intraperitoneal administration of Mtx-loaded pH-NITRA polymersomes in an arthritic animal model is highly effective in the inhibition of the inflammatory arthritic signs. In addition to be highly effective in supressing both local and systemic immune- and inflammatory-mediated responses. More interestingly, unloaded pH-NITRA is able to abrogate arthritic inflammation, as well as, the progression of systemic inflammation, in the same model of arthritis. In conclusion, with this study, we demonstrate the beneficial therapeutic effects of pH-NITRA polymersomes and

prove its potential to control the disease inflammatory activity and to hinder arthritis progression. Hence, establishing them as a very promising nanotherapy in the treatment of RA.

References

1 Firestein GS. Evolving concepts of rheumatoid arthritis. Nature 2003;423(6937):356-61.

2 Smolen JS, Steiner G. Therapeutic strategies for rheumatoid arthritis. Nat Rev Drug Discov 2003;2(6):473-88.

3 Gouveia V, Lima S, Nunes C, Reis S. Non-Biologic Nanodelivery Therapies for Rheumatoid Arthritis. Journal of Biomedical Nanotechnology 2015;11(10):1701-21.

4 van der Linden MP, le Cessie S, Raza K, et al. Long-term impact of delay in assessment of patients with early arthritis. Arthritis Rheum 2010;62(12):3537-46.

5 Müller-Ladner U, Pap T, Gay RE, Neidhart M, Gay S. Mechanisms of disease: the molecular and cellular basis of joint destruction in rheumatoid arthritis. Nat Clin Pract Rheumatol 2005;1(2):102-10.

6 Gouveia VM, Lima SA, Nunes C, Reis S. Non-Biologic Nanodelivery Therapies for Rheumatoid Arthritis. J Biomed Nanotechnol 2015;11(10):1701-21.

7 Quan LD, Thiele GM, Tian J, Wang D. The Development of Novel Therapies for Rheumatoid Arthritis. Expert Opin Ther Pat 2008;18(7):723-38.

8 Lundkvist J, Kastäng F, Kobelt G. The burden of rheumatoid arthritis and access to treatment: health burden and costs. Eur J Health Econ 2008;8 Suppl 2:S49-60.

9 Upchurch KS, Kay J. Evolution of treatment for rheumatoid arthritis. Rheumatology (Oxford) 2012;51 Suppl 6:vi28-36.

10 McInnes IB, Schett G. The pathogenesis of rheumatoid arthritis. N Engl J Med 2011;365(23):2205-19.

11 Kinne RW, Stuhlmüller B, Burmester GR. Cells of the synovium in rheumatoid arthritis. Macrophages. Arthritis Res Ther 2007;9(6):224.

12 Bustamante MF, Garcia-Carbonell R, Whisenant KD, Guma M. Fibroblast-like synoviocyte metabolism in the pathogenesis of rheumatoid arthritis. Arthritis Res Ther 2017;19(1):110.

13 Szekanecz Z, Besenyei T, Szentpétery A, Koch AE. Angiogenesis and vasculogenesis in rheumatoid arthritis. Curr Opin Rheumatol 2010;22(3):299-306.

14 Maracle CX, Kucharzewska P, Helder B, et al. Targeting non-canonical nuclear factor-κB signalling attenuates neovascularization in a novel 3D model of rheumatoid arthritis synovial angiogenesis. Rheumatology (Oxford) 2017;56(2):294-302.

15 Karouzakis E, Neidhart M, Gay RE, Gay S. Molecular and cellular basis of rheumatoid joint destruction. Immunol Lett 2006;106(1):8-13.

16 Singh JA, Saag KG, Bridges SL, et al. 2015 American College of Rheumatology Guideline for the Treatment of Rheumatoid Arthritis. Arthritis Rheumatol 2016;68(1):1-26.

17 Kay J, Upchurch KS. ACR/EULAR 2010 rheumatoid arthritis classification criteria. Rheumatology (Oxford) 2012;51 Suppl 6:vi5-9.

18 Smolen JS, Landewé R, Breedveld FC, et al. EULAR recommendations for the management of rheumatoid arthritis with synthetic and biological disease-modifying antirheumatic drugs: 2013 update. Ann Rheum Dis 2014;73(3):492-509.

19 Brown PM, Pratt AG, Isaacs JD. Mechanism of action of methotrexate in rheumatoid arthritis, and the search for biomarkers. Nat Rev Rheumatol 2016;12(12):731-42.

20 Favalli EG, Biggioggero M, Meroni PL. Methotrexate for the treatment of rheumatoid arthritis in the biologic era: still an "anchor" drug? Autoimmun Rev 2014;13(11):1102-8.

21 Visser K, van der Heijde DM. Risk and management of liver toxicity during methotrexate treatment in rheumatoid and psoriatic arthritis: a systematic review of the literature. Clin Exp Rheumatol 2009;27(6):1017-25.

22 Virgínia Moura Gouveia CNaSR. Innovative target-to-treat nanostrategies for rheumatoid arthritis. In: Reis ARNaS, ed. *Nanoparticles in Life Sciences and Nanomedicine*. Pan Stanford Publishing Pte. Ltd. Singapore: Pan Stanford Publishing; 2018.

23 Abolmaali SS, Tamaddon AM, Dinarvand R. A review of therapeutic challenges and achievements of methotrexate delivery systems for treatment of cancer and rheumatoid arthritis. Cancer Chemother Pharmacol 2013;71(5):1115-30.

24 Kannan K, Ortmann RA, Kimpel D. Animal models of rheumatoid arthritis and their relevance to human disease. Pathophysiology 2005;12(3):167-81.

25 Schopf LR, Anderson K, Jaffee BD. Rat models of arthritis: Similarities, differences, advantages, and disadvantages in the identification of novel therapeutics. In: Stevenson CS, Marshall LA, Morgan DW, eds. *In Vivo Models of Inflammation*. Birkhäuser Verlag Basel, Switzerland; 2006.

26 Schett G, Gravallese E. Bone erosion in rheumatoid arthritis: mechanisms, diagnosis and treatment. Nat Rev Rheumatol 2012;8(11):656-64.

27 Canton I, Massignani M, Patikarnmonthon N, et al. Fully synthetic polymer vesicles for intracellular delivery of antibodies in live cells. FASEB J 2013;27(1):98-108.

28 Robertson JD, Rizzello L, Avila-Olias M, et al. Purification of Nanoparticles by Size and Shape. Sci Rep 2016;6:27494.

29 Gaitzsch J, Delahaye M, Poma A, Du Prez F, Battaglia G. Comparison of metal free polymer-dye conjugation strategies in protic solvents. Polymer Chemistry 2016;7(17):3046-55.

30 Fetsch C, Gaitzsch J, Messager L, Battaglia G, Luxenhofer R. Self-Assembly of Amphiphilic Block Copolypeptoids - Micelles, Worms and Polymersomes. Sci Rep 2016;6:33491.

31 Ruiz-Pérez L, Messager L, Gaitzsch J, et al. Molecular engineering of polymersome surface topology. Sci Adv 2016;2(4):e1500948.

32 Gouveia VM, Rizzello L, Nunes C, et al. Macrophage Targeting pH Responsive Polymersomes for Glucocorticoid Therapy. Pharmaceutics 2019;11(11).

33 Wang L, Chierico L, Little D, et al. Encapsulation of biomacromolecules within polymersomes by electroporation. Angew Chem Int Ed Engl 2012;51(44):11122-5.

34 Cascao R, Vidal B, Raquel H, et al. Effective treatment of rat adjuvant-induced arthritis by celastrol. Autoimmun Rev 2012;11(12):856-62.

35 Vidal B, Cascão R, Vale AC, et al. Arthritis induces early bone high turnover, structural degradation and mechanical weakness. PLoS One 2015;10(1):e0117100.

36 Vidal B, Cascão R, Finnilä MAJ, et al. Early arthritis induces disturbances at bone nanostructural level reflected in decreased tissue hardness in an animal model of arthritis. PLoS One 2018;13(1):e0190920.

37 Szekanecz Z, Halloran MM, Volin MV, et al. Temporal expression of inflammatory cytokines and chemokines in rat adjuvant-induced arthritis. Arthritis Rheum 2000;43(6):1266-77.

38 Tas SW, Maracle CX, Balogh E, Szekanecz Z. Targeting of proangiogenic signalling pathways in chronic inflammation. Nat Rev Rheumatol 2016;12(2):111-22.

39 Bartok B, Firestein GS. Fibroblast-like synoviocytes: key effector cells in rheumatoid arthritis. Immunol Rev 2010;233(1):233-55.

40 Bartok B, Hammaker D, Firestein GS. Phosphoinositide 3-kinase δ regulates migration and invasion of synoviocytes in rheumatoid arthritis. J Immunol 2014;192(5):2063-70.

41 Leblond A, Allanore Y, Avouac J. Targeting synovial neoangiogenesis in rheumatoid arthritis. Autoimmun Rev 2017;16(6):594-601.

42 Abdelhalim MA. Uptake of gold nanoparticles in several rat organs after intraperitoneal administration in vivo: a fluorescence study. Biomed Res Int 2013;2013:353695.

43 Dirnena-Fusini I, Åm MK, Fougner AL, Carlsen SM, Christiansen SC. Intraperitoneal, subcutaneous and intravenous glucagon delivery and subsequent glucose response in rats: a randomized controlled crossover trial. BMJ Open Diabetes Res Care 2018;6(1):e000560.

44 Choy E. Understanding the dynamics: pathways involved in the pathogenesis of rheumatoid arthritis. Rheumatology (Oxford) 2012;51 Suppl 5:v3-11.

45 Narazaki M, Tanaka T, Kishimoto T. The role and therapeutic targeting of IL-6 in rheumatoid arthritis. Expert Rev Clin Immunol 2017;13(6):535-51.

46 Fonseca JE, Santos MJ, Canhão H, Choy E. Interleukin-6 as a key player in systemic inflammation and joint destruction. Autoimmun Rev 2009;8(7):538-42.

47 Treede I, Braun A, Sparla R, et al. Anti-inflammatory effects of phosphatidylcholine. Journal of Biological Chemistry 2007;282(37):27155-64.

48 Linton MF, Tao H, Linton EF, Yancey PG. SR-BI: A Multifunctional Receptor in Cholesterol Homeostasis and Atherosclerosis. Trends Endocrinol Metab 2017;28(6):461-72.

Chapter 4

Conclusion and future perspectives

Rheumatoid arthritis (RA) is a chronic systemic inflammatory and autoimmune disease characterised by progressive synovial inflammation of joints. The treatment of RA remains a challenge as there is no resolutive cure so far. Conventional therapies for the early treatment intervention include glucocorticoids (GCs) and disease-modifying anti-rheumatic drugs (DMARDs), such as prednisolone and methotrexate, respectively [1, 2]. Still, the prolonged administration of these drugs not only entails deleterious side effects, risk of infection and intolerance issues, but also medical and indirect costs associated with the chronic treatment [1, 2]. This often limits the well-known therapeutic potential of these drugs to achieve disease complete remission.

Owing to these drawbacks, the aim of this thesis was to enhance RA treatment by designing innovative nanotherapies with therapeutic potential to target and treat synovial inflammation. And hence, to overcome the limitations related to the long-term use of well-establish conventional drugs – prednisolone and methotrexate.

A better understanding of the disease pathogenesis uncovers the inflamed synovium and the increased presence of macrophages and synoviocytes found within it as the targets to improve RA treatment. The lipid- and polymer-based nanomedicines (liposomes and polymersomes, respectively) presented on Chapter 3 of this thesis were specifically designed to target the inflamed synovium based on the principles of passive and active targeting. The uniqueness of the developed nanomedicines relies on their physicochemical properties tailored to enable the selective and effective drug delivery into target disease-inflamed site, in a way to improve its release when required. In this sense, as demonstrated on Chapter 3 of this thesis:

(i) The nanomedicines provide protection and stability of the loaded drug from degradation in physiologic fluids and hence from off-target systemic activation.

(ii) The nanomedicines are made of biocompatible lipids and polymers, thus not causing cytotoxicity, neither any inflammatory or immunogenic responses by themselves.

(iii) The stealth properties of these nanomedicines can delay the recognition and clearance by the mononuclear phagocyte system in circulation, by providing a hydrophilic and steric barrier against opsonisation.

(iv) The size and morphology of the nanomedicines enhances their ability to passively accumulate within the inflamed synovia via the enhanced

permeability and retention phenomenon by taking advantage of inflamed synovial neovascularisation.

(v) The nanomedicines active targeting ability, bestowed either by the hyaluronic acid or the poly(2-methacryloyloxyethyl phosphorylcholine, enables binding specificity and hence uptake by synovial macrophages and synoviocytes.

(vi) The pH-responsive properties of these nanomedicines ensure the controlled drug delivery and on-site intracellular release.

By taking advantage of the stability, selectivity and pH sensitivity of these nanomedicines, both *in vitro* and *in vivo* studies prove the potential of this step-by-step approach to target inflamed synovial tissues and cells. Hence, to enhance on-site bioavailability, activity and therapeutic effectiveness of loaded conventional drugs. More importantly, *in vivo* studies demonstrate the great potential of the developed nanotherapy in the resolution of chronic synovial inflammation and in the abrogation of disease progression. This can significantly impact current treatment guidelines, in which the control of disease progression is recommended at 6 to 12 months as an approach to improve RA treatment and advanced prognosis [1, 2]. So, unlike conventional therapies, the developed nanotherapy promises to efficiently target and treat arthritic inflammation, while potentially limiting off-site systemic toxicity.

The proposed nanomedicines offer many potential therapeutic advantages, still there are factors to be considered and limitations to overcome before future clinical implementation. The safety and biocompatibility of nanomedicines in chronic RA therapy must be considered, since the nanomedicine alone should not cause any cytotoxic, inflammatory or immunogenic effect. Indeed, *in vivo* subacute systemic toxicity was assessed after daily administration for 15 days. Although, given the chronic component of the disease, sub-chronic and chronic toxicity studies should be also assessed. These include full clinical pathology (clinical biochemistry and hematology), organ weights and histopathology. This is particularly crucial for the organs belonging to the mononuclear phagocyte system, responsible for the body clearance of nanomedicines. In addition to assess *in vivo* immunotoxicology, the batch-to-batch consistency of the developed nanomedicines, their physicochemical stability and sterility are key factors for the production scale-up. The assessment and validation of all these factors is crucial in order to eliminate potential toxicity-

related clinical failure. This may be a costly and time-consuming process that may reduce the speed of translation into clinical trials.

Furthermore, the route of administration should be chosen based on clinical relevance as well as practicality for future implementation. In the case of intra-articular administration of nanomedicines, the number of injections needs to be reduced. As, a part of being extremely painful to the patient, repeated needle punctures may increase the risk of infection or septic arthritis. Also, the intra-articular injection of gel-type formulations can cause an increased viscosity of the synovial fluid, which, in turn, leads to an increased pressure within the joint and further synovial tissue damage. On the other hand, parenteral formulations should ideally have long-lasting therapeutic effect, as daily intraperitoneal or intravenous injection are unlikely to improve patient compliance.

Nonetheless, the proposed nanomedicines have the potential to revolutionize and improve the RA treatment, as their properties may allow the clinical prolonged administration of conventional DMARDs and GCs, with less risk of off-target deleterious effects. Thus also, possibly decreasing high costs associated with the use of biologic therapy.

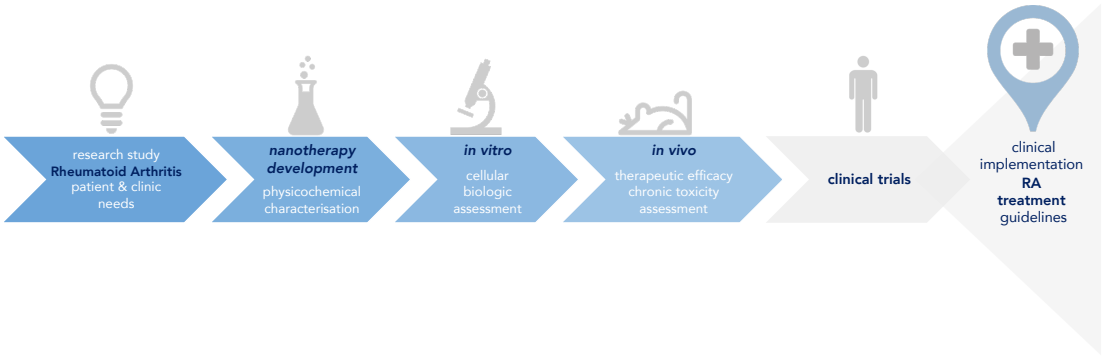

Figure 1. Target-to-treat nanotherapy for rheumatoid arthritis: from idea to clinics.

Moreover, arthritis and the conventional drugs used in this study are not limited in their application neither to the disease. Thereby, the developed nanotherapies might also have an impact in other arthritic inflammatory conditions that employ similar treatment guidelines, namely osteoarthritis, enteropathic arthritis, fibromyalgia, gout, ankylosing and cervical spondylitis [1]. Particularly, the improved therapeutic targeting of methotrexate could also have potential applications in the treatment of several other auto-immune diseases, such as lupus, psoriasis, myasthenia gravis and inflammatory bowel disease. Therefore, the proposed pH-responsive nanomedicine exhibits potential to be immensely

beneficial to patients suffering also from other inflammatory and autoimmune disorders.

Concluding, I am confident that the target-to-treat nanotherapy presented in this thesis has the potential to be clinically translated in the near future for the treatment of chronic inflammatory autoimmune disorders (Figure 1). Patients with RA will benefit from a safe and improved therapeutic efficiency with negligible side effects and less dose frequency. Not only this may lead to an improved patient commitment to the treatment, but also to a substantial improvement of their quality of life. Thereby, in addition to improve the current clinical limitations, target-to-treat nanotherapy may also have an impact on healthcare and socioeconomic associated costs with RA treatment.

Reference

1 Kay J, Upchurch KS. ACR/EULAR 2010 rheumatoid arthritis classification criteria. Rheumatology (Oxford) 2012;51 Suppl 6:vi5-9.

2 Smolen JS, Landewé R, Breedveld FC, et al. EULAR recommendations for the management of rheumatoid arthritis with synthetic and biological disease-modifying antirheumatic drugs: 2013 update. Ann Rheum Dis 2014;73(3):492-509.